Saint-Petersburg state university

Sibirev Aleksei Vladimirovich

Thermal cycling temperature range optimization for stabilization of the force-displacement characteristics of NiTi shape memory alloy

Scientific specialization
1.1.8. Solid Mechanics

The dissertation is submitted for the degree of
Doctor of Physical and Mathematical Sciences

Translation from Russian

Saint Petersburg – 2024

Contents

Introduction 5

Chapter 1. Relationship between defect density and functional properties of NiTi alloy during thermal cycling 24

1.1. Relationship between variation in defect density and parameters of martensitic transitions during thermal cycling without external load 24

1.1.1. The Influence of Isothermal Holdings Between Thermal Cycles on the Recovery of Martensitic Transformation Temperatures in NiTi Alloy 27

1.1.2. The Influence of the Upper Temperature on the Reversible Change in the Kinetics of Multistage Transformations in NiTi Alloy during Thermal Cycling. 37

1.1.3. Relationship between variation in defect density and parameters of martensitic transformations in NiTi alloys during thermocycling 42

1.1.4. Direct observations of the movement of interphase and intermartensitic boundaries during multiple thermal cycles in NiTi alloy in the annealed state. 52

1.2. The influence of stress on the relationship between defect density and variation in the functional properties of NiTi alloy during thermal cycling under stress 65

1.3. Influence of isothermal holdings on reversible and irreversible strain in NiTi shape memory alloy. 73

1.4. Variations in the SMA properties during multiple thermal cycling in the work production cycle. 77

1.5. Conclusions to Chapter 1 87

Chapter 2. Variations in the NiTi SMA properties during thermal cycling under constant stress through the range of incomplete martensitic transformations 89

2.1. Thermal cycling of the $Ni_{50}Ti_{50}$ alloy under constant load in the temperature range of incomplete forward martensitic transformation. 91

2.2. Thermal cycling of the $Ni_{50}Ti_{50}$ alloy under load within temperature range of incomplete reverse martensitic transformation..... 100

2.3. The influence of the fraction of the temperature range of forward and reverse martensitic transformation on the variations in properties of the NiTi alloy during thermal cycling under load 108

2.4. Conclusions to Chapter 2 113

Chapter 3. Managing functional properties during thermal cycling of NiTi alloy in actuator mode 115

3.1. The influence of counterbody stiffness, pre-deformation method, and strengthening on the variation of niti alloy properties during thermal cycling in actuator mode 117

3.1.1. Objects and methods used for investigations of NiTi shape memory alloy properties variations during thermal cycling in actuator mode 117

3.1.2. The impact of counterbody stiffness on the variation of functional properties of NiTi alloy 121

3.1.3. Impact of pre-deformation method on functional properties variations of NiTi alloy during thermal cycling in actuator mode 127

3.1.4. Influence of pre-straining in the austenite state on variations in the functional properties of NiTi alloy during thermal cycling in actuator mode 132

3.2. The influence of transformation fraction during thermal cycling in drive mode on variations in the functional properties of NiTi alloy..... 136

3.3. The influence of the temperature cycle position relative to the martensitic transition temperatures on the variation of the NiTi alloy functional properties during thermal cycling in drive mode within an incomplete temperature range 146

3.4. Variations in the functional properties of a torsional actuator with an working body made of NiTi alloy at high numbers of thermal cycles. 153

3.5. Conclusions to Chapter 3 161

Conclusions 164

References 168

Introduction

The study relevance

Shape memory alloys (SMAs) are one of the prominent representatives of the functional (smart) materials class. SMAs exhibit unique mechanical properties: the superelasticity effect (the ability to recover large deformations up to 10% upon unloading), the shape memory effect (the ability to recover large non-elastic deformations up to 10% upon heating), and the two-way shape memory effect (cyclic deformation up to 4.5% during thermal cycling in the free state). Such unusual behavior is associated with the SMA's experience of thermoelastic martensitic transformations [1,2]. The strain recovery is observed even under opposing external loads, meaning SMAs can directly convert thermal energy into mechanical work. Thanks to these unique properties, SMAs have already found wide applications in aerospace, aviation, medicine, microelectronics, and other industrial sectors [3–9]. The demand for SMAs in the economy is growing every year. According to industry forecasts, the SMA market size is projected to reach $19.8 billion by 2027, with an average growth rate of 10.2% from 2022 to 2027 [10].

All applications of SMAs can be roughly divided into two groups. The first group includes single-actuation devices, where the required action must occur only once. Such devices include thermal mechanical couplings, medical stents, prostheses and clamps, deployment and unfolding devices used in the space industry, and others [9]. The second group consists of multi-action devices, where actions need to be repeated with each heating cycle. Such devices include sensors, thermal actuators, heat engines, and others [6,9,11–16]. Among the large number of SMA devices, the majority are multi-action drives. The use of SMAs as the working body of a drive provides several advantages, such as simplifying the drive's design, smooth and reliable operation, reducing the mass and volume of the product, and the ability to control displacement and forces by controlling thermal cycling modes [9,17–23]. For instance, the NiTi alloy has a specific work capacity of 10 J/cm^3, which is 25 times higher than that of electric motors [9]. Such a high value is achieved due to both high developed forces (over 400 MPa) and large

displacements (up to 10% reversible strain). The smaller the device size, the greater the advantage of SMA-based drives over traditional analogs since the scaling effect almost does not affect the device's performance characteristics. In addition to the aforementioned advantages, NiTi-based SMAs also possess high wear resistance and corrosion resistance, allowing the use of these drives in the presence of aggressive environments (e.g., salty water) [9,19–22,24,25].

In multi-action drives, a pre-deformed working element made of SMA is connected to an elastic counter-body. During heating, the deformation in the SMA's working element is restored, leading to deformation of the counter-body, which acts as an elastic energy accumulator. Upon further cooling, during the direct martensitic transformation, the accumulated potential elastic energy is used to deform the SMA's working element [24–28]. Upon subsequent heating, the deformation in the SMA element is restored again, and the deformation of the counter-body occurs, repeating the described procedure. Thus, drives with working elements made of SMAs are capable of repeatedly changing deformation and exerting forces, i.e., performing necessary actions during thermal cycles. For reliable device operation, it is necessary for the drive's operating parameters (displacements, generated forces, temperature activation intervals) to remain unchanged during multiple thermal cycles. In other words, the functional properties of SMAs during thermal cycling through the martensitic transformation temperature range should either remain unchanged or undergo minimal variations that do not affect the device's performance characteristics. However, it is known that thermal cycling of SMAs is accompanied by changes in structure, an increase in defect density, resulting in changes in mechanical and functional properties (accumulation of plastic deformation, changes in the magnitude of the shape memory effect and martensitic transition temperatures). Changes in the properties of the working body directly affect the functional and force parameters of the device. Therefore, an important property of SMAs is the thermo-mechanical stability of functional properties during thermal cycling.

The most widely used SMAs are based on NiTi (nickel titanium). They demonstrate high values of recoverable strain and developed forces, possess high corrosion resistance and wear resistance [3–6,9,29,30]. For most applications, it is

necessary for the martensitic transformation temperatures of the alloy to be above room temperature. Transformations at such temperatures are observed in NiTi alloys with a chemical composition close to equiatomic. However, equiatomic NiTi alloy demonstrates low thermo-mechanical stability of functional properties [26,31–37]. Numerous data show that during multiple thermal cycles, changes occur in the NiTi-based SMAs' recoverable strain (the shape memory effect values) [26,38–42], generated stresses [3,26,41,43], martensitic transition temperatures [37,44–46], transformation stages [33,41,47], and significant irreversible strain accumulation [26,48–50]. Such changes are undesirable as they lead to changes in the geometric and force characteristics of the device's working body, consequently reducing the drive's operational life. Therefore, an urgent task for the mechanics and physics of functional shape memory materials is the development of effective methods to enhance the thermo-cyclic stability of functional properties of NiTi-based SMA alloys.

Dissertation aims and tasks

It is assumed that the variations in the NiTi alloy properties during thermal cycling are primarily associated with an increase in defect density. Therefore, the main methods to improve the stability of this alloy's properties have been those that allow increasing the dislocation yield strength, which would suppress or significantly slow down the process of defect density increase during thermal cycling. Such methods include various alloy strengthening techniques, such as solid-phase strengthening, dispersion strengthening, pre-straining, and others. However, all these methods directly affect the mechanical properties and thermoelastic transformations. For example, solid-phase strengthening through alloying NiTi alloy changes the temperatures and sequence of transitions, reduces the reversible strain and generated stress values, and decreases strain until failure. This prevents the direct use of commercial NiTi alloys in devices, leading to increased drive costs and limiting their application areas. Another alternative method to improve the stability of NiTi alloy properties during thermal cycling could be the optimization of temperature and stress-strain parameters of the cycle. This would allow controlling the change in defect density and thereby the change in functional properties of the NiTi alloy

during thermal cycling without altering the mechanical properties of the NiTi alloy or martensitic transition parameters. However, this approach to stabilizing the properties of NiTi alloy has not been used before, although simple physical considerations suggest its effectiveness. Optimization of the temperature-force characteristics of the operational cycle would enable the use of commercial NiTi alloys as working elements of drives, significantly reducing their cost and expanding their application areas.

Thus, the aim of this study was to investigate the dependences of strain and generated forces values during thermal cycling of the NiTi alloy within an incomplete range of martensitic transition temperatures at various stresses to develop optimal temperature, and stress-strain parameters for the operational cycle of a NiTi alloy-based drive, demonstrating high stability in parameters during multiple thermal cycles.

To achieve this goal, the following tasks needed to be addressed:

1. Establish the relationship between the variation in defect density and the variation in martensitic transition temperatures during thermal cycling of the NiTi alloy in a stress-free state.
2. Determine the regularities of structural changes in the NiTi alloy during multiple martensitic transformations through direct observations of interphase boundary movements in situ using a transmission electron microscope.
3. Establish the correlation between the variations in defect density and the variations in martensitic transition temperatures, reversible and irreversible strain during thermal cycling under stress.
4. Determine the influence of the fraction of forward and reverse transformations on the change in reversible and irreversible strains, as well as the work output during heating, during thermal cycling of the NiTi alloy under constant stress through a temperature range of incomplete transformations.
5. Investigate the influence of drive parameters (stiffness of the counter-body, method of pre-deformation of the NiTi alloy element, pre-strain value) on the variations in reversible and irreversible strain, forces generated during heating, and work output during heating on thermal cycling of the NiTi alloy in a drive mode.

6. Determine the influence of the fraction of forward and reverse transformations on the variations in reversible and irreversible deformation, forces generated during heating, and work done during heating on thermal cycling of the NiTi alloy in a drive mode with optimal parameters.
7. Develop a methodology for optimizing the temperature-stress-strain parameters of the operational cycle of a NiTi SMA drive during thermal cycling, in which minimal variations in the device's operational characteristics are observed, and validate this methodology on a prototype drive (based on no fewer than 1000 operational cycles).

Scientific novelty

Within the dissertation framework following novel results were achieved:

1. **Impact of Isothermal Holdings**: For the first time, the influence of isothermal holdings on the recovery of temperatures and the sequence of martensitic transformations in NiTi alloy subjected to thermal cycling has been investigated. It has been demonstrated that the effect of temperature and holding duration on the martensitic transition temperatures recovery is determined by recovery processes, which occur more intensively at higher temperatures. It has been shown that holdings in the martensitic state reduces defect density and leads to the recovery of martensitic transition temperatures.
2. **Correlation between Defect Density and Transition Temperatures**: The correlation between the variation in defect density and martensitic transition temperatures has been established for the first time. It has been shown that the transition temperatures dependencies on defect density can be divided into a nonlinear segment at the initial stage of thermal cycling and a subsequent linear segment. It is hypothesized that the nonlinear dependence of martensitic transition temperatures on defect density is due to the fact that, at the initial stage of thermal cycling, transition temperatures are influenced not only by defect density but also by their distribution.

3. **Features of Interphase Boundary Movement**: The peculiarities of interphase boundary movement during martensitic transformation in NiTi alloy after annealing and after pre-deformation in the martensitic phase have been investigated for the first time. It has been shown that in annealed alloy, microstructural memory is not observed, and the sequence of appearance of martensitic crystals during cooling and their disappearance during heating is not opposite. It has been established that the dislocation structure formed as a result of deformation is stable during repeated transformations, hence microstructural memory is observed during martensitic transformations in deformed samples, and the sequence of martensitic crystal disappearance during heating is reverse to their sequence of appearance during cooling.
4. **Influence of Forward and Reverse Transitions**: The influence of the fractions of forward and reverse transitions included in the thermal cycling interval on the change in functional properties of NiTi alloy during thermal cycling under stress or in drive mode has been established for the first time. It has been shown that during thermal cycling of NiTi alloy, irreversible deformation predominantly accumulates in the second half of the forward transition. To suppress irreversible deformation and stabilize properties during thermal cycling under constant stress, it is necessary to exclude the involvement of the second half of the forward transition from the temperature cycle. In the case of drive mode thermal cycling, it is sufficient to exclude the last 10% of the forward transition during cooling from the temperature interval of thermal cycling to reduce irreversible deformation by 5 times.
5. **Effectiveness of Reducing Forward Transition**: It has been established for the first time that reducing the fraction of the forward transition during thermal cycling is more effective for suppressing plastic deformation and improving the stability of functional properties of NiTi alloy than reducing the fraction of the reverse transition. This is due to the fact that defect density intensively increases during the forward transition, and limiting this transition fraction allows slowing down the process of defect accumulation during thermal cycling. During the reverse

transition, dislocation density decreases due to the activation of recovery processes, facilitating the increase in defect density during subsequent cooling.

6. **Nonlinear Relationship between Reactive Stress and Reversible Deformation**: It has been established for the first time that the diagram "reactive stress-reversible deformation" is nonlinear. This is due to the fact that at high counter-body stiffnesses, the reactive stress increases only to the yield stress of the austenitic phase.
7. **Impact of Temperature Positions in the Cycle**: The influence of the positions of maximum and minimum temperatures in the cycle relative to the martensitic transition temperatures on the change in functional properties of NiTi alloy during drive-mode thermal cycling has been established for the first time. It has been shown that to stabilize the properties of the alloy, it is necessary to select the minimum temperature to maximize the exclusion of the second half of the forward transition during cooling, and the maximum temperature of the cycle should be lower than the reverse transformation finish temperature to suppress recovery processes.
8. **Development of Recommendations**: For the first time, recommendations have been developed for selecting optimal temperature, strain and stress conditions for thermal cycling of NiTi alloy, minimizing changes in its properties.
9. **Validation of Recommendations**: The developed recommendations for selecting optimal temperature, deformation, and stress conditions for thermal cycling of NiTi alloy have been validated during the operation of a torsional drive for over 1000 cycles. It has been shown that with the selected optimal cycle parameters, changes in drive characteristics are minimal compared to thermal cycling over the full range of transition temperatures.

Theoretical and practical significance

The theoretical significance of the study lies in the acquisition of new fundamental knowledge about the relationship between defect density, on one hand, and martensitic transition temperatures, reversible and irreversible strain, and reactive stresses values, on

the other hand, during thermal cycling of NiTi alloy in various modes. For the first time, the influence of the fractions of forward and reverse transitions realized in the thermal cycling interval on the variations in functional properties of NiTi alloy operating in drive mode has been established. The obtained results will serve as a basis for developing new models for describing and predicting changes in the properties of shape memory alloys during thermal cycling, taking into account the crucial link between the material's defect structure and its functional properties. Such models can be used to calculate the operational characteristics of drives and devices for multiple cycles.

The practical significance of the research results lies in the development of recommendations for engineers designing drives based on shape memory alloys regarding the selection of force-displacement and temperature operating modes of devices, ensuring minimal changes in the functional properties of NiTi alloy, and consequently, the operational characteristics of devices during thermal cycling.

Methods

The experimental work involved the application of both well-established and proven research methods, such as differential scanning calorimetry, electrical resistivity measurement, transmission electron microscopy, and investigation of strain variations during cooling and heating under constant load. Additionally, specially developed research methodologies were utilized, such as the method for studying strain variation during thermal cycling through different fractions of the temperature interval of forward or reverse martensitic transformation under constant stress or in drive mode. This method involved interrupting the cooling or heating of the sample upon reaching a specified fraction of the temperature range of martensitic transformation. This approach enabled the derivation of dependencies of the values shape memory effects, as well as the values of accumulated plastic deformation during thermal cycling of NiTi alloy, on the fraction of the temperature interval of forward or reverse martensitic transformation.

Within the scope of the study to determine the relationship between defect density and martensitic transformation temperatures, a methodology for determining dislocation density based on variations in resistivity was developed.

The reliability and validation of the results

The results reliability is justified by the application of modern research techniques and equipment, the repeatability of experimental results, and the comparison of the obtained results with those of other foreign and domestic scientific groups.

The results of the study were presented and discussed at various Russian and international conferences:

1. The 9th European Symposium on Martensitic Transformations (ESOMAT), Saint Petersburg, Russia, September 09, 2012 - September 16, 2012.
2. Conference "Shape Memory Alloys: Properties, Technologies, Prospects", Vitebsk, Belarus, May 26, 2014 - May 30, 2014.
3. International Conference on Martensitic Transformations (ICOMAT 2014), Bilbao, Spain, July 06, 2014 - July 11, 2014.
4. 10th European Symposium on Martensitic Transformations (ESOMAT 2015), Antwerp, Belgium, September 14, 2015 - September 11, 2015.
5. XXII St. Petersburg Readings on Strength Problems, Saint Petersburg, Russia, April 12, 2016 - April 14, 2016.
6. Second International Conference "Shape Memory Alloys", Saint Petersburg, Russia, September 19, 2016 - September 23, 2016.
7. CIMTEC 2016 - 7th Forum on New Materials, Perugia, Italy, June 05, 2016 - June 09, 2016.
8. ISPMA 14 - 14th INTERNATIONAL SYMPOSIUM ON PHYSICS OF MATERIALS, Prague, Czech Republic, September 10, 2017 - September 15, 2017.
9. LVIII International Conference "Current Problems of Strength", Perm, Russia, May 16, 2017 - May 19, 2017.
10. 11th European Symposium on Martensitic Transformations (ESOMAT 2018), Metz, France, August 26, 2018 - September 02, 2018.
11. Third International Scientific Conference "Shape Memory Alloys", Chelyabinsk, Russia, August 16, 2018 - August 20, 2018.

12. International Scientific Conference "Current Problems of Strength", Vitebsk, Belarus, May 14, 2018 - May 18, 2018.
13. International Scientific Conference "Current Problems of Strength", Brest, Belarus, May 27, 2018 - May 31, 2018.
14. "Bernstein Readings 2019", Moscow, Russia, October 22, 2019 - October 25, 2019.
15. Fourth International Conference "Shape Memory Alloys", Moscow, Russian Federation, September 13, 2021 - September 17, 2021.
16. LXV International Scientific Conference "Current Problems of Strength" (2022-CPP), Vitebsk, Belarus, May 23, 2022 - May 27, 2022.
17. 12th European Symposium on Martensitic Transformations "ESOMAT 2022", Ankara, Turkey, September 04, 2022 - September 10, 2022.
18. 14th Scientific and Technical Seminar "Bernstein Readings on Thermo-Mechanical Treatment of Metallic Materials", Moscow, Russian Federation, October 24, 2022 - October 27, 2022.
19. International Symposium "Perspective Materials and Technologies", Minsk, Belarus, August 21, 2023 - August 25, 2023.
20. V International Conference "Shape Memory Alloys", Saint Petersburg, Russian Federation, September 27, 2023 - October 01, 2023.
21. Third China-Russia Scientific and Technical Forum, Harbin, China, October 22, 2023 - October 26, 2023.
22. XXIV St. Petersburg Readings on Strength Problems and III Youth School-Seminar "Mechanics, Chemistry, and New Materials", Saint Petersburg, Russia, April 23, 2024 - April 25, 2024.

Publications

The main results on the dissertation topic are presented in 33 papers, out of which 17 are published in journals recommended by Higher Attestation Commission or cited by WoS, and Scopus (7 articles are published in Q1 journals according to SJR). In total, the author has published 61 papers, including 28 papers in refereed international and domestic journals indexed by Scopus, Web of Science, and RSCI.

Works cited by Scopus, Web of Science, and RSCI

1. Sibirev A., Belyaev S., Resnina N. Improvement of the NiTi actuator performance stability by decreasing its operating temperature range // Sensors and Actuators A: Physical. 2023. No. 114743 (363). (Q1)

2. Sibirev A. V., Belyaev S. P., Resnina N. N. Influence of temperature range on NiTi SMA actuator performance during thermal cycling // Letters on Materials. 2023. No. 3 (13). Pp. 249–254.

3. Resnina N., Sibirev, A., Belyaev S., Ubyivovk, E., In situ TEM observation of the martensite interface movement on heating – cooling – heating of the pre-deformed NiTi shape memory alloy // Materials Letters. 2023. No. 134641 (347).

4. Sibirev, A., Ubyivovk, E., Belyaev, S., Resnina, N. In situ transmission electron microscopy study of martensite boundaries movement on cooling and heating of the NiTi shape memory alloy // Materials Letters. 2022. No. 132267 (319).

5. Sibirev A. V., Belyaev S. P., Resnina N. N. Influence of preliminary straining on the recovery stress in TiNi shape memory alloy working element // Letters on Materials. 2021. No. 2 (11). Pp. 209–212.

6. Sibirev A., Belyaev S., Resnina N. The influence of counter-body stiffness on working parameters of NiTi actuator // Sensors and Actuators A: Physical. 2021. No. 112568 (319). (Q1)

7. Sibirev, A., Belyaev, S., Resnina, N., Timashov, R., Averkin, A., Nikolaev, V. Shape Memory Effects and Work Output of [001] Ni55Fe18Ga27 Single Crystals in Torsion Mode // Journal of Materials Engineering and Performance. 2020. No. 4 (29). Pp. 2185–2189.

8. Belyaev, S., Resnina, N., Nikolaev, V., Timashov, R., Saveleva, A., Gazizullina, A., Krymov, V., Sibirev, A. Influence of Detwinning on the Shape Memory Effect in Ni55Fe18Ga27 Single Crystals // Journal of Materials Engineering and Performance. 2019. No. 7 (28). Pp. 4234–4240.

9. Sibirev A., Belyaev S., Resnina N. Influence of holding between the thermal cycles on recovery in martensitic transformation temperatures in TiNi alloy // Letters on Materials. 2019. No. 1 (9). Pp. 103–106.

10. Sibirev A., Resnina N., Belyaev S. Relationship between the variation in transformation temperatures, resistivity and dislocation density during thermal cycling of Ni50Ti50 shape memory alloy // International Journal of Materials Research. 2019. No. 5 (110). Pp. 387–392.

11. Sibirev A., Belyaev S., Resnina N. Variation in TiNi Alloy Properties on Room Temperature Holding // Acta Physica Polonica A. 2018. No. 3 (134). Pp. 671–674.

12. Belyaev, S., Resnina, N., Nikolaev, V., Timashov, R., Gazizullina, A., Sibirev, A., Averkin, A. Krymov, V. Shape memory effects in [001] Ni 55 Fe 18 Ga 27 single crystal // Smart Materials and Structures. 2017. No. 095003 (26). (Q1)

13. Sibirev A., Belyaev S., Resnina N. Softening process during reverse martensitic transformation in TiNi shape memory alloy // Journal of Alloys and Compounds. 2016. (661). Pp. 155–160. (Q1)

14. Belyaev S., Resnina N., Sibirev A. Accumulation of Residual Strain in TiNi Alloy During Thermal Cycling // Journal of Materials Engineering and Performance. 2014. No. 7 (23). Pp. 2339–2342.

15. Belyaev, S., Resnina, N., Sibirev, A., Lomakin, I. Variation in kinetics of martensitic transformation during partial thermal cycling of the TiNi alloy // Thermochimica Acta. 2014. (582). Pp. 46–52., 2014 (Q1)

16. Sibirev A., Belyaev S., Resnina N. Unusual Multistage Martensitic Transformation in TiNi Shape Memory Alloy after Thermal Cycling // Materials Science Forum. 2013. No. 0 (738–739). Pp. 372–376.

17. Belyaev S., Resnina N., Sibirev A. Peculiarities of residual strain accumulation during thermal cycling of TiNi alloy // Journal of Alloys and Compounds. 2012. (542). Pp. 37–42. (Q1)

Other publications in RSCI (not included in the RSCI core):

18. Resnina, N., Sibirev, A., Belyaev, S. & Gracheva, A. The effect of isothermal holding on reversible and irreversible strain in TiNi shape memory alloy // Materials Today: Proceedings. 2017. No. 3 (4). Pp. 4748–4752.

19. Sibirev A.V., Belyaev S.P., Resnina N.N. Multicycle functional fatigue of NiTi used as the working body of a torsional drive / Proceedings of the conference "XXIV Petersburg Readings on Strength Problems and III Youth School-Seminar 'Mechanics, Chemistry, and New Materials' 2024. (In Russian)

20. Sibirev A.V., Belyaev S.P., Resnina N.N. Thermocycling in an incomplete transformation temperature interval as a way to improve the stability of drives based on SMAs. / Shape Memory Alloys (SMA-2023). Materials of the V International Conference. St. Petersburg, 2023. P. 60. (In Russian)

21. Sibirev A.V., Belyaev S.P., Resnina N.N. Features of the operation of a drive based on SMAs TiNi during thermocycling in an incomplete temperature interval of martensitic transformations. / Actual Problems of Strength. Materials of the International Scientific Conference. Minsk, 2022. P. 17. (In Russian)

22. Resnina N.N., Sibirev A.V., Belyaev S.P., Ubyivovk E.V. Direct observation of martensitic transformation in TiNi alloy. / Bernstein Readings on Thermo-Mechanical Processing of Metallic Materials: Collection of Abstracts. Scientific and Technical Seminar. Moscow, 2022. (In Russian)

23. Sibirev A.V., Belyaev S.P., Resnina N.N. Influence of the temperature interval of thermocycling on the parameters of the torsional drive based on SEPF TiNi. / Bernstein Readings on Thermo-Mechanical Processing of Metallic Materials: Collection of Abstracts. Scientific and Technical Seminar. Moscow, 2022. P. 47. (In Russian)

24. Sibirev A.V., Belyaev S.P., Resnina N.N. Influence of the stiffness of the counterbody on the characteristics of the drive with a working body made of TiNi shape memory alloy. / Shape Memory Alloys: Collection of Abstracts of the Fourth International Conference. Moscow, 2021. P. 73. (In Russian)

25. Sibirev A.V., Belyaev S.P., Resnina N.N. Influence of the stiffness of the counterbody on the functional properties of the drive with a working body made of TiNi shape memory alloy. / Phase Transformations and Strength of Crystals: Collection of Abstracts of the XI International Conference. 2020. P. 153. (In Russian)

26. Sibirev A.V., Belyaev S.P., Resnina N.N. Influence of the stiffness of the counterbody on the functional properties of the shape memory drive. / Actual Problems

of Strength. Materials of the International Scientific Conference. Edited by V.V. Rubanik. 2020. P. 90-91. (In Russian)

27. Sibirev A.V., Belyaev S.P., Resnina N.N. Recovery of properties in thermocycled TiNi alloy during isothermal holds. / XXIII Petersburg Readings on Strength Problems, dedicated to the 100th anniversary of the Ioffe Institute and the 110th anniversary of the birth of corresponding member of the USSR Academy of Sciences A.V. Stepanov. Collection of Materials. 2018. P. 144. (In Russian)

28. Sibirev A.V., Belyaev S.P., Resnina N.N., Nikolaev V.I., Timashov R.B., Krymov V.M. NiFeGa alloy as a working body material for converting thermal energy into work. / 60th International Scientific Conference "Current Problems of Strength". 2018. P. 357. (In Russian)

29. Belyaev S.P., Nikolaev V.I., Resnina N.N., Timashov R.B., Sibirev A.V., Averkin A.I., Gazizullina A.R. Features of plasticity transformation and shape memory effects in [001] single crystals of Ni-Fe-Ga alloy. / Promising Materials and Technologies. Materials of the International Symposium. In 2 parts. Edited by V.V. Rubanik. 2017. P. 137-139. (In Russian)

30. Sibirev A.V., Resnina N.N., Belyaev S.P. Generation of reactive stresses and shape memory effects during thermocycling of TiNi alloy in torsional mode. / Bernstein Readings on Thermo-Mechanical Processing of Metallic Materials. Scientific and Technical Seminar dedicated to the 100th anniversary of Professor M.L. Bernstein. 2019. P. 94. (In Russian)

31. Resnina N.N., Belyaev S.P., Sibirev A.V., Grachyova A.G. Influence of isothermal holding on irreversible deformation of TiNi alloy. / XXII Petersburg Readings on Strength Problems. To the 110th anniversary of the birth of academician S.N. Zhurkov and the 85th anniversary of the birth of professor V.A. Likhachev: collection of materials. St. Petersburg: Publishing House of the St. Petersburg State Polytechnic University, 2016. P. 104-106. (In Russian)

32. Sibirev A.V., Belyaev S.P., Resnina N.N. Influence of the maximum temperature of the thermocycle on martensitic transformations in TiNi alloy. / XXII Petersburg Readings on Strength Problems. To the 110th anniversary of the birth of

academician S.N. Zhurkov and the 85th anniversary of the birth of professor V.A. Likhachev: collection of materials. St. Petersburg: Publishing House of the St. Petersburg State Polytechnic University, 2016. P. 345-347. (In Russian)

33. Resnina N.N., Belyaev S.P., Sibirev A.V. Processes responsible for changing the functional properties of TiNi alloy during thermocycling. / Perspective Materials and Technologies. International Symposium dedicated to the 40th anniversary of the Institute of Technology of the National Academy of Sciences of Belarus. Vitebsk, 2015. P. 40-43. (In Russian)

Author's personal contribution

In papers 1-7, 9-11, 13, 14, 16-28, 30, 32-33, the candidate conducted experimental work, performed data processing and analysis, and prepared publications. Belyaev S.P. and Resnina N.N. participated in defining the research tasks and discussing the obtained data. In papers 8, 12, 15, 29, 31, the candidate conducted some experiments and contributed to the discussion of results and preparation of publications.

Dissertation structure

The dissertation consists of an introduction, 3 chapters, conclusions, 86 figures, 5 tables, and a bibliography containing 160 references. The volume of the dissertation is 181 pages.

The first chapter is dedicated to the study of property changes in NiTi and NiFeGa shape memory alloys (SMAs) during thermal cycling through the martensitic transformation temperature interval under various conditions. It discusses the influence of isothermal holds on property changes in NiTi SMAs subjected to multiple thermal cycles through the martensitic transformation temperature interval in free state or under constant stress, as well as the peculiarities of martensite crystal nucleation and disappearance during the cooling and heating of NiTi alloy, and the relationship between dislocation density and martensitic transformation temperatures in NiTi SMAs.

The second chapter focuses on the study of property changes in NiTi SMAs during thermal cycling through the temperature interval of incomplete martensitic transformations in the free state and under constant stress.

The third chapter addresses the influence of various factors such as the actuation method of the drive, stiffness of the elastic counterbody, pre-straining of the austenitic phase, achievable level of functionality, and relative position of the temperature cycling interval on property changes in NiTi SMAs when applied as the working element of torsional drives.

Main scientific results

• It has been established that holding the pre-thermocycled NiTi alloy (in free state or under constant stress) at various temperatures (both in martensitic and austenitic states), as well as increasing the maximum temperature in the cycle, lead to an increase in the martensitic transition temperatures and affect reversible and irreversible strain values. This is due to the recovery processes, which result in changes in the density and distribution of defects. Published in articles [51–54] and conference materials No. 27, 31, 32 (Personal contribution not less than 80%).

• A nonlinear relationship between defect density and martensitic transformation temperatures in NiTi alloy during multiple thermal cycles has been established. Published in article [55] (Personal contribution not less than 80%).

• It has been established that in annealed NiTi alloy, the sequence of disappearance of martensite crystals upon heating does not correspond to the sequence of their appearance upon previous cooling. It has been shown that there is no microstructural memory in annealed NiTi alloy, i.e., the sequence of martensite crystal appearance during cooling in different cycles is not repeated. It is assumed that this is due to changes in the defect structure and distribution of internal stresses during thermal cycling. Published in articles [56,57] and conference materials No. 22 (Personal contribution not less than 80%).

• The influence of the forward and reverse martensitic transformation fractions included in the temperature cycling interval on the variations in the alloy properties during cycling under constant stress or in drive mode has been established. It has been shown

that reducing the fraction of forward transformation reduces the accumulation of irreversible deformation and stabilizes the functional properties of NiTi alloy during cycling. Published in articles [58–61] and conference materials No. 33 (Personal contribution not less than 80%).

• A nonlinear relationship between the maximum reactive stress and the recovered strain values during heating of NiTi alloy in drive mode has been established. It has been shown that at high counterbody stiffness, the increase in reactive stress ceases once its values reaches the yield stress of the austenitic phase. This leads to a non-monotonic dependence of the work output by the alloy during heating on the stiffness of the counterbody. The maximum work performed is observed at a stiffness of 6-10 GPa. It has been established that the pre-deformation method of the NiTi alloy element does not affect the variations in functional properties during cycling. Published in articles [62,63] and conference materials No. 24-26, 30 (Personal contribution not less than 80%).

• The influence of the positions of the minimum and maximum cycle temperatures relative to the martensitic transition temperatures on the variations in functional properties and accumulation of irreversible deformation during cycling of NiTi alloy in drive mode has been established. The optimal position of the cycle temperatures has been determined, at which the work output by the alloy during heating is maximum, while the accumulated plastic strain and property changes during cycling are minimal. Published in articles [64,65] and conference materials No. 19-21, 23 (Personal contribution not less than 80%).

• It has been shown that despite the good stability of functional properties during thermal cycling, single crystals of NiFeGa alloy demonstrate useful work 10 times less than NiTi-based alloys, making their use as the working element of power drives inefficient. Published in articles [66–68] and conference materials No. 28, 29 (Personal contribution not less than 80%).

Thesis statements for dissertation defense

1. The principle of optimizing temperature cycling conditions for elements made of NiTi-based alloys to enhance the stability of martensitic transformation temperatures and

functional properties, which stipulates that the maximum and minimum cycle temperatures should fall within the ranges of reverse and forward transformations.

2. Dependences of reversible strain and irreversible strain values on cycle number during cycling within incomplete ranges of martensitic transformations, indicating that the stability of stress-strain characteristics of the drive improves with decreasing fractions of forward and reverse transformations.

3. The non-monotonic dependence of work output during heating on the stiffness of the counter body, exhibiting a maximum at a stiffness of 6-10 GPa, resulting from the nonlinear relationship between generated stresses and reversible deformation on one hand, and resistance stiffness on the other.

4. Variations in martensitic transformation temperatures during cycling are determined not only by an increase in the defects density in the crystal structure, determined by resistivity, but also by the stress acting in the cycle.

5. Direct observations using an electron microscope revealed a disruption in the sequence of martensite crystal formation and disappearance during cycling, and the absence of microstructural memory in the NiTi alloy.

6. The phenomenon of martensitic transformation temperature recovery during isothermal holding after cycling.

Financial support

The dissertation work was carried out with the support of 5 grants under the personal supervision of the author, including 2 grants from the Russian Science Foundation (19-79-00106, 22-29-20021), 2 grants from the Russian Foundation for Basic Research (16-31-60043, 14-08-31085), and 1 grant from the President of the Russian Federation for young candidates of sciences (MK-1261.2017.8). Some of the results were obtained with the support of grants from the Russian Foundation for Basic Research (16-08-00346) and the Ministry of Science and Higher Education of the Russian Federation (megagrant No. 075-15-2022-1114).

The acknowledgments

The author of the dissertation expresses deepest gratitude to Dr. Sc. (N.N. Resnina and Dr. Sc. S.P. Belyaev for their direct involvement in formulating the tasks of all the research and discussing their results. The author also extends thanks to all co-authors who participated in conducting the research and preparing the publications. The TEM studies were conducted using the equipment of the Interdisciplinary Resource Center of St. Petersburg State University in the field of "Nanotechnologies". X-ray structural studies were carried out using the equipment of the resource center "X-ray Diffraction Research Methods" at St. Petersburg State University.

Chapter 1. Relationship between defect density and functional properties of NiTi alloy during thermal cycling

1.1. Relationship between variation in defect density and parameters of martensitic transitions during thermal cycling without external load

References [69, 70] were among the first to note that martensitic transformations (MT) in shape memory alloys are accompanied by irreversible processes related to plastic relaxation of internal local stresses arising during transformation. In [71], it is suggested that an increase in defect density, which serves as a source of internal stresses, leads to variation in the kinetics of MT in the alloy, shifts in transformation temperatures, and changes in transformation staginess [3, 26, 48, 72–78]. The increase in defect density during direct transformation is associated with stress accommodation caused by the incompatibility of the austenitic and martensitic phase crystal lattices [35, 79, 80].

Changes in the martensitic transformations' kinetics (values of MT temperatures, transformation staginess, transformation type) depend on the alloy composition and type of martensitic transition. For example, in the Cu-Zn-Al system, the M_s temperature (start temperature of forward transformation) decreases if the DO3→18R transition occurs during thermal cycling and increases if the B2→9R transition takes place [81–83]. In Ti-Ni-Cu [76], Ti-Ni-Hf [84], and Ti-Ni-Cu-Hf [85] alloys, MT temperatures decrease with an increase in the number of thermal cycles, as in the binary NiTi alloy. In the Ni-Mn-Ga alloy system, MT temperatures depend non-monotonically on the number of thermal cycles: at the beginning of thermal cycling, MT temperatures decrease, but after the hundredth cycle, MT temperatures increase [86].

Among the wide class of shape memory alloys, NiTi-based alloys are most widely demanded by industry due to their good combination of functional and operational properties. In the high-temperature (austenitic) state, the NiTi alloy exists in a cubic B2 phase, ordered according to the CsCl type [3]. Upon cooling, the martensitic monoclinic B19′ phase is formed directly from the B2 phase or through the formation of an

intermediate R-phase [3, 37, 41, 45, 87, 88]. The martensitic R-phase has a rhombohedral structure [89]. The transformation from B2 to B19′ is accompanied by significant lattice deformation incompatibility [3], leading to the emergence of high local stresses at the phase boundary. Relaxation of these stresses leads to the accumulation of plastic deformation and irreversible changes in the martensitic transformations' kinetics in each thermal cycle.

One of the early studies dedicated to examining the influence of multiple thermal cycles on the kinetics of martensitic transformations in NiTi alloys with varying nickel concentrations from 49.8 to 51.6 at.%, was the work [37]. It was shown that with an increase in the number of cycles, the temperature range of transformations shifts towards lower temperatures. The authors of this study hypothesized that the main cause of this behavior was microplastic deformation occurring during transformation, due to the large stresses created by growing martensite crystals. Microplastic deformation, in turn, leads to an increase in dislocation density, resulting in a decrease in transformation temperatures. Additionally, not only do transformation temperatures decrease, but their sequence can also change. For instance, in annealed Ni50Ti50 alloy, cooling leads to a B2→B19′ transformation. After a certain number of thermal cycles, a multi-stage B2→R→B19′ transformation is observed during cooling [45, 47, 48, 90]. This is because during thermal cycling, the defect density increases non-uniformly, leading to the formation of heterogeneous fields of internal stresses. In regions with high internal stresses, the transformation from the B2 phase to the B19′ phase occurs with the formation of the R-phase during cooling, thus altering the sequence of transformations.

Therefore, existing understandings of the variations in NiTi alloy properties during thermal cycling are solely attributed to changes in defect density. However, there are only a few studies that directly examined dislocation densities in NiTi alloy before and after thermal cycling using direct methods [37, 48, 91]. These studies revealed that the dislocation density in NiTi alloy increases. Nevertheless, the investigations were not conducted on a single sample subjected to thermal cycling and examined for defect density before and after cycling, but on several samples subjected to different numbers of thermal cycles. Moreover, it is known that the dislocation density changes non-uniformly,

and the fact that changes in dislocation density were detected in some very small areas of the sample does not allow us to definitively correlate the changes in martensitic transition parameters with an increase in defect density. Without understanding the relationships between defect density changes and changes in martensitic transition parameters, it is impossible to develop methods to improve the stability of alloy functional properties during thermal cycling. Therefore, one of the important tasks of this dissertation was to establish the relationship between changes in defect density and changes in martensitic transition temperatures during thermal cycling of NiTi alloy in the free state (without stress) and direct observations (in situ) of interphase boundary movement during direct martensitic transitions in NiTi alloy in an electron microscope column. The results of these studies are presented in section 1.1 and published in works [52–57].

1.1.1. The Influence of Isothermal Holdings Between Thermal Cycles on the Recovery of Martensitic Transformation Temperatures in NiTi Alloy

If the variation in functional properties of the NiTi alloy during thermal cycling is due to variations in defect density, then it can be assumed that reducing the defect density will lead to the recovery of the martensitic transformations' kinetics (temperatures and sequence of martensitic transformations). Defect density reduction in the thermally cycled alloy can be achieved through isothermal holdings at temperatures above 100°C, where dislocation structure annihilation and redistribution will occur [92]. Obviously, the higher the holding temperature, the more intensively the defect density decreases, which should affect the MT parameters. To investigate this issue, the influence of holding temperature on the change in temperatures and sequence of martensitic transformations in NiTi alloy subjected to preliminary thermal cycling was studied.

The research was conducted on wire samples of $Ni_{50}Ti_{50}$ alloy (d = 0.5 mm), water-quenched from 700°C, and annealed at 500°C for two hours. After annealing, the alloy underwent the B2→B19′ martensitic transformation upon cooling (M_s = 64°C and M_f = 48°C) and the B19′→B2 transformation upon heating (A_s = 84°C and A_f = 98°C). The samples underwent twenty thermal cycles in the temperature range of 200°C to 0°C with a cooling/heating rate of 7°C/min. After preliminary thermal cycling, the samples were held at a constant temperature from 100°C to 300°C for 60 minutes and subjected to one thermal cycle to compare the MT temperatures before and after holding. During thermal cycling and after holding, electrical resistivity was measured (using the four-probe method), from which the temperatures and type of martensitic transformation were determined, and the defect density variation during holding was assessed.

Figure 1 shows the dependencies of electrical resistivity on temperature obtained in the NiTi alloy in the first and twentieth thermal cycles in the temperature range of 200÷0°C. It can be seen that in the first thermal cycle, an anomalous decrease in electrical resistivity is observed during cooling on curve ρ(T), and during heating, an anomalous increase in resistivity is observed, associated with the B2↔B19′ martensitic transformation [33, 90, 93, 94]. In the twentieth thermal cycle, a peak is observed on

curve ρ(T) during cooling, indicating a change in the transformation sequence from B2→B19′ (in the first cycle) to B2→R→B19′ (in the twentieth cycle), which is in good agreement with the data [47, 57]. The R-phase has a higher electrical resistivity compared to the B2 and B19′ phases, so during the B2→R transformation, electrical resistivity sharply increases, while the R→B19′ transformation leads to a sharp decrease in resistivity [37, 93, 95, 96]. The characteristic transformation temperatures were determined from the ρ(T) curves as points of intersection of tangent lines (Figure 1), where T_{B2-R} is the start temperature of the B2→R transformation, M_f is the finish temperature of the direct martensitic transformation, and A_s, A_f are the start and finish temperatures of the reverse martensitic transformation (in the twentieth thermal cycle: T_{B2-R} = 58°C, M_f = 34°C, A_s = 76°C, A_f = 84°C). Over twenty thermal cycles, transformation temperatures decreased, and electrical resistivity increased (the ρ(T) curve shifted towards higher electrical resistivity values). It is assumed that both phenomena are caused by an increase in defect density [34, 37, 46, 47].

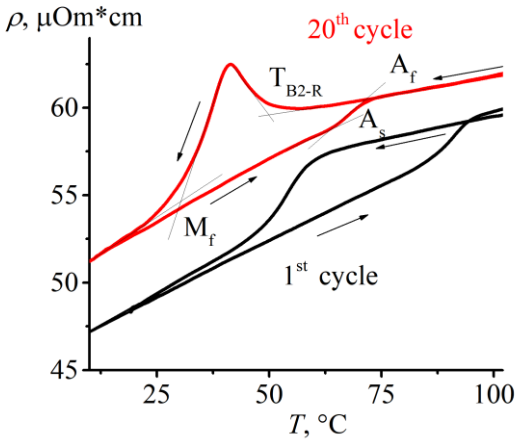

Figure 1 Dependencies of the resistivity on temperature obtained in the NiTi alloy during the first and twentieth thermal cycles in the temperature range from 200°C to 0°C.

In Figure 2a, the dependencies of resistivity on temperature obtained in the twentieth thermal cycle and after isothermal holding at a temperature of 300°C for 60 minutes are shown. It can be observed that the holding leads to a decrease in the resistivity of the alloy, a shift of anomalies on the resistivity curve to higher temperatures, and a

reduction in the peak caused by the formation of the R-phase. Figure 2b illustrates the variation in

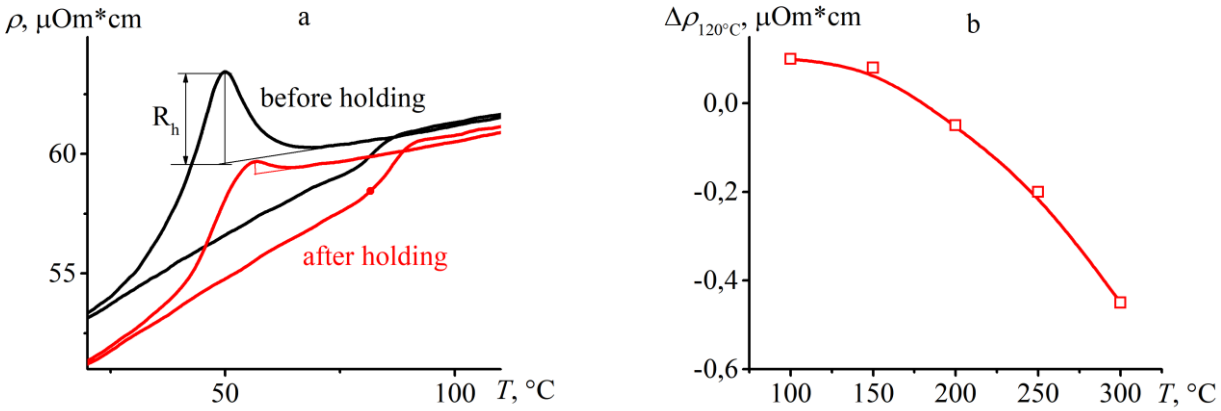

Figure 2. The dependencies of the resistivity on temperature obtained in the NiTi alloy after the twentieth thermal cycle and after a hold at 300°C for 60 minutes (a), and the variations in electrical resistivity in the austenitic state after holds at 120°C (b).

the resistivity measured in the austenitic state after holding at a temperature of 120°C decreased. If the holding temperature exceeded 200°C, the resistivity decreased after the holds, while if the holding temperature was below 200°C, the resistivity increased, similar to the behavior observed during thermal cycling without intermediate holds. The higher the holding temperature, the greater the reduction in resistivity. For instance, after one-hour holding at 200°C, the resistivity changed by -0.05 μΩcm, whereas after holding at 300°C, the change was -0.45 μΩcm.

On Figure 3, the variations in temperatures $T_{B2\text{-}R}$, M_f, A_s, A_f measured in the thermal cycle after isothermal holding at various temperatures for 1 hour are shown compared to the temperatures in the 20th thermal cycle. It can be observed that after holding at temperatures below 200°C (the maximum temperature reached in the 20th thermal cycle), transformation temperatures decreased. This indicates that holding at 100°C and 150°C has no effect on the subsequent cycle's transition temperature variations. The temperatures continued to decrease, similar to before the holding. If the holding temperature exceeded 200°C, then the transformation temperatures increased compared to those in the 20th cycle.

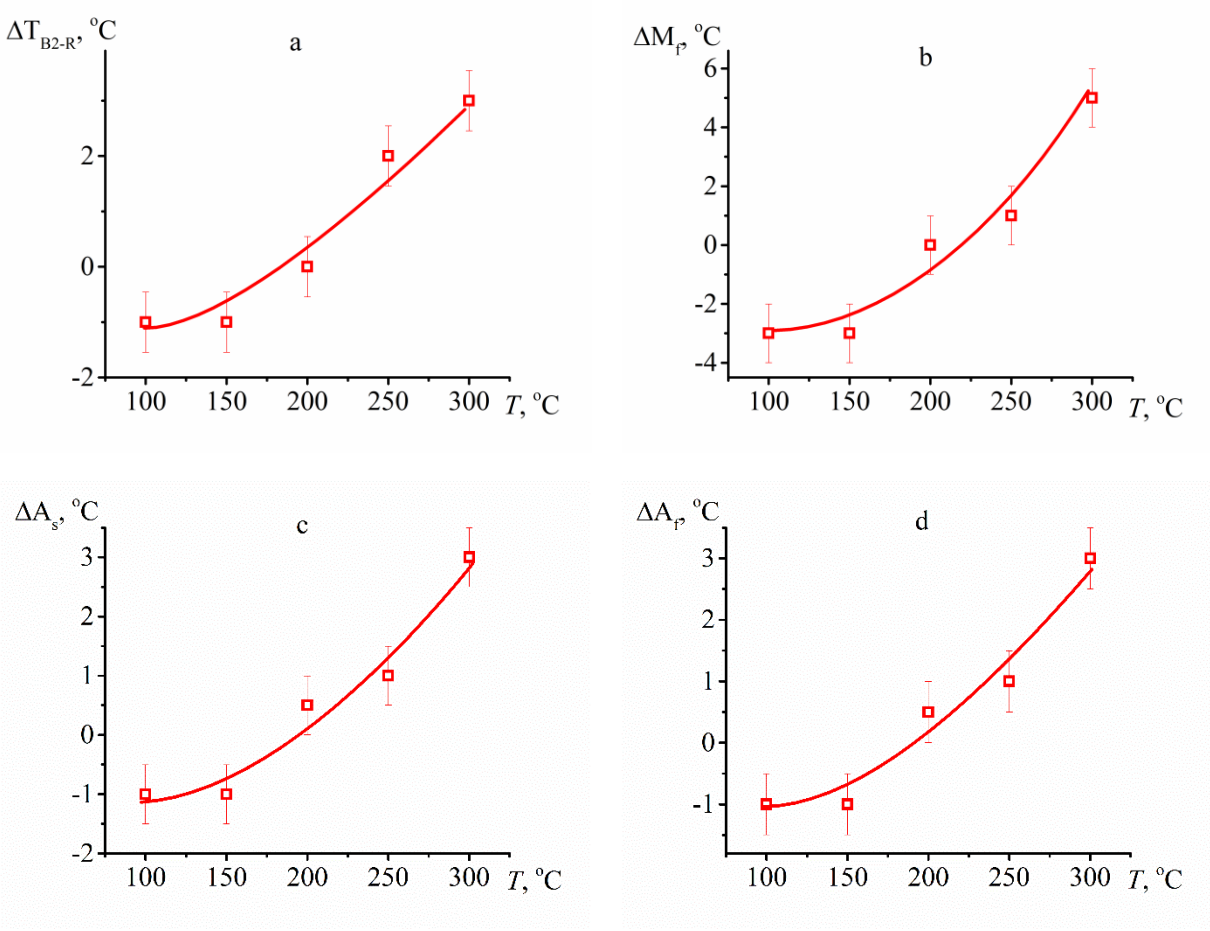

Figure 3. Variations in transformation temperatures T_{B2-R} (a), M_f (b), A_s (c), A_f (d) after a 1-hour hold compared to temperatures in the 20th cycle, at various hold temperatures.

In equiatomic NiTi alloy, the R-phase forms during cooling under conditions of existence of areas of the alloy with high internal stresses, which are created by defects arising during thermal cycling. Thus, it can be assumed that the volume fraction of the alloy undergoing B2→R transformation correlates with the defect density on one side and with the peak height on the ρ(T) curve on the other side. The change in peak height was calculated as $\Delta R_h = (R_{h1} - R_{h0})/R_{h0} \times 100\%$, where R_{h1} is the peak height measured on the ρ(T) curve immediately after holding, and R_{h0} is the peak height measured in the 20th thermal cycle (before holding). The dependence of ΔR_h on the holding temperature is shown in Figure 4b. It can be seen that the peak height of the resistivity curve remains unchanged if the holding temperature is below 200°C, and it decreases if the holding occurs at temperatures above 200°C. Thus, the data on the variation in peak height on the ρ(T) curve indirectly confirm the fact that holding at temperatures above 200°C reduces the defect density and restores the parameters of the martensitic transition.

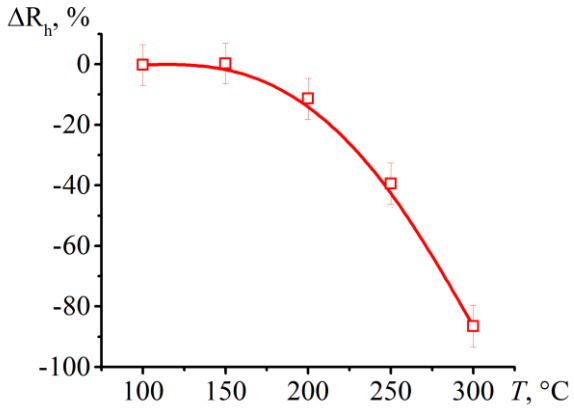

Figure 4. Variations in the peak height on the resistivity-temperature (ρ(T)) curve due to the B2→R transformation, depending on the temperature of the 1-hour holding.

Thus, the research results indicate that post-cycling holding of the sample at temperatures exceeding the maximum temperature in the cycle leads to an increase in transformation temperatures, a decrease in the absolute value of resistivity, and a reduction in the peak height on the ρ(T) curve. If the holding temperature was lower than the maximum temperature during preliminary cycling, no variations in properties were observed. Since defects appear during preliminary cycling in the temperature range from 200 to 0°C, it is logical to assume that they are characterized by a stable configuration and distribution that does not change upon heating to 200°C. In this case, holding at temperatures below 200°C does not affect the defect density and their distribution, and therefore, the alloy properties remain unchanged. If the holding temperature exceeds 200°C, the defects become unstable, their density decreases, as evidenced by the decrease in the overall resistivity level, and their distribution changes, which partially restores the alloy properties. The higher the holding temperature, the more intense the recovery processes, the greater the decrease in defect density, and the more intensive the restoration of alloy properties. Thus, the study results demonstrated a direct correlation between defect density and martensitic transition temperatures. Moreover, it was established that the properties of NiTi alloy can be restored by holding at temperatures above the maximum temperature in the cycle, which can be applied to already operating devices.

Recovery processes in metals are thermoactivated, and their intensity depends on the holding temperature. The lower the holding temperature, the lower the intensity of

recovery processes, but this does not mean their complete cessation. Holding at low temperatures for one hour does not result in the restoration of martensitic transformation temperatures. However, it is possible that longer holding durations may influence the defect distribution and, consequently, the kinetics of martensitic transformations in the NiTi alloy.

To test this hypothesis, we conducted a study on the effect of holdings at room temperature on the kinetics of martensitic transformations in the same NiTi alloy previously examined at high holding temperatures. Samples underwent thermal cycling in the temperature range from 140°C to 0°C at a cooling/heating rate of 7°C/min. After the 5th, 10th, and 15th thermal cycles, the samples were held at room temperature. The duration of holding was 15 hours after the 5th and 15th cycles and 85 hours after the 10th cycle. The dependencies of martensitic transformation temperatures on the cycle number are shown in Figure 5. It can be observed that all transformation temperatures decrease

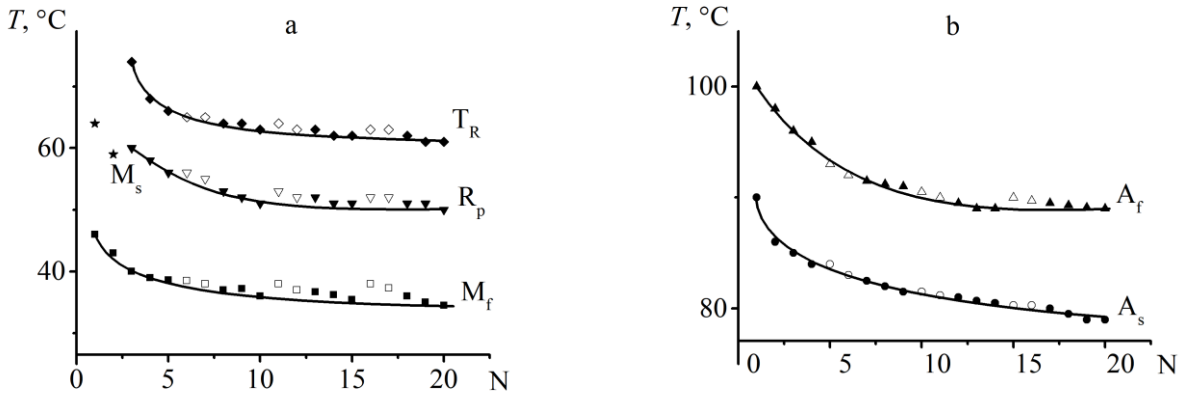

Figure 5. Dependencies of direct (a) and reverse (b) martensitic transformation temperatures on the number of thermal cycles obtained during thermal cycling of the NiTi alloy.

during thermal cycling. Holding after the 5th cycle did not have a noticeable effect on the change in transformation temperatures. Holding after the 10th and 15th cycles led to an increase in transformation temperatures measured in the cycles following the holding (highlighted by open symbols in Figure 5). Subsequent thermal cycling of the samples after holding resulted in a decrease in transformation temperatures to "normal" values

(within 2-3 cycles) that would be expected in the alloy if no holding had been performed (indicated by the solid line).

Deviations of transformation temperatures T_R, M_f, A_s, measured immediately after annealing, from the normal values of martensitic transformation temperatures (lines), are presented in Table 1.

Table 1. Changes in transformation temperatures and resistivity during holdings at room temperature of NiTi alloy subjected to thermal cycling in the range of 140÷0°C. N - number of cycles before holding; t - duration of holding.

N	*t*, h	ΔT_R, °C	ΔM_f, °C	$\Delta\rho_{20}$, %	ΔA_s, °C	ΔA_f, °C	$\Delta\rho_{120}$, %
5	15	0	0	-0,12	0	-0.5	0
10	85	1,5	2,5	-0,34	0	0	-0,12
15	15	1,5	3	-0,41	0.5	1.5	-0,28

It can be observed that the variation in transformation temperatures for direct transformation is greater than for reverse transformation. It was found that the variation in transformation temperatures was maximal during holding after the 15th cycle, despite the fact that the holding after the 10th cycle was 5.5 times longer in duration than after the 15th cycle. Thus, increasing the holding time from 15 to 85 hours does not affect the variation in transformation temperatures, emphasizing the importance of the initial defect density before holding.

To assess the variation in defect density during thermal cycling, the variation in resistivity at constant temperatures of 20°C (martensite) and 120°C (austenite) was measured. The resistance dependence on the cycle number is shown in Figure 6. Holding the sample at room temperature leads to a decrease in electrical resistivity in the subsequent cycle (open symbols in Figure 2). The reduction in resistivity after holding is presented in Table 1. It was found that the higher the number of cycles preceding holding, the greater the reduction in resistivity after holding. For instance, the variation in resistivity ($\Delta\rho20$) is -0.34% when holding at room temperature occurs after the tenth cycle, and -0.41% after the fifteenth cycle, despite the longer holding duration of 85 hours after the tenth cycle compared to only 15 hours after the fifteenth cycle. Thus, the

presented data demonstrate that holding at room temperature of NiTi alloy, which has undergone prior thermal cycling, leads to an increase in martensitic transformation temperatures and a decrease in resistivity, consistent with previous findings [97], where authors observed the recovery of transformation temperatures in NiTi alloy after holding at room temperature for two days. It is established that the initial defect density, rather than the duration of holding, is important. The higher the defect density, the more unstable the state of the alloy, leading to more intensive recovery processes during holding.

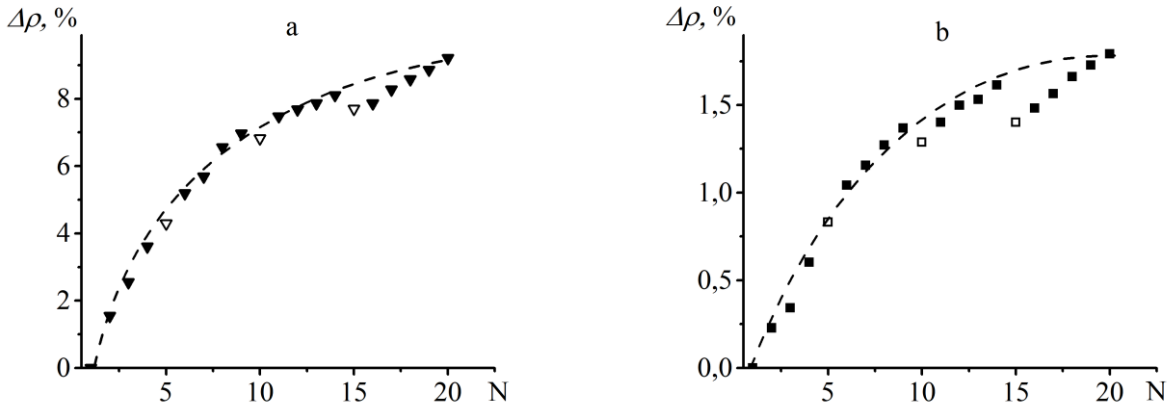

Figure 6. Variations in resistivity change, measured at 20°C (a) and 120°C (b), as a function of cycle number, obtained during thermal cycling of NiTi alloy.

Defects density can increase not only through thermal cycling within the range of martensitic transformations but also through active deformation in the martensitic state. Moreover, the increase in defect density during active deformation is greater than during thermal cycling, so it can be expected that structure relaxation during holding after active deformation of the TiNi alloy will be more intensive. To test this hypothesis, resistivity measurements were conducted after holding for 20 hours on samples of NiTi alloy pre-deformed to 10, 20, and 30% at room temperature (in the martensite state). It was found that even in the sample deformed to 30%, the resistivity value did not change and remained close to the resistance value measured immediately after deformation (Figure 7). This indicates that the defect structure formed during active deformation and during thermal cycling is different. The defect structure formed during thermal cycling is unstable and changes during holding. The defect structure formed during active straining is stable and does not change during holding at low temperatures. This difference may be

related to the fact that during thermal cycling, dislocations form in the austenitic phase since its dislocation limit is lower than in the martensitic phase.

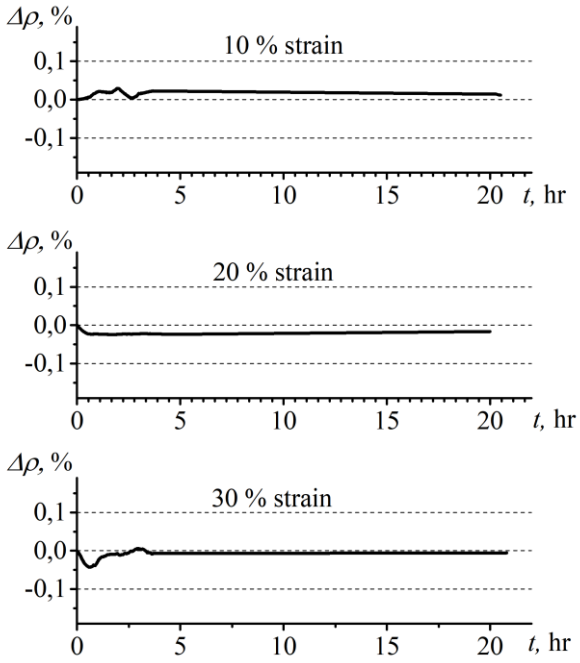

Figure 7. Variations in resistivity in the NiTi alloy during 20-hour holding at room temperature after pre-deformation to 10, 20, or 30% in the martensite state.

The martensitic phase only inherits the dislocation structure of the austenite [48,98,99], so in it, these dislocations are "unnatural." This leads to the formation of high stresses, the relaxation of which during holding, for example, through dislocation splitting, leads to properties restoration. During active deformation in the martensite state, dislocations arise in the martensitic phase, they are stable, and their structure and density do not change during holding at room temperature.

Thus, the results of the study on the effect of isothermal holding on the kinetics of martensitic transformations in the NiTi alloy have shown that there is a clear connection between the defect density and the parameters of martensitic transformations (the values of transformation temperatures and transformation stages). An increase in defect density due to thermal cycling leads to a decrease in transformation temperatures and the appearance of volumes of material undergoing B2→R transformation, while a decrease in defect density during holding leads to an increase (recovery) in transformation

temperatures and a decrease in the proportion of material undergoing B2→R transformation.

1.1.2. The Influence of the Upper Temperature on the Reversible Change in the Kinetics of Multistage Transformations in NiTi Alloy during Thermal Cycling

Section 1.1 has shown that holding the NiTi alloy leads to a partial recovery of the martensitic transition parameters. It has been established that property recovery occurs even with holding at room temperature, where the alloy is in a martensite state. Thus, it has been demonstrated that the recovery processes take place at both low and high temperatures. This indicates that the recovery processes occur not only during holding but also during heating. In this case, the maximum temperature in the cycle should influence the property changes during thermal cycling. To investigate this issue, the study examined the influence of the upper temperature of the cycle on the parameters of the martensitic transition in NiTi alloy samples subjected to thermocycling in the same interval.

$Ni_{50}Ti_{50}$ alloy samples, annealed at 500°C for 1 hour, underwent 30 thermocycles in the temperature range of 120°C to 20°C using a Mettler Toledo 822e differential scanning calorimeter (DSC) at a heating/cooling rate of 10°C/min. The DSC results showed that in the first cycle, the alloy underwent B2 ↔ B19' transformation upon cooling (M_s = 64°C, M_f = 56°C) and B19' → B2 transformation upon heating (A_s = 84°C, A_f = 97°C). After 30 thermocycles, a four-stage martensitic transformation during cooling and a two-stage reverse transformation during heating were observed (Figure 8). During cooling, the peaks were labeled A, B, C, D, and during heating, they were labeled E and F. To determine the nature of these peaks, cycles in the incomplete martensitic transformation range were performed according to the method described in [47]. It was found that peak A is due to the B2 → R transformation, peak B to the B2 → $B19'_1$ transformation, peak C to the B2 → $B19'_2$ transformation, and peak D to the R → $B19'_3$ transition. Thus, during cooling at high temperatures, a portion of the alloy transitions to the R phase (peak A). The remaining untransformed austenite transitions to the B19' phase at different temperatures (peaks B and C). At even lower temperatures, the R phase transitions to the B19' phase (peak D). During heating, peak E is caused by the B19' → B2 transformation in areas where the B19' phase appeared upon cooling directly from austenite, and peak F

is caused by the B19' → B2 transformation in areas where the B19' phase appeared upon cooling from the R phase. Such multistage transformation indicates that thermocycling leads to non-uniform changes in defect density throughout the volume of the alloy, which is the cause of non-uniform distribution of local stresses, which in turn affect the type and temperatures of martensitic transitions.

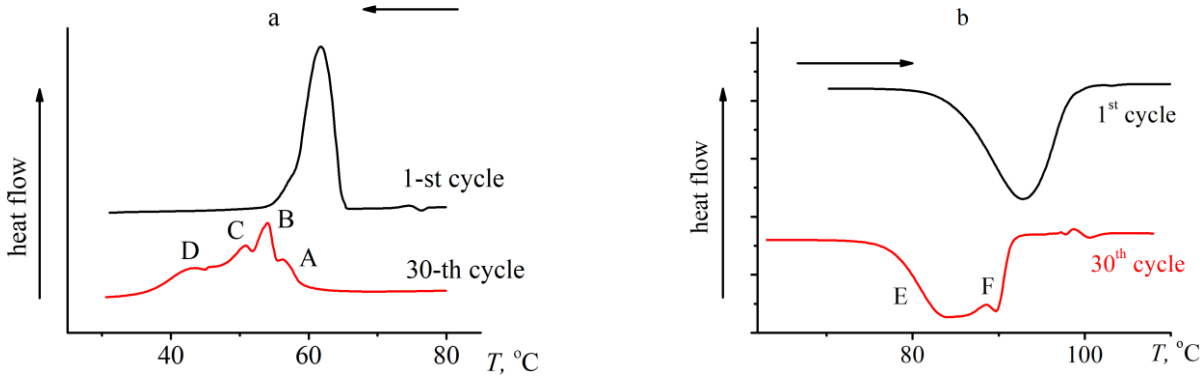

Figure 8. DSC curves obtained during cooling (a) and heating (b) in the first and thirtieth thermocycles in the temperature range of 120°C to 20°C.

After 30 thermocycles, the sample was subjected to thermocycling in the temperature range of 20°C to T_h (maximum temperature during heating), where the temperature T_h varied from 100°C to 240°C. Figure 9 shows the calorimetric curves obtained in cycles where the value of Th was less than 240°C. It can be observed that increasing the maximum temperature in the cycle does not affect the number of peaks either during cooling or heating. However, there is an increase in the temperatures of martensitic transitions and a redistribution of intensities between the calorimetric peaks. It is evident from Figure 9 that increasing T_h from 100°C to 240°C leads to an increase in the intensity of peaks B, C, and E.

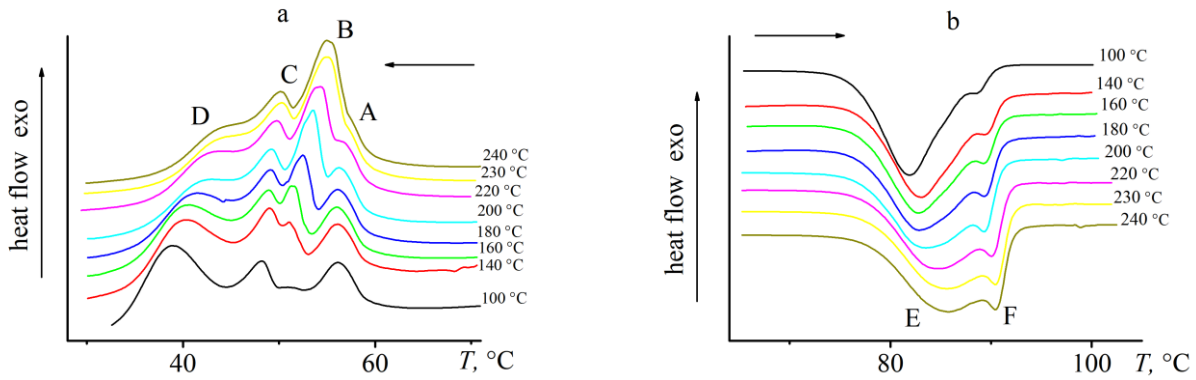

Figure 9. Evolution of calorimetric curves obtained during cooling from different initial temperatures (a) and subsequent heating (b) of the NiTi sample subjected to 30 thermocycles. The numbers on the right represent the values of the T_h temperature.

To determine the parameters of each peak, Origin Pro Peak Analyzer software was used. This software allows for the iterative separation of the contribution of each peak, determining their positions, widths, and areas. This procedure was applied to determine the contribution of each peak by fitting the peaks with a Lorentzian function (Figure 10). The enthalpy of the peaks was calculated as the area under the corresponding peak.

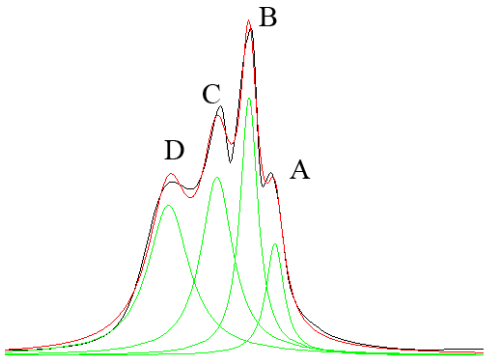

Figure 10. Example of peak separation using Origin Pro Peak Analyzer software. The green lines represent calculated peaks, the red envelope line is equal to the sum of the green curves, and the black line represents the experimental curve.

In Figure 11a, dependencies of enthalpy on the T_h temperature for each of the peaks observed during cooling are presented. It can be seen that with an increase in the T_h temperature, the enthalpy of peaks B and C increased, while the enthalpy of peaks A and D decreased. Since the enthalpy value depends on the volume fraction of the alloy undergoing phase transformation, it can be concluded that the change in T_h temperature

leads to a redistribution of volumes of material experiencing different phase transformations. Since peaks A and D are caused by transformations in volumes with high internal stresses, and their intensity decreased, this indicates that the proportion of such areas decreased due to a decrease in defect density. This assumption is supported by the increase in peak temperatures with increasing T_h, which is associated with a decrease in defect density (Figure 11b).

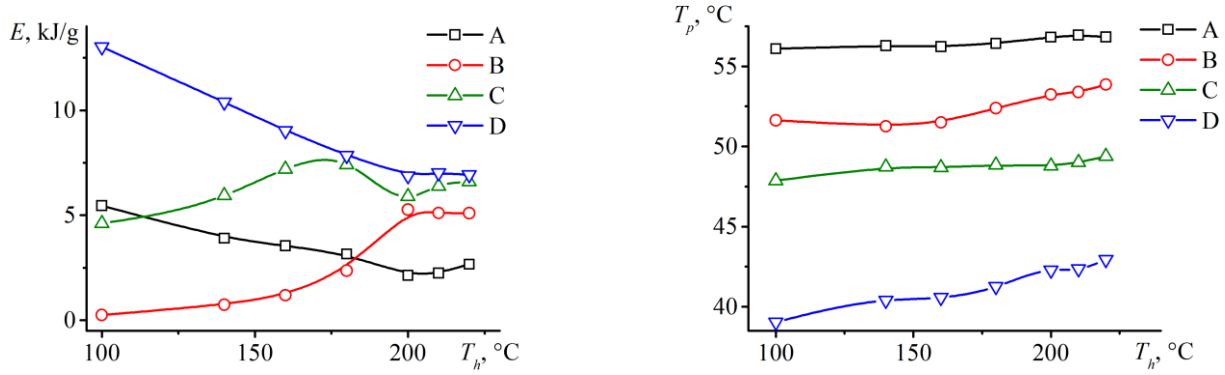

Figure 11. Dependencies of enthalpy of peaks A, B, C, D on the T_h temperature (a) and dependencies of peak temperatures A, B, C, D on the T_h temperature (b).

If the variations in the kinetics of martensitic transformations, observed in this study, is a result of decreasing defect density, then this process should be irreversible. However, Figure 12 presents DSC data obtained during cooling in three consecutive cycles: in the first cycle, the sample was cooled from 200°C to 20°C and then heated to 200°C, after which the sample was cooled again to 20°C. In the second cycle, cooling occurred from 100°C to 20°C, and heating - up to 100°C, after which the sample was cooled again to 20°C. In the third cycle, the sample was cooled from 200°C to 20°C and then heated to 200°C. Thus, the first and third cycles had the same conditions and were separated by a cycle where the T_h temperature was 100°C. It can be seen in Figure 12 that both DSC curves obtained in the first and third cycles are identical, despite the fact that between these cycles the sample underwent a cycle with a T_h temperature of 100°C. Thus, it is found that the change in the kinetics of martensitic transformations with a change in the T_h temperature is reversible. It can be assumed that the defect density decreases upon

heating to 200°C and increases upon cooling through the forward transformation interval. Heating to a temperature of 100°C did not lead to a decrease in dislocation density, so significant changes in the kinetics of martensitic transformations were observed upon cooling from this temperature. Subsequent heating to 200°C led to the annihilation of defects formed in the previous cycle with T_h equal to 100°C, so upon cooling, the same peaks were observed as during the first cooling from 200°C.

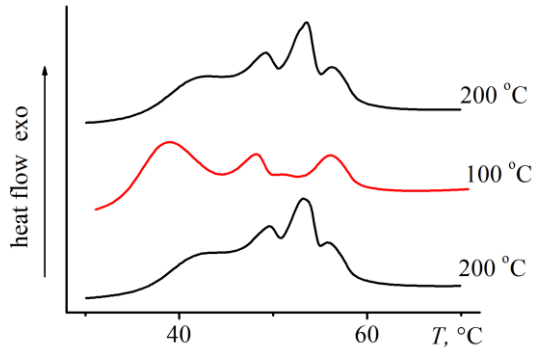

Figure 12. DSC curves obtained in three consecutive thermal cycles with different values of T_h

Thus, heating to higher temperatures leads to the annihilation of dislocation structures with high density formed during the previous thermal cycling. Subsequent cooling results in a reduction in the volume of material undergoing B2→R→B19' transformations, hence the redistribution of released heat among the four calorimetric peaks. The change in the MT kinetics was repeatable and determined only by the value of T_h. That is, one cooling cycle was sufficient to increase the defect density to its previous level (Figure 12). Therefore, during the devices operation, such as sensors, based on NiTi shape memory alloys, brief heating above the normal operating temperature can lead to significant changes in their operating conditions, which must be taken into account in their design.

1.1.3. Relationship between variation in defect density and parameters of martensitic transformations in NiTi alloys during thermocycling

In section 1.1.1, it is shown that there is a clear relationship between variation in defect density and temperatures of martensitic transformations. However, the regularities of this relationship are not established. This is due to the complexity of estimating changes in defect density during thermocycling. Defect density can be estimated based on the broadening of peaks in X-ray diffraction patterns or directly from images obtained in a transmission electron microscope. However, both of these methods are not applicable to NiTi alloys with equiatomic composition, which are in the martensitic phase at room temperature. B19′ martensite exhibits numerous reflections in a narrow range of angles in X-ray diffraction patterns, leading to peak overlap and complicating the measurement of peak broadening [3]. Observing dislocations in the martensitic phase using transmission electron microscopy is also challenging due to the complex contrast provided by the martensitic phase [80]. Pelton et al. [48] estimated changes in defect density during thermocycling in a Ti-50.5Ni alloy, which is in the austenite phase at room temperature, simplifying the assessment of changes in defect density. It was shown that the defect density in the Ti-50.5Ni alloy increased from 10^{12} to 10^{13} m^{-2} during the first thermocycle and further increased to 5×10^{14} m^{-2} over the next hundred thermocycles. However, these data cannot be used to assess variation in defect density in equiatomic NiTi alloys, as demonstrated in numerous studies [33,37,41,100], where it has been shown that property changes during thermocycling depend on the alloy composition. X-ray diffraction patterns or TEM images can be obtained at higher temperatures where equiatomic NiTi alloy is in the austenitic phase. To achieve this, samples are heated to the needed temperature and held at this temperature for about an hour while X-ray diffraction patterns are recorded. However, as shown in previous sections, heating and holding lead to a restructuring of the defect structure, so the defect density will change during the measurement process.

This problem can be solved by estimating changes in defect density based on changes in resistivity. According to Matthiessen's rule, the resistivity of an alloy is equal

to the sum of resistances caused by various sources, including phonons, dislocations, point defects, grain boundaries, etc. [101]. Currently, there is no data regarding the change in the proportion of grain boundaries and the concentration of point defects during thermocycling of shape memory alloys, so it can be assumed that the main change in resistivity observed during thermocycling is associated with an increase in dislocation density [37,48]. The resistivity caused by an increase in dislocation density can be estimated as $\rho_d=\rho^*\cdot\Delta D$, where ΔD is the change in dislocation density, and ρ^* is a constant [102]. Thus, the variation in resistivity measured at a constant temperature in each cycle can be considered as a measure of dislocation density and used to determine the relationship between the decrease in transformation temperatures and the increase in dislocation density during thermocycling of equiatomic NiTi alloys. Such studies were conducted in the present work. Wire samples of $Ni_{50}Ti_{50}$ alloy with a diameter of 0.5 mm and a length of 140 mm were quenched in water at a temperature of 700°C (for 15 minutes) and annealed at a temperature of 500°C for 1 hour. After annealing, martensitic transformations from the cubic B2 phase to the monoclinic B19' phase during cooling and from B19' to B2 during heating were observed in the alloy.

Thermocycling was performed in two different temperature ranges from 140°C to 0°C and from 200°C to 0°C, as the upper temperature in the cycle may affect the changes in the parameters of martensitic transformations and defect density during thermocycling. Samples were subjected to 20 thermocycles at the selected temperature ranges in a Shimadzu thermal chamber, providing cooling and heating at the specified rate (7°C/min). During thermocycles, the resistance of the samples was measured using a four-probe method, and the temperature was measured in the middle of the sample using a thermocouple.

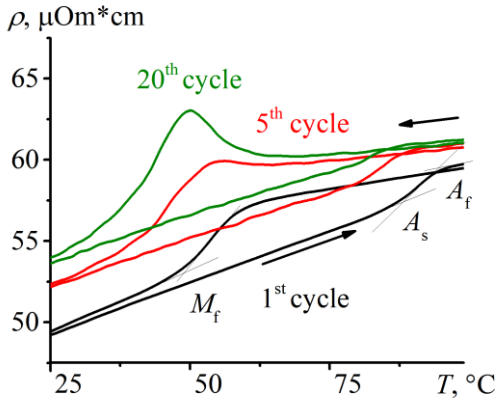

Figure 13. Dependencies of resistivity on temperature obtained in the first, fifth, and twentieth cycles during the thermocycling of the NiTi alloy in the temperature range from 200°C to 0°C.

In Figure 13, the dependencies of resistivity on temperature obtained in the first, fifth, and twentieth cycles in the temperature range from 200°C to 0°C are presented. Anomalies related to martensitic transformations are visible on the ρ(T) curves. With an increase in the number of cycles, these anomalies shifted to lower temperatures, and the ρ(T) curve itself shifted upwards towards higher resistivity values. In the first cycle, the alloy underwent B2↔B19′ transformations. After the fifth cycle, the transformation sequence during cooling changed from B2→B19′ to B2→R→B19′. The temperatures M_f, A_s, and A_f were measured from the ρ(T) curves obtained during thermocycling, as shown in Figure 1, while the M_s temperature was excluded from consideration due to the change in transformation type during thermocycling. To assess variation in defect density, the resistivity at a temperature of 120°C, where the samples were in the austenitic state, was analyzed in each cycle.

Figure 14 shows the dependencies of the M_f, A_s, and A_f temperatures on the cycle number. It can be observed that regardless of the value of the upper thermocycling temperature, the transformation temperatures decreased during thermocycling (Figure 14a,b), while the resistivity increased (Figure 14c). Comparing the data obtained during thermocycling in different temperature intervals demonstrates that the changes in transformation temperatures and resistivity during thermocycling in the temperature

range from 200°C to 0°C are smaller than those in the range from 140°C to 0°C, which is consistent with the results presented in reference [104].

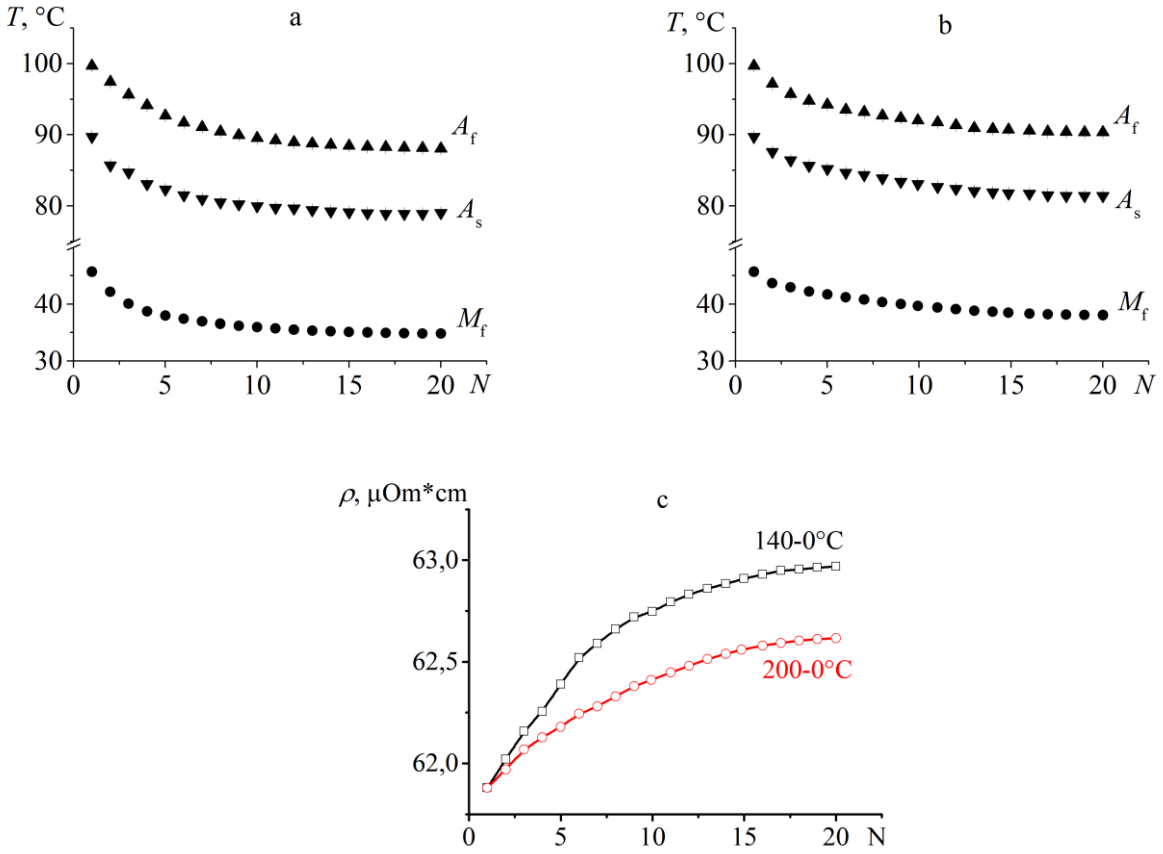

Figure 14. Changes in transformation temperatures (a, b) and resistivity (c) during thermocycling in temperature intervals from 140°C to 0°C (a) and from 200°C to 0°C (b).

The electrical resistivity of a material depends on its composition, microstructure, and concentration of defects such as dislocations, vacancies, impurities, and others. If the defect density in an alloy varies, for example, due to heat treatment or other processes, this can lead to a variation in resistivity. Therefore, analyzing variations in resistivity can provide insight into the state of the material's defect structure. Using the data presented in Figure 14, dependencies of transformation temperatures on resistivity were obtained, as shown in Figure 15. It can be observed that the dependencies of transformation temperatures on resistivity are not linear. This indicates that the temperatures of martensitic transformations nonlinearly depend on variations in defect density during thermocycling.

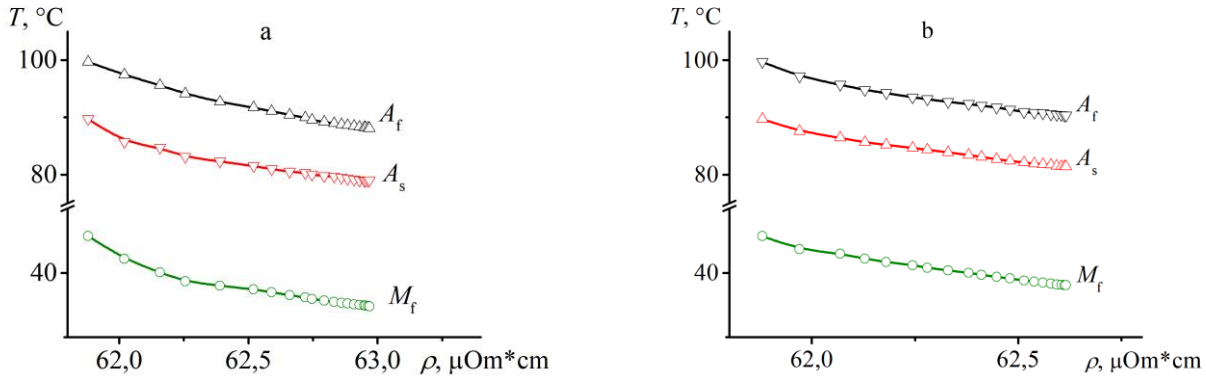

Figure 15. Dependencies of transformation temperatures on resistivity obtained during thermocycling in the temperature ranges of 140°C to 0°C (a) and from 200°C to 0°C (b).

The variation in resistivity caused by an increase in dislocation density can be determined using the following expression:

$$\rho_d = \rho_N - \rho_0 \quad (1.1)$$

where ρ_N is the resistivity measured in the N-th cycle, and ρ_0 is the resistivity measured in the alloy after heat treatment before cycling [101]. At the same time, $\rho_d = \rho^* \cdot \Delta D$ [102], therefore, to estimate the defect density, it is necessary to find the coefficient ρ^* as the ratio of ρd to the change in dislocation density D. Thus, ρ^* can be determined as:

$$\rho^* = \frac{\rho_1 - \rho_0}{D_1 - D_0} \quad (1.2)$$

where ρ_0 and D_0- are the resistivity and dislocation density measured in the sample before cycling, and ρ_1, D_1 are the resistivity and dislocation density measured after the first cycle, respectively. To demonstrate how this analysis can be used to estimate the linear coefficients between transformation temperatures and dislocation density, data from Pelton et al. [48] were used. According to [48], the dislocation density in the uncycled NiTi alloy is $D_0 = 10^8$ cm^{-2}, and it increases to $D_1 = 10^9$ cm^{-2} during the first cycle. Thus, the value of D_1–D_0 is $9 \cdot 10^8$ cm^{-2}. In Figure 14c, it can be seen that ρ_1–ρ_0 is 0.14 μΩ·cm. Therefore, the value of ρ^* is $1.55 \cdot 10^{-6}$ μΩ·cm^3. In this case, the dislocation density in each cycle can be estimated as:

$$D = D_0 + \Delta D = D_0 + \frac{\rho_d}{\rho^*} = D_0 + \frac{\rho_N - \rho_0}{1.55 \cdot 10^{-6}} \quad (1.3)$$

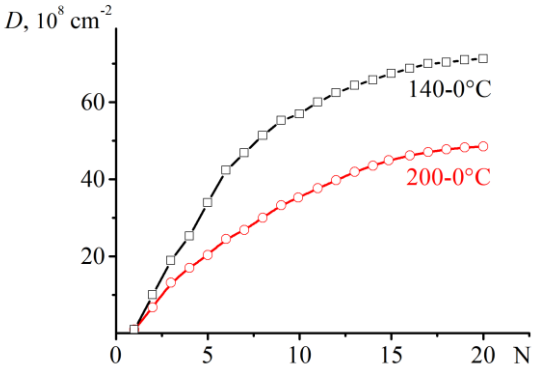

Figure 16. Dependencies of dislocation density on the cycle number, obtained using equation (3).

In Figure 16, the variation of dislocation density with an increasing number of cycles is shown for temperature ranges of 140°C to 0°C and 200°C to 0°C. It can be observed that the increase in dislocation density during thermal cycling in the temperature range from 200°C to 0°C is less compared to the range from 140°C to 0°C, which confirms the assumption proposed by Wang et al. [104] that increasing the upper temperature limit of the cycle leads to a reduction in the variation of dislocation density due to recovery processes.

Using the data presented in Figure 15 and the data on the variation of dislocation density shown in Figure 16, dependencies of the changes in transformation temperatures (ΔA_s, ΔA_f, ΔM_f) on dislocation density were obtained, as depicted in Figure 17. It can be observed that regardless of the temperature range of thermal cycling, the dependencies of transition temperatures on defect density can be divided into two regions – a non-linear region for thermal cycling up to the 5th cycle and a linear region for thermal cycling starting from the 5th cycle. In the linear region, the proportionality coefficient A* was calculated, which equals $-0.09 \pm 0.002 \cdot 10^{-8}$ °C·cm^2 for the curves ΔM_f(D) and ΔA_s(D), and $-0.125 \pm 0.002 \cdot 10^{-8}$ °C·cm^2 for the curve ΔA_f(D) for thermal cycling in the range from 140 to 0°C (Figure 17a), and $-0.130 \pm 0.002 \cdot 10^{-8}$ °C cm^2 for the curve ΔM_f(D), $-0.140 \pm 0.002 \cdot 10^{-8}$ °C·cm^2 for the curve ΔA_s(D), and $-0.143 \pm 0.002 \cdot 10^{-8}$ °C·cm^2 for the

curve ΔA_f(D) for thermal cycling in the range from 200°C to 0°C (Figure 17b). These obtained data are unexpected, as they show that the rate of variation in transition temperatures with increasing defects density during thermal cycling in the range from 200 to 0°C is higher than in the range from 140 to 0°C, despite the fact that the variation in defect density in the first range is less than in the second (Figure 17). This indicates that the temperatures of martensitic transition are determined not only by defect density. Otherwise, the rate of change in transition temperatures with increasing defect density would be the same.

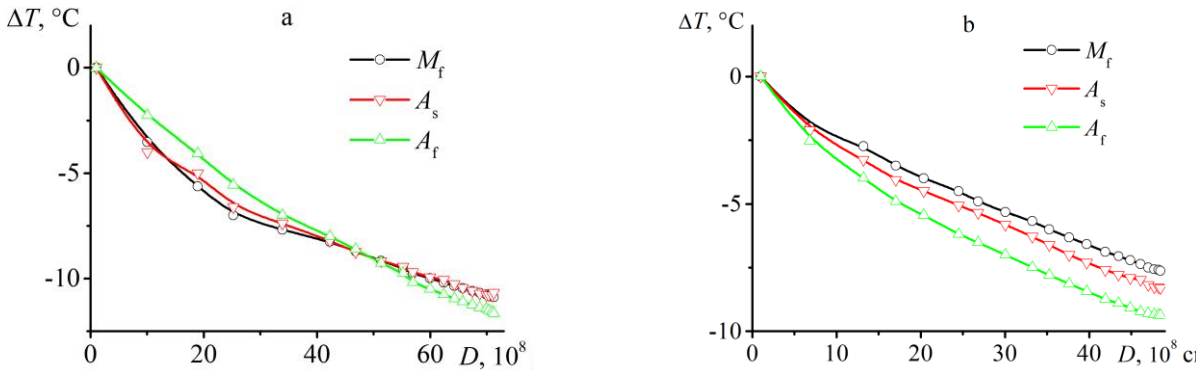

Figure 17. Dependencies of the transformation temperatures increment on dislocation density obtained during thermal cycling in the temperature ranges from 140°C to 0°C (a) and from 200°C to 0°C (b).

The relationship between dislocation density and martensitic transformation temperatures can be determined using the equation of thermodynamic equilibrium. In the first cycle, direct martensitic transformation during cooling occurs when $\Delta G_{ch} = E_d + E_{el}^{A\rightarrow M}$, where ΔG_{ch} is the difference in chemical free energy between austenitic and martensitic phases, Ed is the dissipative energy determining the transformation hysteresis, and $E_{el}^{A\rightarrow M}$ is the elastic energy arising from the growing martensite crystals creating elastic stress fields that must be overcome to advance the martensitic boundary. This energy determines the temperature range of martensitic transformation. The sum $E_d + E_{el}^{A\rightarrow M}$ is referred to as the non-chemical Gibbs energy [46, 105]. According to McCormick and Liu [46], the increase in defect density during thermal cycling results in an additional contribution to elastic energy, which should be included in the equation of thermodynamic equilibrium.

Thus, in the second cycle, direct martensitic transformation during cooling occurs when $\Delta G_{ch} = E_d + E_{el}^{A\to M} + E_{el}^{d}$, where E_{el}^{d} is the elastic energy of defects [46, 105, 106]. Comparing the equations of thermodynamic equilibrium formulated for the first and second cycles shows that if the increase in defect density contributes to thermodynamic equilibrium, then the value of ΔG_{ch} in the second cycle should be greater than the value of ΔG_{ch} in the first cycle. A greater value of ΔG_{ch} can be achieved by additional cooling of the sample, thus, martensitic transformation occurs in the second cycle at lower temperatures than in the first cycle. McCormick and Liu [46] demonstrated that the change in transformation temperatures caused by the increase in elastic energy of defects is given by:

$$\Delta T = -\frac{\left|E_{el}^{d}\right|}{\left|\Delta S\right|} \tag{1.4}$$

where ΔT is the change in martensitic transformation temperatures, and ΔS is the change in transformation entropy. Therefore, the decrease in transformation temperatures is proportional to the increase in elastic energy of defects.

Since it is assumed that the main variation in defect density is associated with the variation in dislocation density, let's consider the energy of an individual dislocation, which can be found as the sum of elastic deformation energy and the dislocation core energy. In [107], it is shown that the energy of the dislocation core does not exceed 10% of its total energy; therefore, this term can be neglected. Thus, the elastic energy of the dislocation can be estimated as indicated in [107]:

$$E_{el}^{d} = \frac{G \cdot b^2 \cdot L}{4\pi \cdot K} \cdot \ln\frac{R}{r_0} \tag{1.5}$$

Where G is the shear modulus, L is the dislocation length, b is the Burgers vector, K is a constant equal to 1 for edge dislocations and $(1-\nu)$ for screw dislocations (ν is the Poisson's ratio), r_0 is the dislocation core radius, and R is the cutoff radius. To estimate the elastic energy contributed by dislocations in metals and alloys, the following expression is used:

$$E_{el}^{d} \approx \frac{G \cdot b^2 \cdot L}{2} \tag{1.6}$$

If the interaction between dislocations is not considered, then the total energy contributed by all dislocations, according to [108], can be estimated as:

$$E_{\mathrm{el}}^{\mathrm{d}} \approx \frac{G \cdot b^2 \cdot \sum L}{2} \tag{1.7}$$

where ΣL is the total dislocation length, which can be expressed as ΣL=D·V, where D is the dislocation density, and V is the volume. Thus, the expression for the elastic energy contributed by dislocations can be written as:

$$E_{\mathrm{el}}^{\mathrm{d}} \approx \frac{G \cdot b^2 \cdot D \cdot V}{2} \tag{1.8}$$

Since G, b, and V are constants, the elastic energy can be estimated as:

$$E_{\mathrm{el}}^{\mathrm{d}} \approx A \cdot D \tag{1.9}$$

where $A = \frac{G \cdot b^2 \cdot V}{2}$. Using equation (4), the variation in transformation temperatures can be estimated as follows: $\Delta T \approx -\frac{A \cdot D}{\Delta S}$ since ΔS is also a constant, this expression can be written as:

$$\Delta T \approx -A^* \cdot D, \tag{1.10}$$

where $A^* = \frac{G \cdot b^2 \cdot V}{2 \cdot \Delta S}$.

According to the thermodynamic approach described in detail in [46,105,106], the increase in dislocation density should lead to a uniform decrease in all transformation temperatures. However, this contradicts the data presented in Figure 17. The difference in the linear coefficients A* for different transformation temperatures may be caused by changes in the shear modulus and Burgers vector of dislocations during the martensitic transformation [3]. Thus, when analyzing the thermodynamic equilibrium equations proposed for different transformation temperatures, it is necessary to consider that the elastic energy of dislocations is different for martensitic and austenitic states and depends on the ratio of the volume fraction of martensitic and austenitic phases.

The decrease in transformation temperatures should linearly depend on the dislocation density, and this is observed experimentally starting from the fifth cycle. During the initial cycles, the decrease in transformation temperatures depends on the

dislocation density in a nonlinear manner, indicating the presence of another (or other) factor(s) influencing the transformation temperatures besides the dislocation density. It can be hypothesized that the structure (distribution) of defects may additionally affect the transformation temperatures. For example, it has been shown in [47,48,57] that thermocycling of equiatomic NiTi alloy led to changes of martensitic transformations type due to the non-uniform distribution of defects throughout the volume of the alloy. Perhaps, the complex dislocation structure may be responsible not only for the manifestation of multi-stage martensitic transformations but also for the additional shifting of transformation temperatures. Thus, the research results have shown that the change in dislocation density is not the sole cause of the decrease in transformation temperatures during thermocycling of equiatomic NiTi alloy.

1.1.4. Direct observations of the movement of interphase and intermartensitic boundaries during multiple thermal cycles in NiTi alloy in the annealed state.

In the previous section, it was shown that the relationship between changes in martensitic transformation temperatures and dislocation density during thermal cycling of NiTi SMA is nonlinear. It can be assumed that additional factors influence transition temperatures in the initial stages of thermal cycling. To ensure the stability of NiTi alloy properties during thermal cycling, it is necessary for interphase boundary movement during reverse martensitic transformation in each cycle to follow a trajectory opposite to their movement during the preceding forward transformation. This ensures the complete reversibility of the structure after the cooling-heating cycle.

Currently, it is believed that during cooling, martensitic crystals heterogeneously nucleate in the austenitic phase and grow until they encounter other crystals. A characteristic feature of thermoelastic martensitic transformations is that upon heating, the reverse transformation from martensite to austenite occurs due to the reverse movement of interphase boundaries. This facilitates the return of atoms to their initial positions, restoring the austenite structure. This assumption has been confirmed by direct observations of interphase boundary movement during thermal cycling of CuAlNi alloy using optical microscopy. Thus, the martensitic crystal that first appeared during cooling disappears last during heating, and vice versa. The sequence of martensite formation during cooling and its disappearance during heating is repeated during multiple thermal cycles across the transformation temperature range, showing a so-called "microstructural" memory. However, "reversible" processes at the microlevel may be "irreversible" at the nano level. Additionally, changes in dislocation density during thermal cycling may affect the movement of interphase boundaries during both cooling and heating. This, in turn, can disrupt the structure's restoration during the reverse transformation, leading to property changes in the subsequent cycle.

To determine how the dislocation structure affects the formation of martensitic crystals during cooling and their disappearance during heating, direct (in situ) observations of interphase boundary movement during cooling and heating were

conducted using transmission electron microscopy (TEM). Foils of $Ni_{50.2}Ti_{49.8}$ alloy were prepared by standard methods, including electrochemical etching in a solution of 10% HClO4 + ethanol at -25°C and 12 mA. The prepared foil was mounted in a two-axis analytical holder (Gatan 652) of the "Libra 200-FE" transmission electron microscope. The sample was cooled and heated through the direct and reverse martensitic transformation temperature intervals, and images of the alloy structure at various temperatures were obtained in bright-field scanning transmission electron microscopy (BF STEM) mode. The equipment of the "Nanotechnology" Resource Center of the Scientific Park of St. Petersburg State University was used for the research.

Figure 18a shows a STEM image of a grain center approximately 5 μm in size obtained at a temperature of 100°C, where the alloy is in the austenitic state. Dislocations already present in the sample, formed during foil preparation and the preliminary cycle (cooling during foil preparation and heating in TEM up to 100°C), can be observed. The dark oval contrast at the bottom of the image represents a Ti_2Ni particle (EDX analysis results).

During the first cooling, two large martensite plates simultaneously formed at 56°C in the lower left and upper right corners (Figure 18b). Upon cooling to 52°C, both martensitic regions expanded, with the upper part of the grain exhibiting more significant growth of the martensite region than the lower part (Figure 18c). This is because the Ti_2Ni particle creates a stress field around itself, hindering the movement of the interfacial boundary of the lower plate, which consists of a single martensite plate composed of two variants. In the right part, the martensitic region contains several plates with different twin orientations (Figure 18c-d). Upon further cooling to 40°C, the large martensite plate in the left region remains unchanged in size, while in the upper right region, the martensite plates continue to grow
until they come into contact with the left plate (Figure 18e). Upon further cooling to 27°C, the transformation completes in the central and lower right regions (to the right of the Ti_2Ni particle) (Figure 18f).

During subsequent heating, the reverse transformation begins at 72°C simultaneously in the upper, lower, and middle regions of the grain (Figure 19a). The area

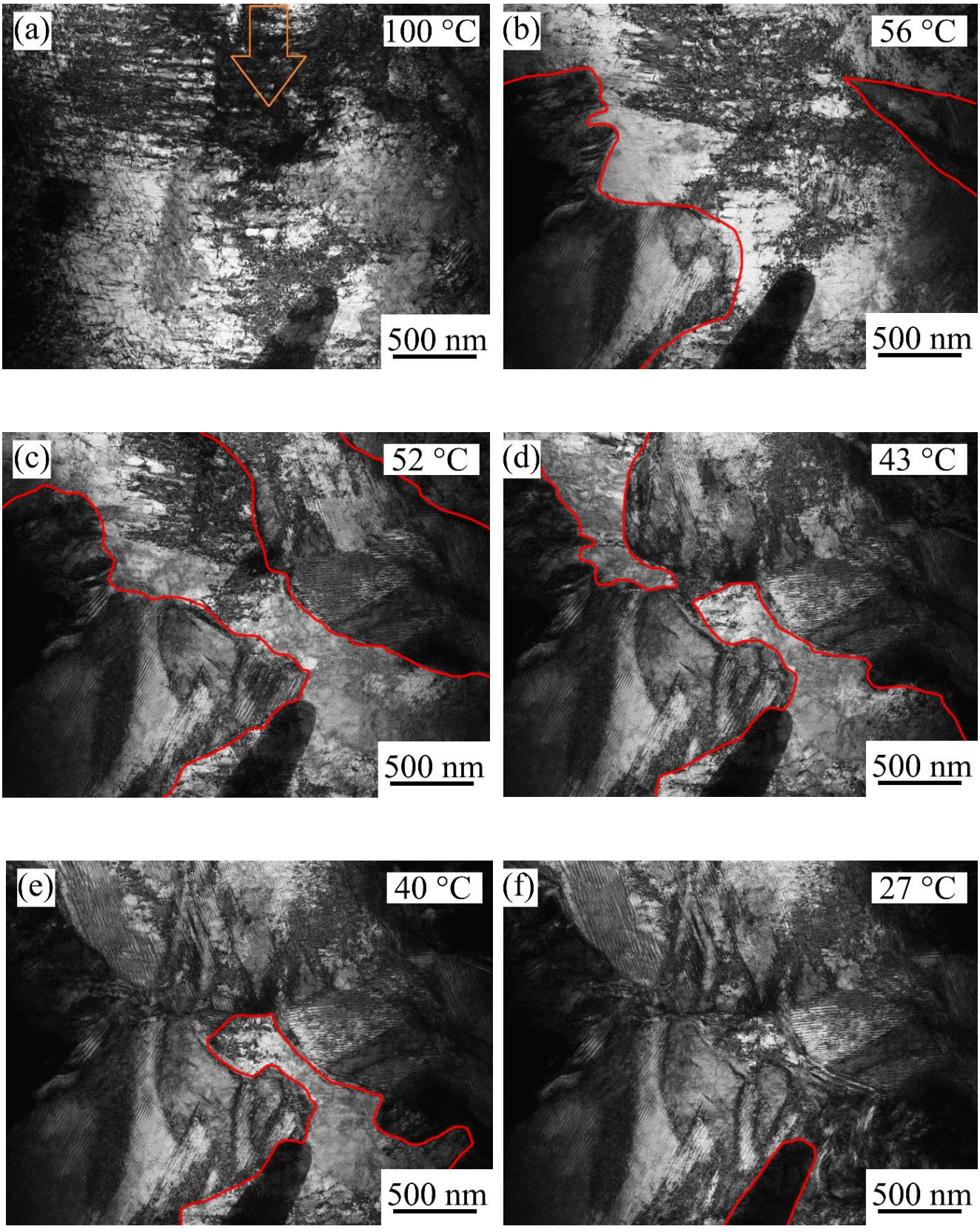

Figure 18. BF STEM images of the NiTi alloy sample during cooling at temperatures 100°C (a), 56°C (b), 52°C (c), 45°C (d), 40°C (e), and 27°C (f). Red lines delineate the boundaries between the austenite and martensite phases.

in the lower part of the grain transformed into martensite last during cooling; therefore, according to current understanding, martensite in this area should have disappeared first upon heating. However, martensite also disappeared in the upper and central parts, where it did not form in the final stage of cooling. This indicates that during heating, the boundaries do not move precisely backward in the same sequence as during cooling (see Figure 18c-e). Upon further heating, the boundaries continue to move in the upper and lower parts of the grain (Figure 19b). In the central part of the grain, two new austenite regions appear (Figure 19b, c), which merge with each other and then with the regions in the upper and lower parts of the grain (Figure 19d). Heating to 89°C leads to the complete disappearance of martensite plates in the right region, while a significant martensite area remains in the left part (Figure 19e), which transforms into austenite upon heating to 100°C (Figure 19f). Thus, the research results demonstrate that the sequence of martensite plate disappearance during heating is not reverse to the sequence of their formation during cooling.

Figure 20 shows BF STEM images obtained during the second cooling. It can be observed that two martensite crystals first appeared, outlined by red lines, merging into a single region (the orientation of the plates is indicated at the junction in Figure 20a). The two crystals can be distinguished by the twinning direction inside the crystal. In the left and right regions, the twins have different crystallographic orientations. It should be noted that this region only partially overlaps with the area where martensite crystals first appeared during the first cooling cycle. Upon further cooling in the second cycle, both crystals continued to grow, and at a temperature of 52°C, half of the grain volume was already in the

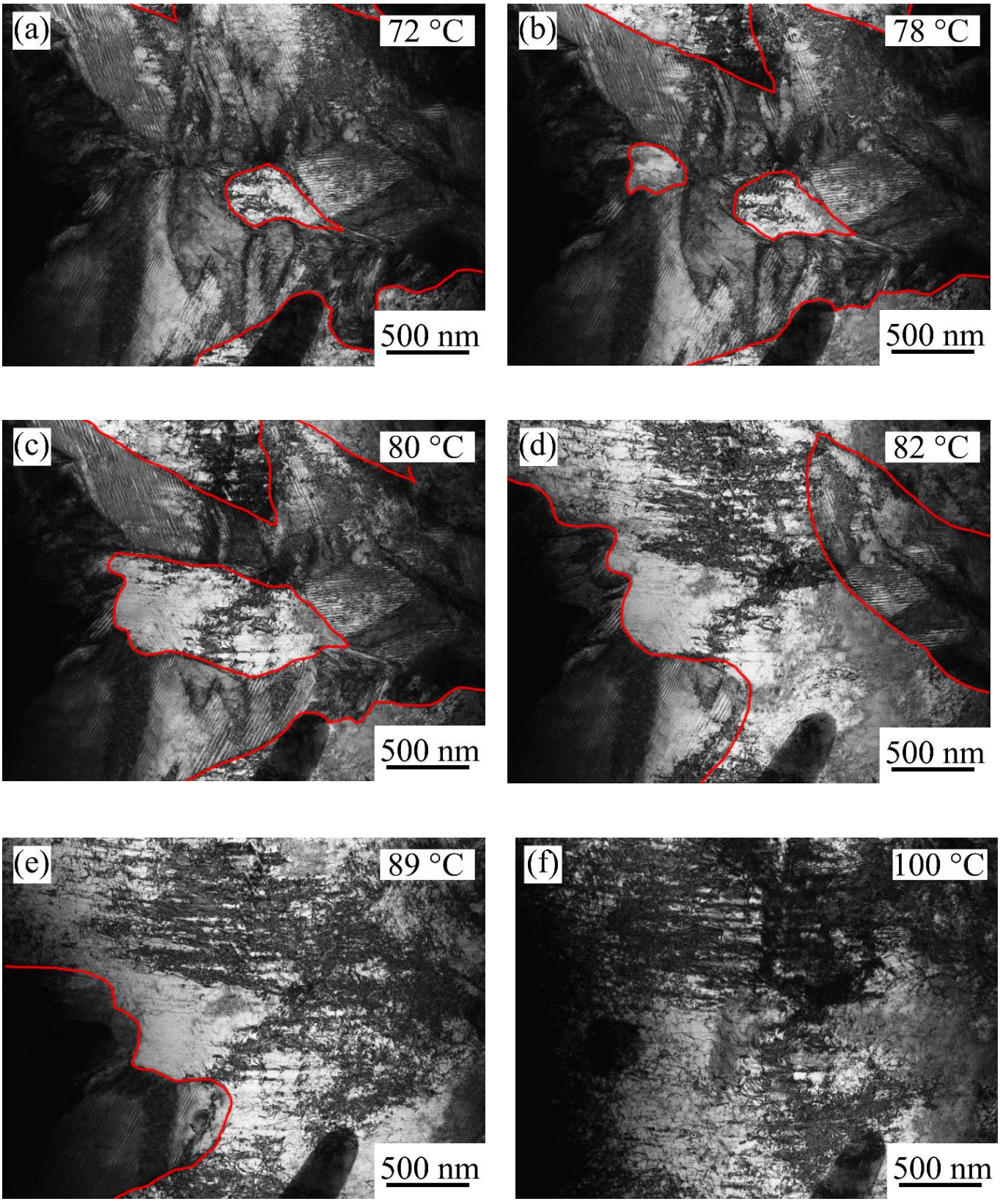

Figure 19. Images obtained in BF STEM mode of NiTi alloy sample during heating at temperatures of 72°C (a), 78°C (b), 80°C (c), 82°C (d), 89°C (e), and 100°C (f), where the red line outlines the austenite/martensite boundary.

martensite state (Figure 20b). Further cooling was accompanied by both the growth of already existing crystals and the appearance of new plates (Figure 20c-e). Forward transformation was completed at 31°C when a large plate appeared in the upper part, occupying the remaining volume of the grain (Figure 20f). Thus, the order of martensite crystal formation during the second cooling differed from the sequence of martensite plates appearance during the first cooling. For example, during the first cooling, the lower part transformed last, while during the second cooling, the last martensite appeared in the upper part of the grain. This indicates the absence of microstructural memory during martensitic transformation in NiTi alloy.

As noted earlier, a region with a high density of dislocations was present in the upper central part of the grain, indicated by the arrow in Figure 18a. Analysis of martensite formation near this region showed that during the first cooling, the first martensite appeared at a temperature of 52°C (Figure 18c), and its formation was completed at 40°C (Figure 18e). During the second cooling, the forward transformation in this area occurred between 35 and 31°C (Figure 20f). This area was not the last to form martensite during the first cooling cycle, nor was it the first where martensite nucleated. Thus, it can be concluded that regions with high defect densities neither facilitate nor hinder the nucleation of martensite crystals.

The results of the study showed that in the original undeformed NiTi alloy, the sequences of martensite crystal appearance during cooling and their disappearance during heating are not preserved. Additionally, there is no microstructural memory, meaning that martensite crystals during cooling in the first and second cycles grow in a non-coordinated manner and form in different locations. However, both phenomena (disruption of the sequence of martensite crystal appearance during cooling and their disappearance during heating, and the absence of microstructural memory) can be caused by stress redistribution in the grain body due to changes in the distribution of defects. As shown in sections 1.1.1 and 1.1.2, the defect structure formed during thermal cycling is unstable, and recovery processes easily occur, leading to the redistribution of defects, and thus stresses, which can

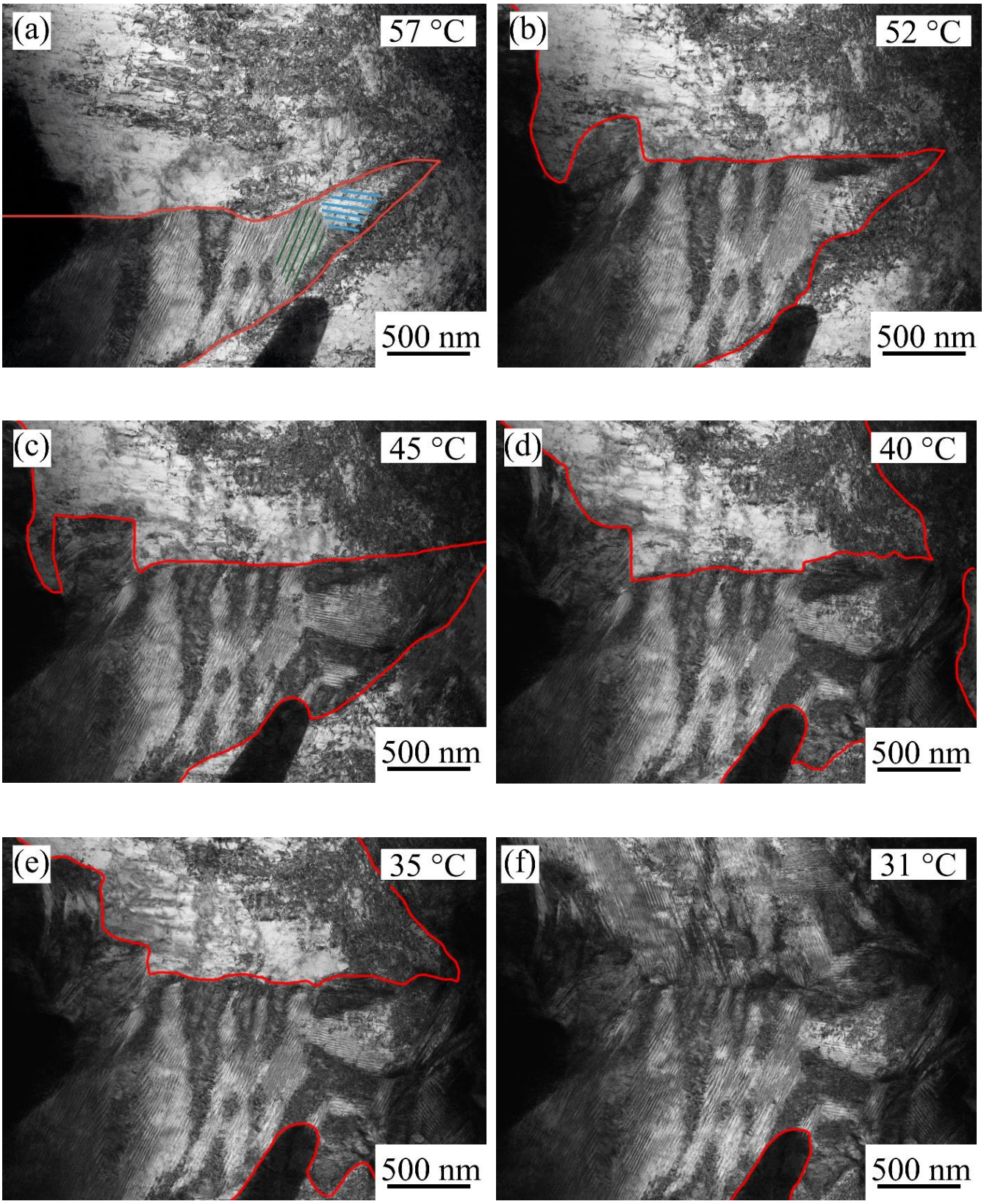

Figure 20. BF STEM images obtained during the second cooling cycle of the NiTi alloy at temperatures of 57°C (a), 52°C (b), 45°C (c), 40°C (d), 35°C (e), and 31°C (f), with the red line outlining the austenite/martensite boundary.

affect transition temperatures. To verify this assumption, the study examined the direct (in situ) method of movement of phase boundaries in NiTi alloy subjected to preliminary stretching, which, as previously shown, forms a stable dislocation structure.

A sample with a working part measuring 20 x 6 x 0.12 mm was deformed by 10% in the martensitic state (Figure 21a) on a Shimadzu AG-X testing machine equipped with a video extensometer for precise deformation measurement. After unloading, disks with a diameter of 3 mm were cut from the working part of the sample using an electrical discharge machine, which were used to obtain foils for TEM according to the methodology described earlier. The obtained foil was installed in a biaxial analytical holder (Gatan 652) TEM (Libra 200-FE), which allowed heating and cooling the foils in the electron microscope column. The foils were heated to a temperature of 150°C, cooled to 25°C, and heated again to 150°C. The need for heating to a temperature significantly higher than A_f is associated with the fact that after deformation of the NiTi alloy in the martensitic state, the martensite stabilization effect manifests itself [112–114], resulting in the alloy undergoing reverse transformation at temperatures significantly higher than the undeformed alloy (Figure 21b). During thermal cycling, images of the alloy structure were obtained in BF STEM mode and the movement of phase boundaries was analyzed as the temperature changed.

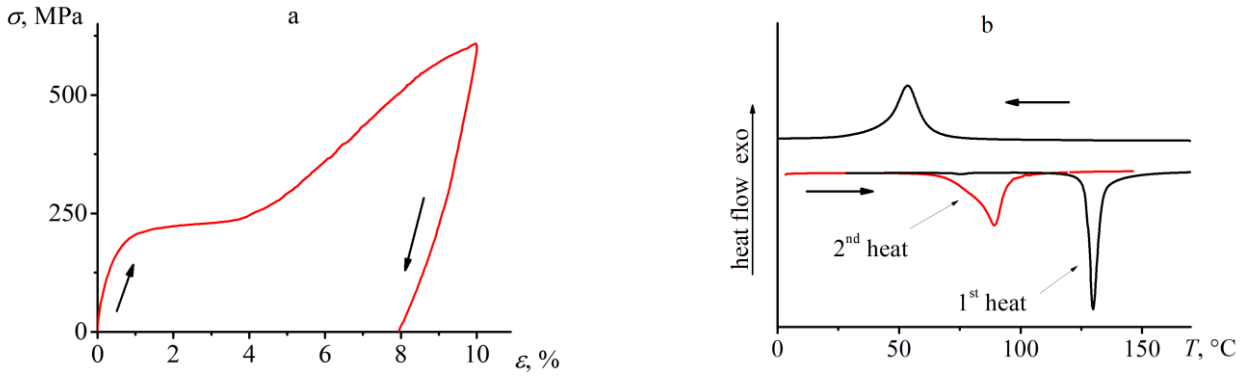

Figure 21. Stress-strain diagram obtained during stretching by 10% and unloading (a), and the DSC curve obtained during heating-cooling-heating of the pre-deformed NiTi specimen (b).

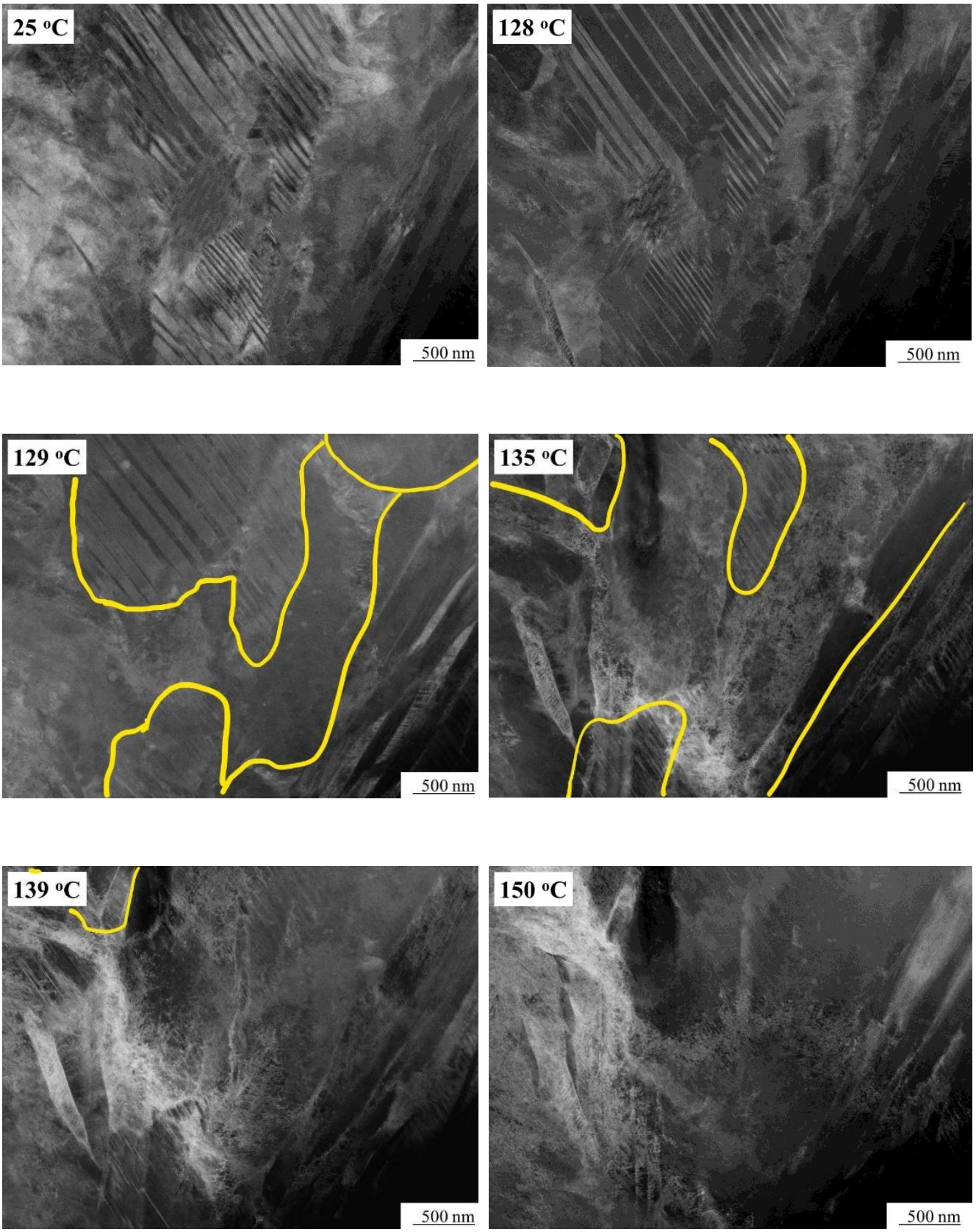

Figure 22. Movement of phase boundaries (shown in yellow) during the first heating of the NiTi sample pre-deformed by 10% in the martensitic state.

Figure 22 shows the evolution of the martensite structures of the pre-deformed sample during the first heating. At room temperature, immediately after pre-deformation, wide martensite plates were observed in the grain. Most of these plates had the same orientation (except for the area in the lower right corner), which is typical for oriented martensite formed as a result of deformation of NiTi samples in the martensitic state. Increasing the sample temperature to 128°C does not affect the sample structure, regardless of the fact that this temperature is 46°C higher than the start temperature of reverse transformation (A_s) in the undeformed sample. Further temperature increase to 129°C results in a sharp transformation of the majority of the sample from martensite to austenite. The remaining part of the sample undergoes reverse transformation as the temperature increases from 129 to 139°C, with small areas of martensite remaining in the sample, but their volumetric fraction is low. At 150°C, the grain is completely in the austenite state, meaning that reverse transformation finishes upon heating to this temperature.

Figure 23 shows the movement of phase boundaries during the subsequent cooling. At 55°C, the first martensite plate with very thin twins appears. As the temperature decreases to 46°C, the plate continues to grow and eventually merges with two other plates that appeared in the lower part of the sample. When the temperature drops to 30°C, martensite occupies a large part of the volume. Comparison of the alloy structure after deformation (25°C in Figure 22) and after heating and cooling (24°C in Figure 23) shows that the martensite twins' orientation is preserved, but their thickness decreases by more than 10 times.

Figure 24 illustrates the structural changes during the second heating of the sample pre-deformed by 10% in the martensite state. It is observed in Figure 24 that the reverse transformation begins at 85°C, which is 43°C lower than during the first heating. With further temperature increase, the volume fraction of martensite gradually decreases, reaching zero at temperatures above 100°C. The sequence of disappearance of crystals was opposite to their appearance during the previous cooling: the first martensite plate to disappear was the one emerging from the upper right corner (Figure 24), which was the

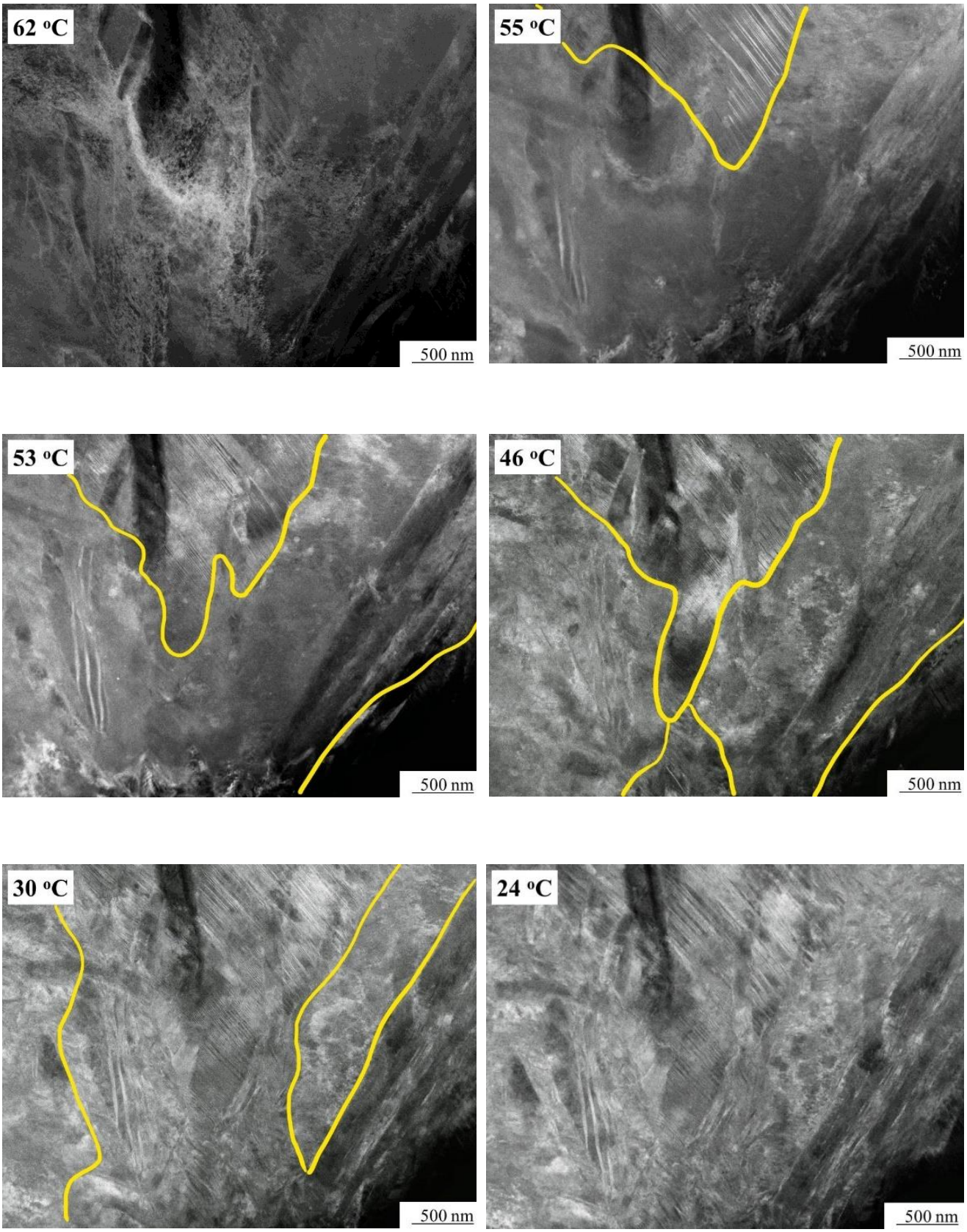

Figure 23. Movement of phase boundaries (shown in yellow) during the cooling of the NiTi sample, pre-deformed by 10% in the martensitic state and heated up to 150°C.

last to appear during cooling (Figure 23). Martensite in the upper part appeared first and disappeared last.

Subsequently, the sample was cooled again to room temperature, revealing that the sequence of martensite crystal appearance during the second cooling was the same as during the first cooling, indicating that the pre-deformed sample with a stable dislocation structure exhibited microstructural memory.

Thus, the results of the study demonstrate that if a stable dislocation structure is formed in the alloy (during active deformation), the sequence of martensite crystal disappearance during heating is opposite to the sequence of their appearance during cooling. Additionally, microstructural memory is retained in the alloy. The stable dislocation structure formed during deformation ensures the stability of internal stresses in the grain. The appearance of additional stresses during the formation and disappearance of martensite crystals does not affect the stable dislocation structure, hence maintaining microstructural memory and the sequence of crystal appearance during cooling and disappearance during heating.

It is worth noting that numerous studies have shown that the stability of transformation temperatures is higher in pre-deformed samples, which is attributed to the stability of the dislocation structure formed during active deformation. In the undeformed alloy, the dislocation structure formed during thermal cycling is unstable and is influenced by stresses arising during the growth and disappearance of martensite crystals. This leads to the redistribution of defects, changes in internal stresses, and consequently, changes in transition temperatures. Thus, the study demonstrates that the redistribution of defects during thermal cycling is another reason for the change in transition temperatures.

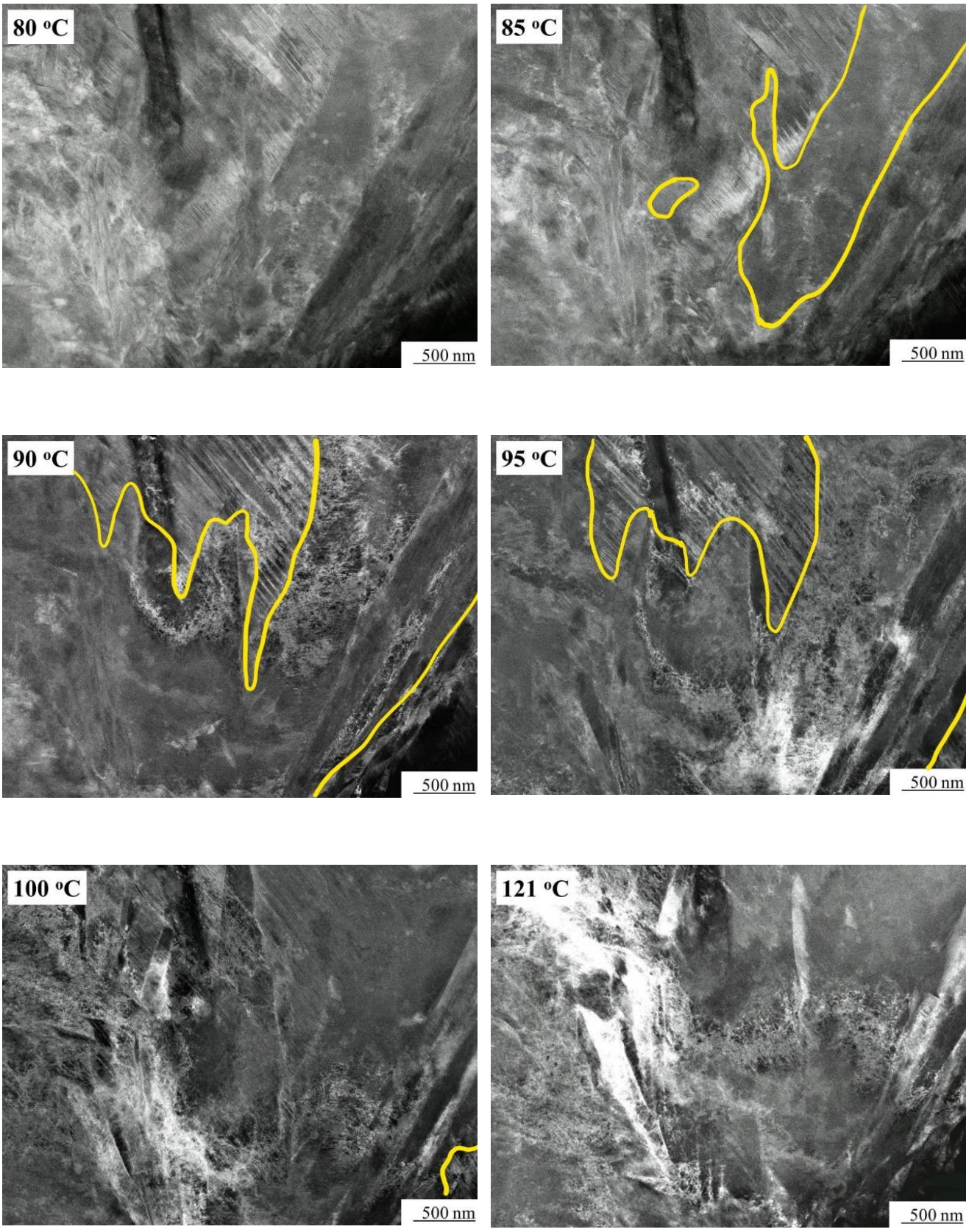

Figure 24. Martensite/Austenite boundaries (shown in yellow) at different temperatures during the second heating of the NiTi sample pre-deformed by 10% in the martensite state.

1.2. The influence of stress on the relationship between defect density and variation in the functional properties of NiTi alloy during thermal cycling under stress

In section 1.1., the relationship between defect density, their distribution, and the variations in the martensitic transformation temperature during thermo-cycling without stress was established. However, in practical applications, shape memory alloys must demonstrate strain variation under stress. Numerous studies show that during multiple thermal cycles through the martensitic transformation temperature range under load, the temperatures of martensitic transitions change. Additionally, reversible strain varies and irreversible strain accumulates [26, 81, 85, 115–120]. Furthermore, it has been shown that variations in the functional properties of NiTi alloy depend on the stress applied during thermal cycling. For instance, in [26], it was demonstrated that under a stress of 37 MPa during thermal cycling, the plastic strain in the alloy changed by 0.2% over 27 thousand cycles, while under a load of 186 MPa, the plastic deformation reached 2.2% in just 800 cycles. Thus, it is evident that the variations of defect density and functional properties during thermo-cycling under stress will differ from those observed without stress.

To develop a methodology for optimizing the temperature-stress-strain cycle for actuators, it is necessary to study the effect of stress on the relationship between dislocation density and functional properties during thermal cycling, which was one of the tasks of this dissertation. The results of this study are presented in section 1.2. and published in [51, 58, 59].

To investigate the influence of stress on the variation in defect density and functional properties, wire samples of $Ni_{50}Ti_{50}$ alloy were subjected to thermal cycling through the martensitic transformation temperature range under stresses of 50 and 200 MPa in the alloy. These loads were chosen so that one of them (50 MPa) was below the martensite reorientation limit, and the other (200 MPa) exceeded this value (the martensite reorientation limit for the investigated alloy was 126 MPa). This choice was based on the findings of [49], which showed that the variation in the properties of NiTi

alloy during thermal cycling under load depends on how the stress during thermal cycling relates to the martensite reorientation limit.

The $Ni_{50}Ti_{50}$ alloy samples were tested in a Lloyd 30 K Plus testing machine equipped with a thermal chamber. The samples were heated to a temperature T_1, at which the entire alloy was in the austenitic state, loaded to stresses of 50 or 200 MPa, and subjected to multiple thermal cycles under constant stress in the temperature range of martensitic transformation $T_1 \div T_2$. If the stress magnitude was 50 MPa, then $T_1 = 130°C$, if it was 200 MPa, then $T_1 = 180°C$. Regardless of the applied stress, $T_2 = 30°C$. From the deformation-temperature dependencies, the values of reversible deformation and accumulated plastic deformation were determined (Figure 25).

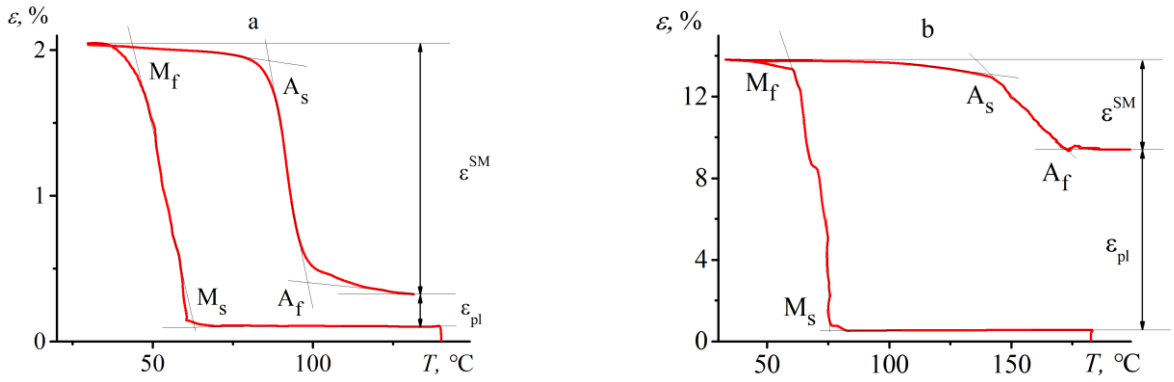

Figure 25. Strain-temperature dependencies obtained during cooling and heating of $Ni_{50}Ti_{50}$ alloy under constant stresses of 50 and 200 MPa.

To assess the change in defect density, variations in resistivity were measured at -196°C after 5, 10, 15, 20, and 30 thermal cycles. The study analyzed changes in plastic strain, the shape memory effect and martensitic transition temperatures values based on the variations in resistivity, which served as a measure of defect density.

Figure 26 shows the dependencies of $\Delta\rho/\rho(N)$ obtained during thermal cycling of NiTi shape memory alloy specimens under free conditions and under constant stress of 50 and 200 MPa. It can be observed that the resistivity varies nonlinearly in all samples, the main changes occur at the beginning of the thermal cycling.

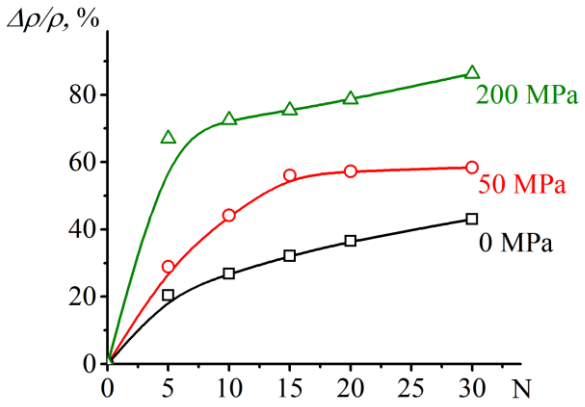

Figure 26. Dependencies of Δρ/ρ(N) obtained during thermal cycling of the $Ni_{50}Ti_{50}$ alloy under loads of 0, 50, and 200 MPa through the martensitic transformation temperature range.

The resistivity increase during thermal cycling under constant stress was greater than during thermal cycling in the free state. After 30 cycles under a stress of 50 MPa, the resistivity increased by 58%, and by 43% during thermal cycling in the free state. With an increase in the applied load to 200 MPa, the resistivity increase over 30 cycles was 86%. The increase in resistivity growth during cycling under stress compared to cycling in the free state is associated with the fact that during cooling under stress, the martensite crystals develop a preferred growth direction, reducing the possibility of elastic accommodation of internal stresses, and consequently increasing the defect density, which leads to an increase in resistivity.

The dependencies of plastic strain on the variations in resistivity (Δρ/ρ) obtained during thermal cycling under constant stress of 50 MPa and 200 MPa are shown in Figure 27. It can be seen that during cycling under a stress of 50 MPa, plastic strain increased linearly with increasing defect density until the value of ε_{pl} reached 2.3% (in the 15th cycle). With larger cycles, the slope of the dependence $\varepsilon_{pl}(\Delta\rho/\rho)$ increased. Apparently, the dislocation density reached some critical value where further dislocation multiplication became difficult. However, the accumulation of plastic strain continued due to the sliding of existing dislocations.

.

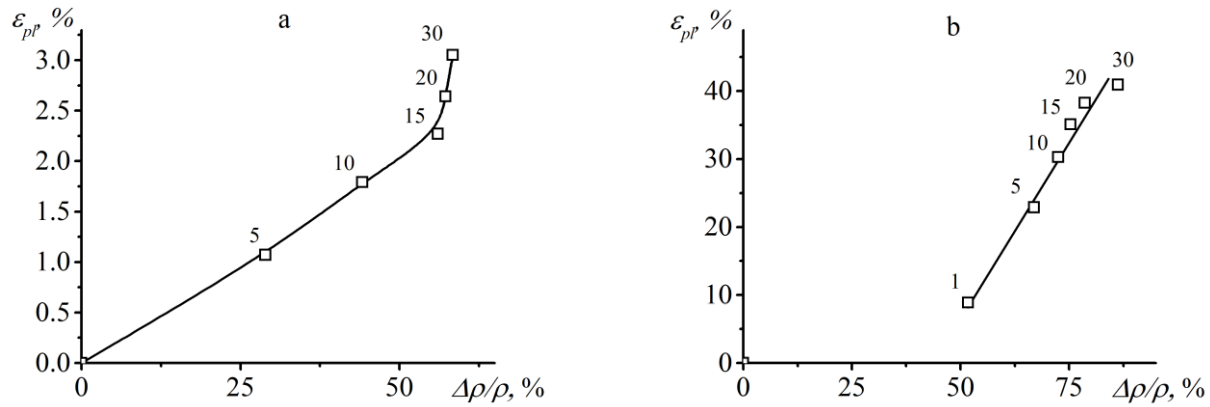

Figure 27. Dependencies of plastic strain values (ε_{pl}) on the variations in resistivity ($\Delta\rho/\rho$) obtained during thermal cycling under constant stress of 50 MPa (a) and 200 MPa (b). The numbers indicate the cycle number.

During thermal cycling under constant stress of 200 MPa, the main increase in dislocation density occurs already in the first cycle, where the l resistivity increases by 52%, and plastic deformation by 8.8%. With an increase in the number of cycles, the dependence of plastic strain on the variations in electrical resistivity (defect density) becomes linear.

Figure 28 shows the dependencies of the recovered strain (ε^{SM}) on the change in electrical resistivity ($\Delta\rho/\rho$) obtained during thermal cycling under constant stress of 50 MPa and 200 MPa. In the $\varepsilon^{SM}(\Delta\rho/\rho)$ dependence obtained during thermal cycling under a constant stress of 50 MPa, two linear sections can be distinguished. For $N < 15$, the slope is 0.04% ε^{SM} per 1 percent change in resistivity, while for $N > 15$, this value increases to 0.12% per 1% increase in resistivity. Similar to plastic strain, a sharp increase in the recovered strain occurred after the 15th cycle (Figure 27a).

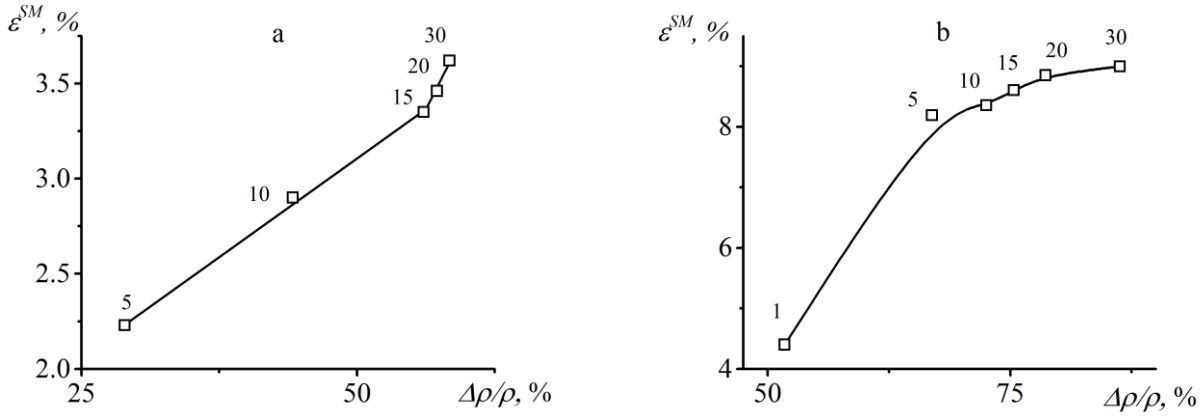

Figure 28. Dependencies of the recovered strain (ε^{SM}) on the change in electrical resistivity ($\Delta\rho/\rho$) obtained during thermal cycling under constant stress of 50 MPa (a) and 200 MPa (b). The numbers indicate the cycle number.

During thermal cycling under constant stress of 200 MPa, the dependence of $\varepsilon^{SM}(\Delta\rho/\rho)$ was nonlinear. This is attributed to the fact that by the fifth cycle, the ε^{SM} reached 8.2%, while the maximum theoretical strain for the B2↔B19' transformation is 11.2%, and the maximum observed reversible strain does not exceed 10% in polycrystals. Thus, by the fifth cycle, most of the newly formed martensite crystals were favorably oriented, leading to smaller changes in ε^{SM} with further increases in dislocation density.

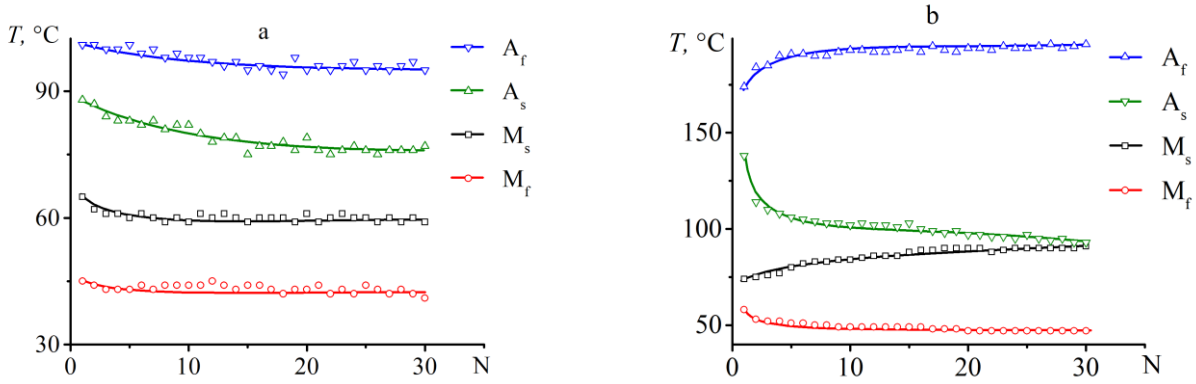

Figure 29. Dependencies of $A_s(N)$, $A_f(N)$, $M_s(N)$, and $M_f(N)$ during thermal cycling of the $Ni_{50}Ti_{50}$ alloy under a load of 50 MPa (a) and 200 MPa (b).

In Figure 29, the dependencies of the strain accumulation temperatures during cooling (M_s, M_f) and strain recovery temperatures during heating (A_s, A_f) are presented as a function of cycle number. It can be observed that during thermal cycling under a stress of 50 MPa, all M_s temperatures decrease with increasing thermal cycles, whereas

during cycling under a load of 200 MPa, A_s and M_f temperatures decrease, while M_s and A_f temperatures increase. The difference in the qualitative nature of these dependencies indicates a fundamental change in the mechanism of the effect of the defect structure on the transformation temperatures. Reference [41] suggests that the increase in the M_s value during thermal cycles under high stress is attributed to the evolving dislocation structure, which promotes the nucleation of favorable martensite variants during cooling. The increase in A_f values may be due to the damage of intermartensitic boundaries at the final stage of forward transformation, leading to the manifestation of the martensite stabilization effect (the stress of 200 MPa exceeds the values of the martensite reorientation limit in the NiTi alloy). Only a portion of the martensite undergoes reorientation. Martensitic variants with undamaged boundaries undergo transformations at "normal" temperatures, so they transform into austenite at low temperatures and are unaffected by the martensite stabilization effect.

On Figure 30, the dependencies of the martensitic transformation temperatures on the change in resistivity ($\Delta\rho/\rho$) are presented. The temperature M_s was not determined during thermal cycling in the free state due to the change in transformation sequence with an increase in the number of cycles (as described in section 1.1). It can be observed that the temperature M_f linearly decreases with increasing defect density in all cases, with the slope values being very close, approximately -0.16°C per 1% change in electrical resistivity, and independent of the applied stress (see Figure 30b). Similarly, the temperature A_s also linearly depends on the change in resistivity (defect density). Increasing the stress from 0 to 50 MPa does not affect the slope on the $A_s(\Delta\rho/\rho)$ curve, which was approximately -0.2°C per 1% change in resistivity. Increasing the stress from 50 to 200 MPa led to a threefold increase in the slope to -0.6°C/% (see Figure 30c). The slope on the $A_f(\Delta\rho/\rho)$ curve remains unchanged as the stress increases from 0 to 50 MPa and is approximately -0.2°C per 1% change in electrical resistivity, which is close to the values determined for the temperatures A_s and M_f. Increasing the stress from 50 to 200 MPa results in a change in the slope sign, with temperatures increasing rather than decreasing with increasing defect density (see Figure 30d). The same observations apply to the temperature M_s (see Figure 30a).

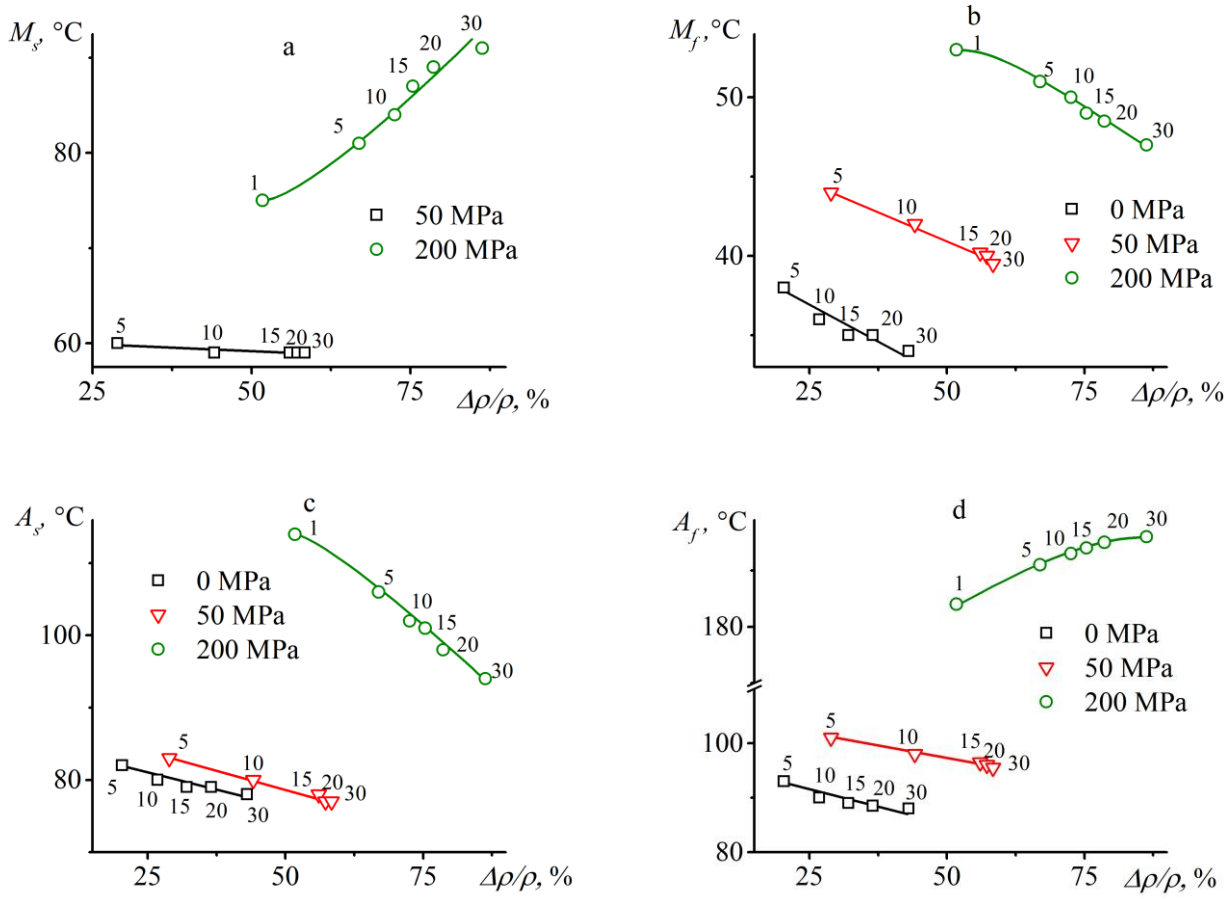

Figure 30. Dependencies of M_s (a), M_f (b), A_s (c), A_f (d) temperatures on the variations in resistivity (Δρ/ρ) obtained during thermal cycling of the NiTi alloy in the free state, under a constant load of 50 MPa, and 200 MPa.

Thus, the research results have revealed patterns in the variations in defect density and functional properties during thermal cycling under stress. It has been demonstrated that if the stress during thermal cycling is below the martensite reorientation limit, the variation in transition temperatures follow the same patterns as in stress-free thermal cycling. Changes in plastic strain are minor, while reversible strain increases by 1.6% over 30 cycles. If the stress during thermal cycling exceeds the reorientation limit, then the changes in transition temperatures qualitatively differ from those observed during stress-free thermal cycling. This is due to the significant plastic strain, which increases by 41% over 30 cycles. The reversible strain value more than doubles, which is associated with the increase in internal stresses, combining with external stresses to increase effective stress, leading to the growth of reversible strain. In conclusion, it is advisable not to select

stresses above the reorientation limit during thermal cycling, as otherwise, the functional properties of the NiTi alloy undergo significant changes, which is undesirable for devices intended for repeated use.

1.3. Influence of isothermal holdings on reversible and irreversible strain in NiTi shape memory alloy.

In section 1.1.1, it is shown that the holding of the NiTi alloy subjected to thermal cycling in the unstressed state affects the temperatures and sequence of martensitic transitions in the next cycle. This is due to the fact that recovery processes occur during the hold, resulting in changes in the distribution and density of dislocations. However, such changes will not only affect the parameters of martensitic transitions but also functional properties, such as reversible and irreversible strain. This issue has not been previously investigated, although the values of these quantities are important parameters for devices with multiple actions, as the reversible strain values affects the movement of the working element, and the accumulation of irreversible strain changes the geometric dimensions of the element. Therefore, one of the tasks of the dissertation was to investigate the effect of temperature and duration of holding under a load of 50 MPa on changes in reversible and irreversible strain. The results are published in [51].

Wire samples of the $Ni_{50}Ti_{50}$ alloy with a length of 120 mm and a diameter of 0.5 mm, quenched in water from a temperature of 700°C and annealed at a temperature of 500°C for 1 hour, were heated to 140°C, loaded to 50 MPa, and cooled to 25°C (lines 1-2, Figure 31a). Then, they were heated to a temperature T_h, which was 130°C, 160°C, or 200°C, at which the alloy was in the austenitic state (line 2-3 in Figure 31a). The sample was then held at this temperature T_h for 0, 15, 30, 60, or 120 minutes (lines 3-4). After that, the sample was cooled to 25°C and heated again to T_h (lines 4-5-6). The vertical lines indicate the time interval of isothermal aging.

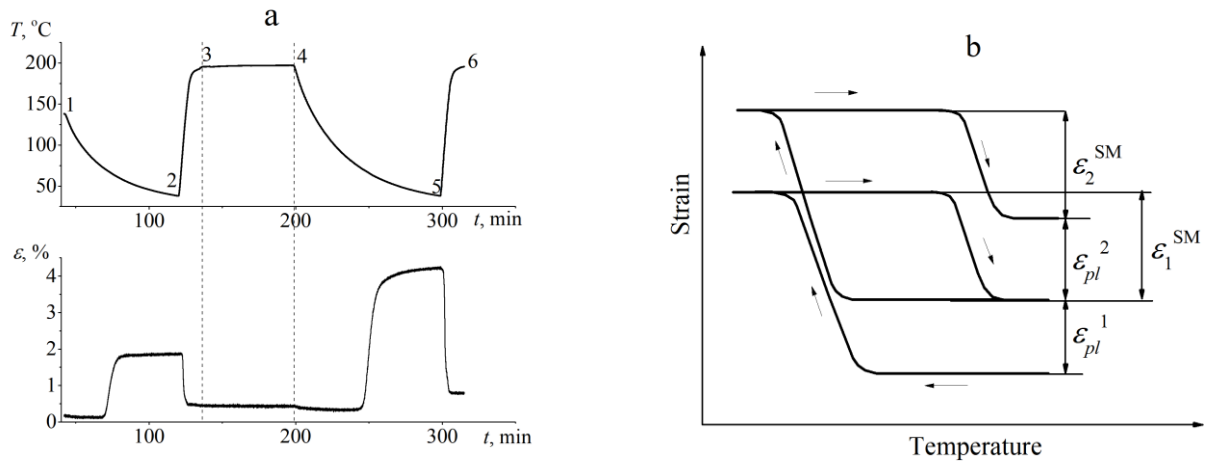

Figure 31. Dependencies of temperature and strain over time measured in the $Ni_{50}Ti_{50}$ alloy using isothermal holding at a temperature of 200°C during thermal cycling (a). Scheme of measuring reversible (ε^{SM}) and irreversible (ε_{pl}) strains in the thermal cycle before (indicated as 1) and after (indicated as 2) isothermal holding (b).

According to the dependencies of strain on temperature, the values of reversible strain were determined as the shape memory effect ε^{SM} and irreversible strain ε_{pl}, which represents the strain that did not return upon heating in the thermal cycle before and after holding, as shown in Figure 31b. The values of $\varepsilon^{SM*} = \varepsilon_2^{SM} / \varepsilon_1^{SM}$ and $\varepsilon_{pl}* = \varepsilon_{pl}^{2} / \varepsilon_{pl}^{1}$ were calculated, where the superscript 1 corresponds to the values measured before aging, and the subscript 2 corresponds to the values measured after aging.

Figure 32a illustrates the dependency of ε^{SM*} on the duration of holding at different temperatures. It can be observed that an increase in the maximum cycle temperature, T_h, even without aging (t=0), leads to an increase in reversible strain in the subsequent thermal cycle. Since no holding was performed, this increase in reversible strain is associated with the manifestation of the training effect. It was established that the higher the temperature in the cycle, the more intense the training process occurs, and the greater the increase in reversible strain with cycles. Thus, if the temperature T_h = 130°C is reached in the cycle, ε^{SM*} equals 1.1, meaning that the reversible deformation measured in the second cycle is 1.1 times greater than in the first cycle.

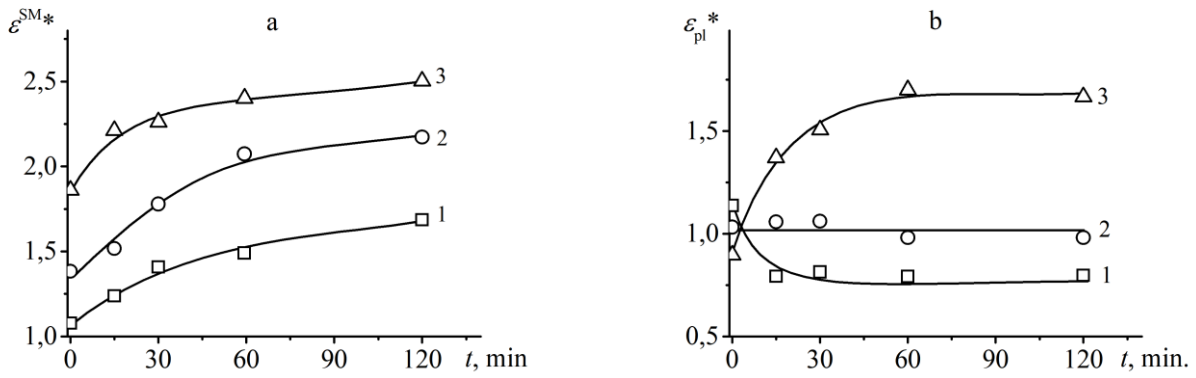

Figure 32. Dependencies of the values of ε^{SM}* (a) and ε_{pl}* (b) on the duration of holding, obtained for the $Ni_{50}Ti_{50}$ alloy. Holding was conducted at temperatures of 130°C (curve 1), 160°C (curve 2), or 200°C (curve 3).

If the maximum temperature in the cycle is 200°C, then the value of ε^{SM}* is 1.8. Similar effects of the maximum temperature of the thermal cycle on the values of shape memory effect were observed in [123]. Holding at the maximum temperature in the cycle additionally increases the reversible strain, and the longer the holding duration, the greater the increase in reversible strain in the cycle after aging compared to the cycle before aging. The increase in reversible strain means that in the second cycle, the volume fraction of oriented martensite crystals has increased. On the other hand, the increase in the volume fraction of oriented martensite crystals may be caused by an increase in stress. Since the value of external stress is constant, the increase in effective stress occurs due to the increase in internal stresses. However, there are no clear reasons that would lead to an increase in internal stresses with increasing upper temperature in the cycle. According to [123], increasing the maximum temperature of the thermal cycle leads to the intensification of relaxation processes. This is likely accompanied by a restructuring of the dislocation structure, leading to an increase in internal stresses; however, this requires further investigation.

Figure 32b shows the dependence of the value of ε_{pl}* on the duration of holding, the appearance of which depends on the temperature at which the aging was conducted. The higher the maximum temperature of the thermal cycle, the less irreversible strain accumulated in the second cycle if aging between cycles was not conducted. On the other hand, increasing the duration of isothermal holding reduces irreversible strain if holding

is conducted at 130°C; it does not affect irreversible strain when holding at 160°C and increases irreversible strain when holding was at 200°C.

Thus, the results of the study have shown that by controlling the maximum temperature of the thermal cycle, the duration and temperature of intermediate holding, it is possible to control not only the temperatures and sequence of martensitic transformations, as shown in section 1.1.1, but also the values of reversible and irreversible strain in NiTi alloys during thermal cycling. This is achieved by controlling the contribution of softening to the process of increasing defect density.

1.4. Variations in the SMA properties during multiple thermal cycling in the work production cycle.

During thermal cycling under constant stress, shape memory alloys (SMAs) are utilized in many repeated actions devices. However, in such a mode, the alloy does not produce useful work, as the work expended during cooling is greater than or equal to the work accomplished during heating. Nevertheless, SMAs can produce useful work, enabling their application as the working element of a thermal engine that directly converts thermal energy into mechanical energy, known as a martensitic engine [9,124]. The possibility of using SMAs for the production of such engines is based on the materials' ability to recover strain under opposing forces. To increase the positive work balance in the thermal engine's operating cycle, it is necessary to reduce the work expended on pre-deformation and increase the work produced during heating as a result of strain recovery. This can be achieved by cooling the sample under constant stress τ_o in the temperature range of forward martensitic transformation and heating it under higher stress τ_h ($\tau_h > \tau_o$) in the temperature range of reverse martensitic transformation [117,124–127]. In [117], it is shown that the Ti-Ni-Cu alloy produces useful work exceeding 10 MJ/m^3. However, significant irreversible strain accumulates during the thermal cycling of the sample. For example, 30 thermal cycles of cooling under 50 MPa stress and heating under 300 MPa stress (in torsion mode) resulted in a 120% accumulation of plastic strain. The accumulation of irreversible strain negatively impacts the parameters of the thermal engine due to changes in the working body's characteristics, such as geometric dimensions and temperatures for the realization of shape memory effects, requiring adjustments to the thermal engine's design and preventing its use in fully automatic mode.

In [39], to reduce plastic strain, it was proposed to use a symmetric cycle in which the stress applied to the sample in each even cycle would be opposite to the stress in odd cycles. In this case, irreversible strain would accumulate in the opposite direction in each cycle, resulting in less overall accumulation of residual plastic strain. It has been shown that the symmetric thermal cycling scheme, implemented in Ti–51.5 at.% Ni and Ti–50.0

at.% Ni alloys, significantly reduced the accumulation of irreversible strain while maintaining high performance. For instance, in the Ti–51.5 at.% Ni alloy, the amount of plastic strain accumulated in the sample after 30 thermal cycles in the "symmetric" scheme, heating under 400 MPa stress, was less than the strain accumulated after 30 thermal cycles in the "asymmetric" scheme, heating under a load of 200 MPa. It is worth noting that despite the successful application of the "symmetric" working cycle to reduce the accumulation of irreversible strain in one direction, the use of this scheme does not reduce the variation in defect density during thermal cycling. Additionally, the practical implementation of the symmetric scheme proves challenging as it requires a mechanism for constantly changing the direction of the applied load. Therefore, the use of an asymmetric (conventional) cycle, in which the load acts in the same direction during both cooling and heating, remains preferable.

Since the properties of equiatomic NiTi-based alloys vary during thermal cycling, and as the results of section 1.2. show, the higher the stresses, the more significant the property changes, it makes sense to consider using other alloys instead of NiTi-based ones. Recently, alloys based on Ni-Fe-Ga Heusler alloys have attracted wide attention, first synthesized in 2002 [128], as possible alloys exhibiting magnetic shape memory and possessing increased ductility compared to Ni2MnGa alloys. However, it was found that the reversible strain in Ni_2FeGa alloys, which can be initiated by a magnetic field, is small due to the high value of the reorientation stress [129]. Nevertheless, it was discovered that these materials exhibit excellent functional properties, such as a wide temperature range of superelasticity, large reversible strain (up to 12% [130,131]), and high stability of functional properties during mechanical and thermal cycling [130,132–135]. It can be assumed that these alloys may be applicable as the working body of a martensitic engine or actuators. The functional properties of Ni-Fe-Ga-based alloys have been well studied [130,131,134–141], but their work production has not been investigated. To assess the prospects of replacing NiTi-based alloys with Ni-Fe-Ga-based alloys as power elements of thermal engines or actuators, the performance of single crystals of Ni_2FeGa alloy was studied in the dissertation, as polycrystalline samples proved to be very brittle and unsuitable for application. The research results are published in [62–64].

The study focused on single crystals of the $Ni_{55}Fe_{18}Ga_{27}$ alloy with [001] and [011] orientations, grown using the Czochralski method. The samples underwent quenching at 900°C for 20 minutes in water and annealing at 600°C for 2 hours. After this heat treatment, the $Ni_{55}Fe_{18}Ga_{27}$ alloy contained a primary martensitic phase 10M and secondary γ phase particles (Figure 33a). The presence of 10M martensitic phase reflexes in the X-ray diffraction pattern obtained at room temperature indicates that the alloy underwent L21↔10M transformation. L_21 cubic lattice, characteristic of Heusler alloys [142], transforms into a modulated tetragonal martensite [142–144] upon cooling. In modulated structures, unlike simple tetragonal structures, atomic positions deviate periodically; the number indicates the modulation period. Differential scanning calorimetry data (Figure 33b) determined the martensitic transition temperatures: M_s = 50°C, M_f = 40°C, A_s = 53°C, and A_f = 63°C.

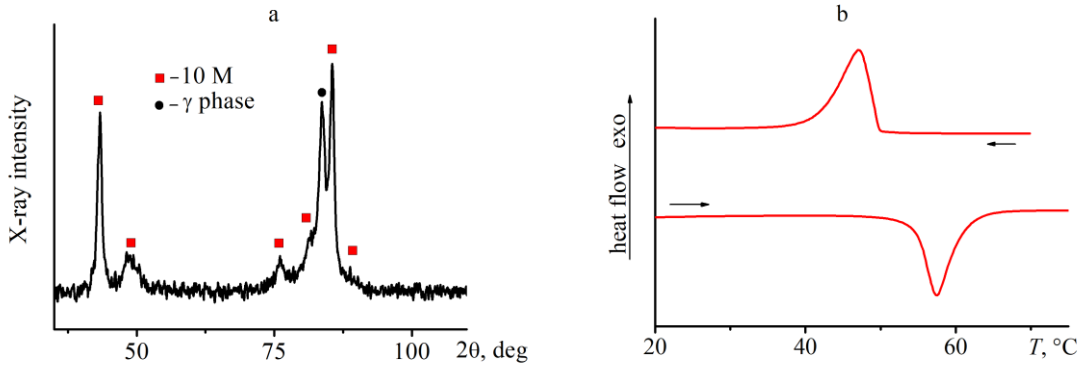

Figure 33. X-ray diffraction pattern obtained at room temperature (a) and calorimetric curves obtained during cooling and heating (b) of the [001] oriented single crystal of $Ni_{55}Fe_{18}Ga_{27}$ after annealing at 600°C for 2 hours. [62]

Before investigating the performance of these alloys, it was necessary to study their functional properties, which may depend on both the crystal growth method and its orientation. To examine the functional properties, samples sized 3x3x6 mm were cut from the grown crystals (using electrical discharge machining), with the long axis parallel to the [001] or [011] axis. Tests were conducted under compression using a "Lloyd 30k Plus" testing machine equipped with a reverse frame for compression, a thermal chamber, and a video extensometer. At room temperature, where the crystal was in the martensitic

state, the sample was compressed along the long axis to a certain strain value, unloaded, and heated to 140°C. From the ε(T) dependencies, the recovered strain (shape memory effect) and irreversible strain were measured, as shown in Figure 25.

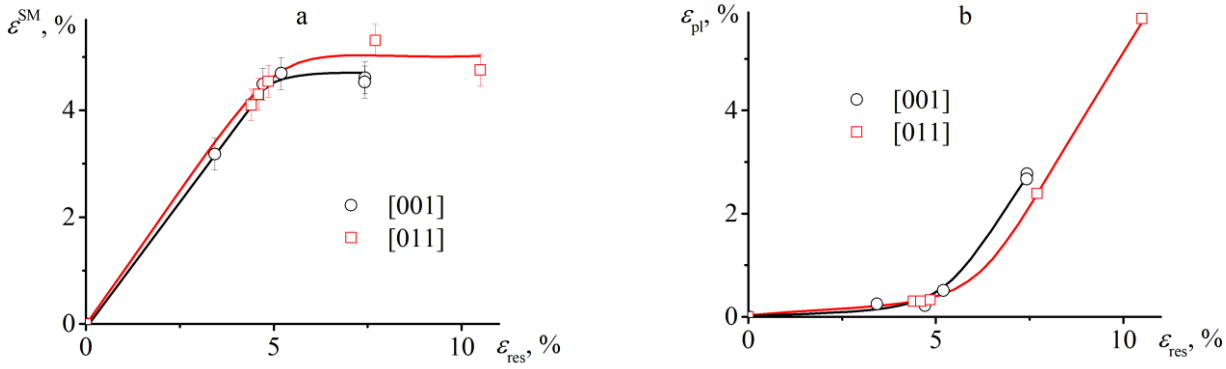

Figure 34. Dependencies of the shape memory effect ε^{SM} (a) and irreversible strain (ε_{pl}) (b) on residual strain (ε_{res}) obtained for samples of $Ni_{55}Fe_{18}Ga_{27}$ crystals in [001] and [011] orientations.

Comparison of dependencies of the shape memory effect and irreversible strain on residual strain is presented in Figure 34. It can be observed that the crystal orientation practically does not affect the shape of these dependencies $\varepsilon^{SM}(\varepsilon_{res})$. The maximum recoverable strain (shape memory effect) is 4.7% in [001] oriented crystals and 5% in [011] oriented crystals (Figure 34a). If the residual strain did not exceed 5%, the plastic strain was not more than 0.3%. If the residual strain exceeded 5.5%, plastic strain actively accumulated in the alloy, with a value exceeding 2%. Thus, it is evident that to avoid the accumulation of irreversible strain in the alloy, it is necessary to limit the residual strain to 5%. Since in this case, the orientation of the single crystal does not affect the functional properties, the performance evaluation was conducted on [001] oriented single crystals. To allow for load variation in the cycle, the performance evaluation was conducted in a torsional mode.

Samples of [001] single crystal with square cross-sections sized 2×2×40 mm (long axis parallel to [001]) were cooled to 23°C under constant stress τ_{cool}, then loaded to 150 MPa and heated again to 140°C, followed by unloading to τ_{cool}, and repeating the cycle. The stress value during cooling (τ_{cool}) was varied from 0 to 100 MPa, and heating was always carried out under a stress of 150 MPa, as heating under higher stress leads to active

accumulation of irreversible strain and premature failure of the samples. For instance, increasing τ_{cool} to 200 MPa during the thermal cycling of the $Ni_{55}Fe_{18}Ga_{27}$ single crystal led to sample failure in the second cycle. The value of stress in the outer layer was estimated as $\tau = \frac{M}{0.208*a^3}$, where M — the applied torque, a — the width of the sample (2 mm). Shear strain was calculated as $\gamma = \frac{\varphi*a}{2*l} * 100\%$, where φ — the angle of rotation, and l — the length of the sample.

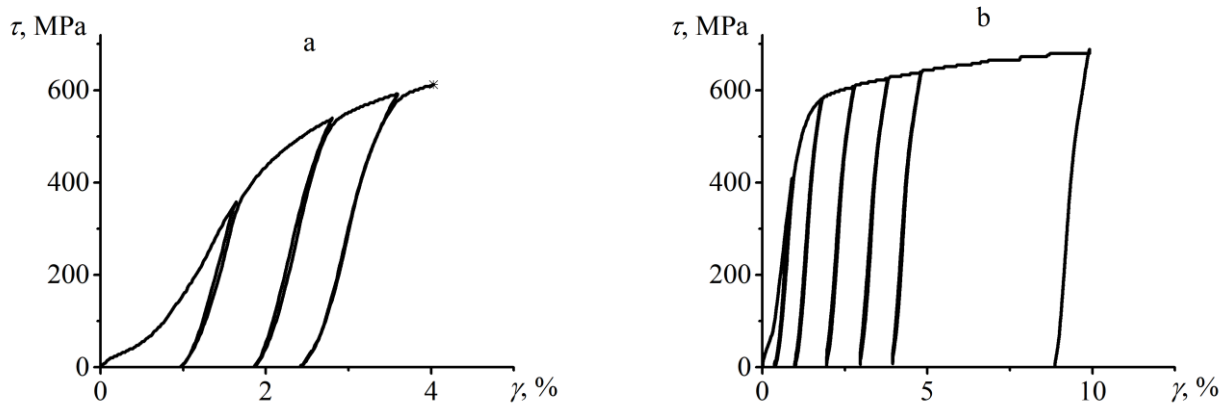

Figure 35. Deformation diagrams of [001] single crystal $Ni_{55}Fe_{18}Ga_{27}$ obtained in torsion mode at temperatures of 23°C (a) (martensite state) or 140°C (b) (austenite state).

Figure 35 depicts deformation diagrams obtained in torsion mode for a single crystal of $Ni_{55}Fe_{18}Ga_{27}$ alloy with [001] orientation at temperatures of 23°C (in the martensite state) and 140°C (in the austenite state). It can be observed that the deformation curve obtained for the alloy in the martensite state exhibits a small plateau at 20 MPa (Figure 35a). This might be associated either with martensitic reorientation or with intermartensitic transformations 10M↔14M. The dislocation yield strength in the martensite state was 492 MPa, with a deformation to failure of 4%. When deforming in the austenite state, a plateau at 15 MPa was observed on the τ(γ) curve (Figure 35b), which may be related to the formation of a small volume of tetragonal martensitic phase under load, as noted in [134,140,145]. The dislocation yield strength at a temperature of 140°C was 585 MPa, with a deformation to failure of 15.2%.

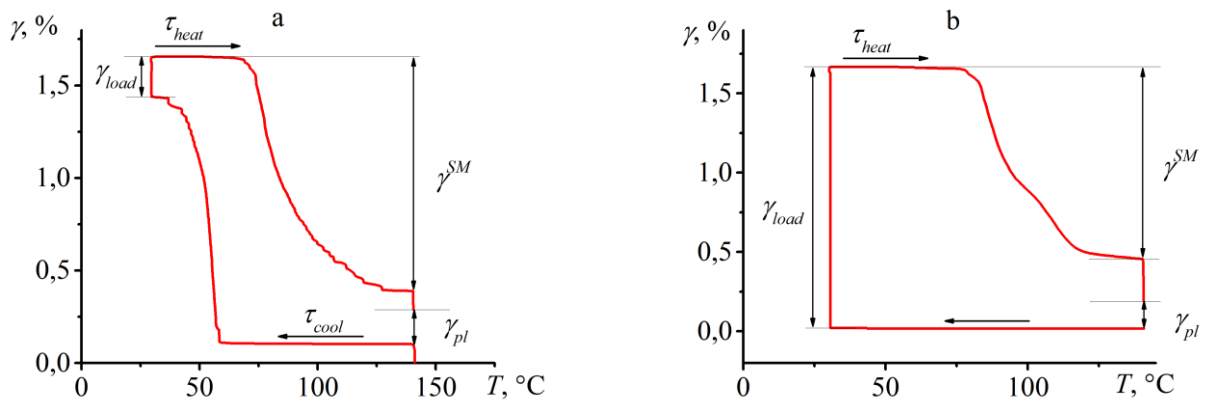

Figure 36. Strain-Temperature dependencies obtained in the first thermal cycle for a single crystal [001] of $Ni_{55}Fe_{18}Ga_{27}$, cooled under constant stress of 100 MPa (a) and without load (b), deformed to 150 MPa and heated under stress of 150 MPa.

Figure 36 depicts strain-temperature dependencies obtained in the first thermal cycle, where cooling was conducted under a load of 100 MPa (a) or without stress (b). Subsequently, the sample was loaded to 150 MPa and heated under a constant stress of 150 MPa. In Figure 36a, it can be observed that the sample accumulated strain during cooling in the temperature range of the forward martensitic transformation. With an increase in stress from 100 to 150 MPa, the sample accumulated additional strain – γ_{load}. During subsequent heating, the shape memory effect was realized, and the sample recovered deformation - γ^{SM}. Since the recovery of deformation was not complete, irreversible deformation (γ_{pl}) was measured after heating and unloading to 100 MPa. If the sample was cooled without stress (Figure 36b), deformation upon loading occurred due to martensite reorientation, and then it partially recovered during heating.

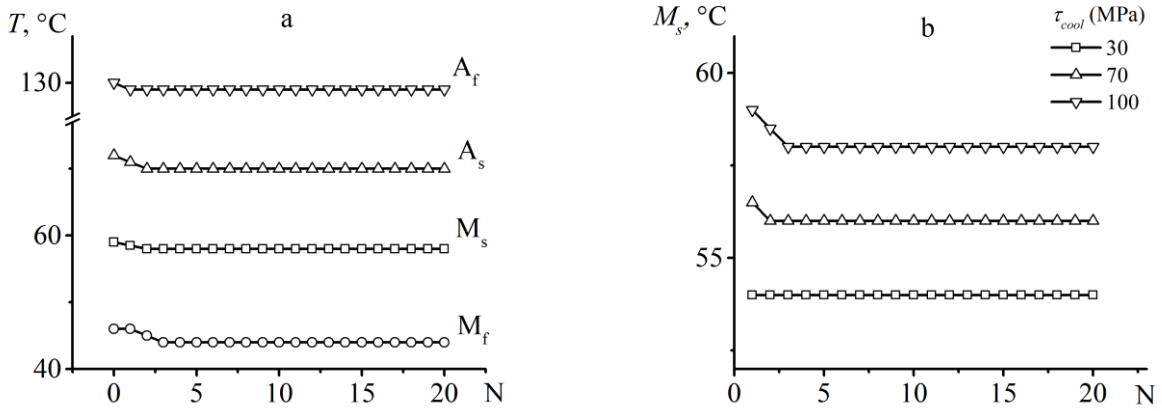

Figure 37. Dependencies of martensitic transformation temperatures on the cycle number obtained for the single crystal $Ni_{55}Fe_{18}Ga_{27}$ with [001] orientation at τ_{cool} = 100 MPa and τ_{heat} = 150 MPa (a), and dependencies of the start temperature of the forward martensitic transformation (M_s) on the cycle number obtained during cooling under different stresses (b).

Variations in the temperatures of martensitic transformations during cycling, where τ_{cool} = 100 MPa and τ_{heat} = 150 MPa, are shown in Figure 37a. It can be observed that all temperatures decrease during the first few cycles and then stabilize. Figure 37b presents the dependencies of the start temperatures of the forward transformation M_s on the cycle number obtained during cycling at different values of τ_{cool}. Increasing τ_{cool} leads to an increase in the M_s temperature according to the Clausius-Clapeyron equation with a coefficient of $dM_s/d\tau$ = 0.086 °C/MPa. It has been established that, despite the different stress levels during cooling, the M_s temperature changes only in the first few cycles and then remains constant. The other temperatures of martensitic transformations vary during cycling similarly to the M_s temperature. Thus, during cycling, the parameters of martensitic transformations in single crystals of the $Ni_{55}Fe_{18}Ga_{27}$ alloy with [001] orientation remain stable compared to NiTi alloys.

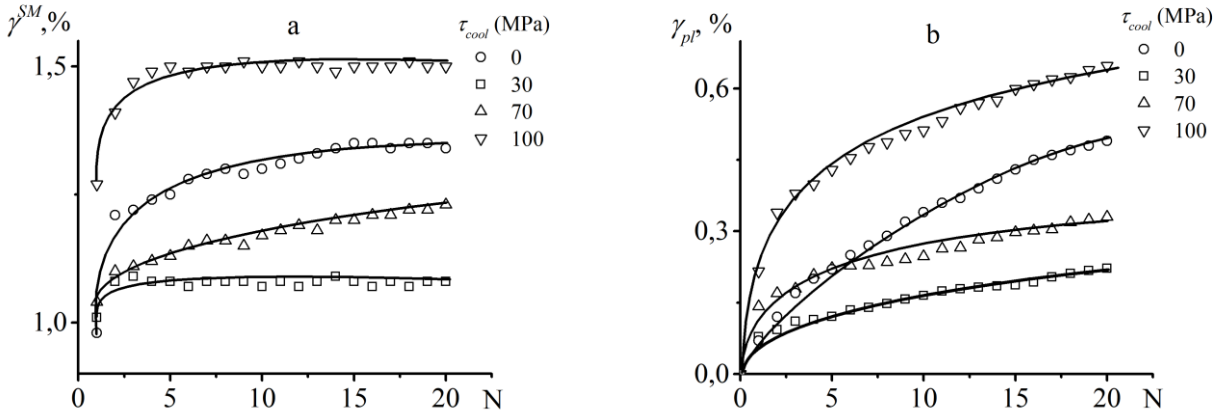

Figure 38. Dependencies of the values of γ^{SM} (a) and γ_{pl} (b) on the cycle number obtained during cycling of single crystals of $Ni_{55}Fe_{18}Ga_{27}$ with [001] orientation.

Figure 38a illustrates the dependencies of the values of the shape memory effect (γ^{SM}) on the number of cycles for various values of the cooling stress (τ_{cool}). It can be observed that regardless of the value of τ_{cool}, the values of γ^{SM} increase during cycling, except for τ_{cool} = 30 MPa, where the deformation only increased in the first three cycles and then remained constant. Overall, it can be noted that the change in reversible strain during cycling is less compared to NiTi-based alloys.

In Figure 38b, it is shown that irreversible strain accumulates with an increase in the number of cycles. The magnitude of the cooling stress (τ_{cool}) influenced plastic strain non-monotonically. The smallest value of irreversible strain was obtained at τ_{cool} = 30 MPa, whereas the maximum value of irreversible strain was found at τ_{cool} = 100 MPa. The irreversible strain value at τ_{cool} = 0 MPa (0.5% in the 20th cycle) was greater than at τ_{cool} = 30 MPa (0.22% in the 20th cycle). Therefore, the reorientation of martensitic variants in the $Ni_{55}Fe_{18}Ga_{27}$ alloy during deformation in the martensitic state is accompanied by the accumulation of greater plastic strain than when oriented martensite is formed directly from austenite during cooling under constant stress. Thus, despite the fact that in the $Ni_{55}Fe_{18}Ga_{27}$ alloy during cycling, variations in reversible strain (γ^{SM}) and martensitic transformation temperatures (M_s) are less than in NiTi, the accumulation of plastic strain occurs, similar to cycling in binary NiTi alloys.

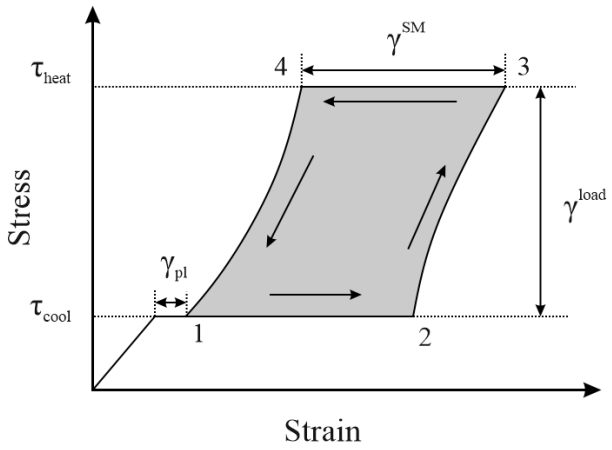

Figure 39. Scheme for calculating the performance of the alloy based on the stress-strain diagram.

Since the strain recovery during heating occurs under a higher stress than the stress required to accumulate strain during cooling, the alloy performs useful work in each thermocycle [117,126,127]. The working cycle is presented in Figure 39 in the "stress-strain" coordinates: work is expended to accumulate strain during cooling under constant stress (path 1-2 in Figure 39) and upon loading to 150 MPa (2-3) at room temperature. The specimen performs work during heating, recovering strain under a stress of 150 MPa (3-4 in Figure 39), and unloading to τ_{cool} (path 4-1). Useful work can be calculated as the difference between total and expended work, which equals the area marked by the gray fill in Figure 39 [117,126,127]. Figure 40 shows the dependencies of the useful work values on the cycle number. It can be seen that thermocycling leads to an increase in performance, regardless of the stress value during cooling. The maximum performance in the 20th cycle was 1.15 MJ/m^3 at τ_{cool} = 30 MPa.

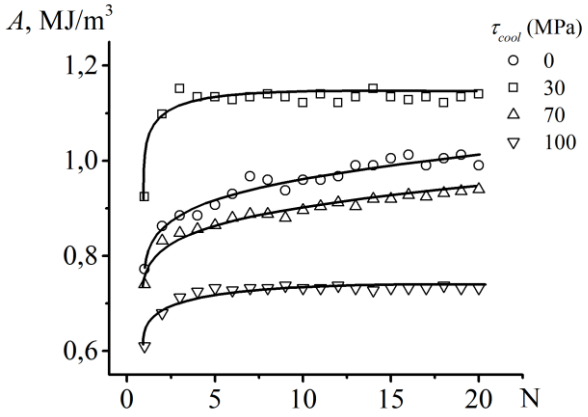

Figure 40. Dependencies of useful work on the cycle number for the [001] single crystal of $Ni_{55}Fe_{18}Ga_{27}$, obtained during cooling under constant stress τ_{cool} and heating under stress of 150 MPa.

Thus, the research results indicate that [001] $Ni_{55}Fe_{18}Ga_{27}$ single crystals cannot compete with NiTi-based alloys as the material for the working body of a martensite engine. The maximum value of γ^{SM} during the twisting of the $Ni_{55}Fe_{18}Ga_{27}$ single crystal is 1.5%, significantly lower than in equiatomic NiTi alloy, where γ^{SM} reaches 8.5% at τ_{cool} = 50 MPa and τ_{heat} = 200 MPa [126]. The maximum useful work in the $Ni_{55}Fe_{18}Ga_{27}$ alloy is nine times less than in NiTi-based alloys [126,127,146]. It is worth noting that the growth of single crystals is a labor-intensive and expensive process, and in the polycrystalline state, the $Ni_{55}Fe_{18}Ga_{27}$ alloy is so brittle that its practical application becomes impossible. Obviously, the search for new shape memory alloy systems with stable properties will continue, but so far, none of the new alloys has surpassed the combination of properties of NiTi-based alloys. Therefore, methods for improving the stability of their properties need to be developed.

1.5. Conclusions to Chapter 1

In the first chapter, the relationship between variations in defect density during thermal cycling and the functional properties of NiTi alloy (Martensitic Transformation (MT) temperatures, reversible and irreversible strain, useful work) is examined. Based on the results of this chapter, the following conclusions can be drawn:

1. Dependencies of MT temperatures changes on defect density are nonlinear, indicating additional factors influencing transformation temperatures during thermal cycling. A stationary region, where a linear dependence of transformation temperatures on defect density is observed, begins from the 5^{th} cycle.
2. The rate of transformation temperature variations in NiTi alloy with increasing defect density depends on the maximum temperature in the cycle. The higher the maximum temperature, the smaller the change in MT temperatures in the initial cycles, but the greater the changes in temperatures with increasing defect density in the stationary region where a linear relationship between transformation temperatures and dislocation density is observed. Since dislocation density increases slower in cycles with a maximum temperature of 200°C compared to those with a maximum temperature of 140°C, while temperatures increase faster with increasing dislocation density, this indicates that redistribution of defect density during heating from 140°C to 200°C also influences the transformation temperatures.
3. Isothermal holding in the martensite and austenite states of NiTi alloy, where a defects structure was formed during thermal cycling, leads to partial restoration of the alloy's properties. After holding, transformation temperatures increase, and restivity decreases. Holding under stress allows control of reversible strain and irreversible strain values by changing the intensity of structure relaxation (softening).
4. The dislocation structure formed during thermal cycling is unstable and changes with variations in the maximum cycle temperature, holding, or changes in stress.

This is because during thermal cycling, dislocations form in the austenitic phase, where the yield stress is lower than in the martensitic phase. The martensitic phase inherits the dislocation structure of the austenitic phase, leading to high internal stresses that relax with temperature changes or holds, and change during phase transition. This results in changes in the defective structure, particularly in the initial cycles, leading to additional reduction in transformation temperatures.

5. Direct observations of interphase boundary movement during cooling and heating of NiTi alloy in an electron microscope column showed that on thermal cycling of annealed NiTi alloy, there is no correspondence between the sequences of crystal appearance during cooling and their disappearance during heating. Moreover, no microstructural memory is observed, i.e., the martensite structure is not reproduced during thermo-cycling. This may be caused by the redistribution of defects, which leads to variation in internal stresses and additionally affects the transformation temperatures. If a dislocation structure is formed in the alloy during active deformation, microstructural memory is observed, and there is correspondence between the sequences of martensite crystal appearance during cooling and their disappearance during heating.
6. If thermal cycling is performed under a stress of 50 MPa, which is below the martensite reorientation limit, the dependences of transformation temperature on defect density are the same as those during thermal cycling without load. Reversible strain in the cycle is small and does not exceed a few percent. However, if thermal cycling is conducted under a stress of 200 MPa, exceeding the martensite reorientation limit, the dependencies of MT temperatures on defect density qualitatively change: temperatures A_s and M_f decrease, while temperatures A_f and M_s increase with increasing defect density. The value of reversible strain in the cycle doubles, and the plastic strain accumulated over 30 cycles exceeds 40%.
7. Single crystals of Ni_2FeGa alloy demonstrate better stability of functional properties during thermal cycling compared to NiTi alloys; however, the useful work they produce is an order of magnitude lower.

Chapter 2. Variations in the NiTi SMA properties during thermal cycling under constant stress through the range of incomplete martensitic transformations

The main method of enhancing the stability of NiTi alloy properties is by increasing the dislocation yield strength. However, as demonstrated by the results of Chapter 1, not only the density of dislocations affects the changes in transition temperatures during thermo-cycling, but also their distribution (configuration). Therefore, increasing the dislocation yield strength may not always have a positive effect on the stability of NiTi alloy properties. It is necessary to develop other alternative methods to improve the stability of functional properties of NiTi-based alloys for use in multi-action devices. One such alternative method is to limit the temperature range of thermal cycling. For instance, in [147], it was shown that thermal cycling of $Ni_{50.2}Ti_{49.8}$ alloy through an incomplete temperature range of the forward transformation leads to a smaller shift in the martensitic transformation temperatures compared to thermal cycling through the full transformation range. It was suggested that thermal cycling through an incomplete temperature range of the forward transformation results in significantly less material damage. In other words, during thermal cycling in an incomplete transition interval, the change in dislocation density will be smaller than during thermal cycling in a full range. In this case, the variaitons in the properties of NiTi alloy during thermal cycling should depend on the fractions of the temperature transition range. It can be assumed that the patterns of changes in the properties of NiTi alloys during thermal cycling will depend differently on the proportion of forward and reverse transition ranges since the increase in dislocation density during forward and reverse transitions may be caused by different reasons. These questions remain unexplored to date. However, knowledge about the dependence of functional properties of NiTi alloy on the proportion of the temperature interval of forward or reverse transitions would allow the development of recommendations for choosing the optimal temperature cycling interval that would ensure the best stability of functional properties. Thus, one of the tasks of this study was

to investigate the influence of the fraction of the temperature interval of forward and reverse transitions on the changes in transition temperatures, reversible and irreversible strain, and the work performed during heating during thermo-cycling under constant stress. The results of the study are presented in this chapter and published in works [58–60].

2.1. Thermal cycling of the $Ni_{50}Ti_{50}$ alloy under constant load in the temperature range of incomplete forward martensitic transformation.

The influence of the fraction of forward transformation on the variations in the properties of the NiTi alloy during thermal cycling in the free state has already been studied in several works. For example, in the study [147], it was found that the reduction in the A_s temperature after 80 cycles through an incomplete temperature range of forward transformation is less than after 40 cycles through the full temperature range (Figure 40).

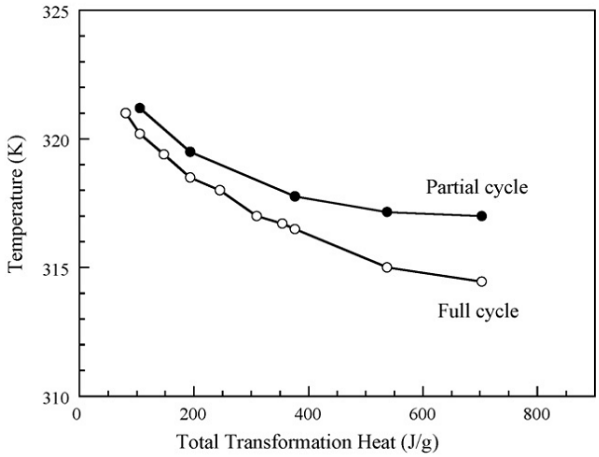

Figure 41. Dependence of the change in the A_s temperature on the total accumulated transformation heat during thermal cycling in the temperature range of full and incomplete forward martensitic transformation [147].

In [61], the authors investigated the effect of thermal cycling through an incomplete temperature range of the forward transition on the properties of $Ni_{50}Ti_{50}$ alloy. It was found that the M_s temperature always decreases from 64.5°C to 59°C, regardless of the fraction of the forward martensitic transformation implemented in the "partial cooling" cycles (Figure 41). However, the smaller the fraction of the forward transformation, the more "partial cooling" cycles are required to decrease the M_s temperature to 59°C. Nevertheless, the difference in the number of cycles at which the M_s temperature reaches 59°C is small. For example, if 75% of the forward martensitic transformation is achieved during cooling (ΔT = 4.5°C), then M_s = 59°C is reached starting from the 7th cycle, similar to thermal cycling through the full range of martensitic transformations. If the

fraction of the forward martensitic transformation is 10% (ΔT = 0.8°C), then M_s = 59°C is reached by the 10th cycle. The temperature of 59°C corresponds to the onset temperature of the B2→R transformation, which is stable [87,127]. Thus, the change in the M_s temperature during thermal cycling ceased as soon as the transformation type changed from B2→B19′ to B2→R.

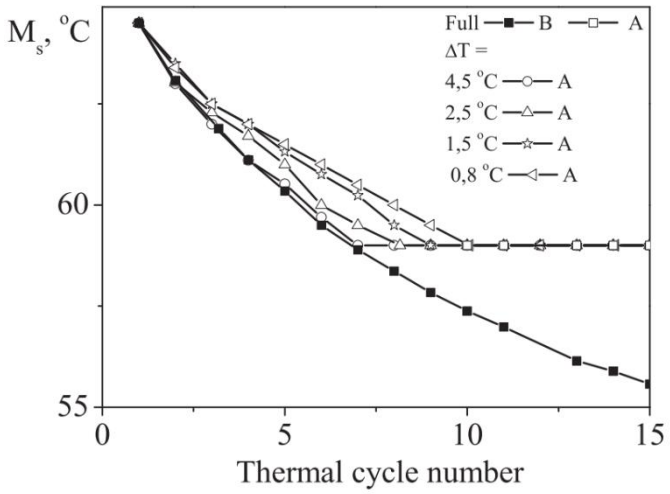

Figure 42. Dependencies of the temperatures of the onset of the forward martensitic transformation M_s, determined by the tangent method using the first peak on the DSC curve (A) and the second peak (B), on the number of "partial cooling" cycles, where cooling was interrupted at T* = M_s - ΔT. The values of ΔT are indicated in the figure [61].

Thus, prior to this study, little attention has been paid to examining the relationship between the fraction of the temperature range of the forward transition and the variations in the properties of NiTi alloy during thermal cycling. Moreover, in existing studies, thermal cycling was conducted without load (in a stress-free state), whereas it is known that the changes in the properties of NiTi-based alloys during thermal cycling under stress differ from the behavior of the material during thermal cycles without load. However, in real devices, components made of NiTi alloy are always under load (constant or variable).

To determine the influence of the fraction of the forward transition range on the properties of NiTi alloy during thermal cycling under stress, two stress values of 50 and 200 MPa were chosen, similar to those used in thermal cycling through the full transformation range (described in 1.2). The experiments were conducted using a Lloyd

30K Plus testing machine equipped with a thermal chamber and a video extensometer. Wire specimens with a diameter of 0.5 mm of $Ni_{50}Ti_{50}$ alloy were annealed at a temperature of 500°C for 1 hour. DSC results showed that after the heat treatment, the alloy underwent B2↔B19′ martensitic transformation at temperatures M_s = 64°C, M_f = 55°C, A_s = 84°C, A_f = 97°C. The samples were heated to a temperature T (130°C for 50 MPa and 200°C for 200 MPa), at which the entire volume of the alloy was in the austenitic state, loaded to a stress of 50 MPa or 200 MPa, and subjected to repeated thermal cycling under constant stress in the temperature range of incomplete forward martensitic transformation. To determine the boundaries of the temperature intervals of incomplete forward transition, based on the strain-temperature dependencies obtained in the first cycle through the full forward martensitic transformation interval (obtained during the study described in section 1.2), the temperature interval of the forward transition $\Delta T = M_s - M_f$ was determined separately for cycles under 50 MPa and 200 MPa stress. Temperature ranges were calculated at which 25, 50, and 75% of the temperature interval of the forward transition were realized, and temperatures ($T_1 = M_s - ¾\Delta T$, $T_2 = M_s - ½\Delta T$, $T_3 = M_s - ¼\Delta T$) at which cooling should be stopped were determined. This is schematically shown in Figure 43. Thus, the $Ni_{50}Ti_{50}$ alloy samples were heated to T,

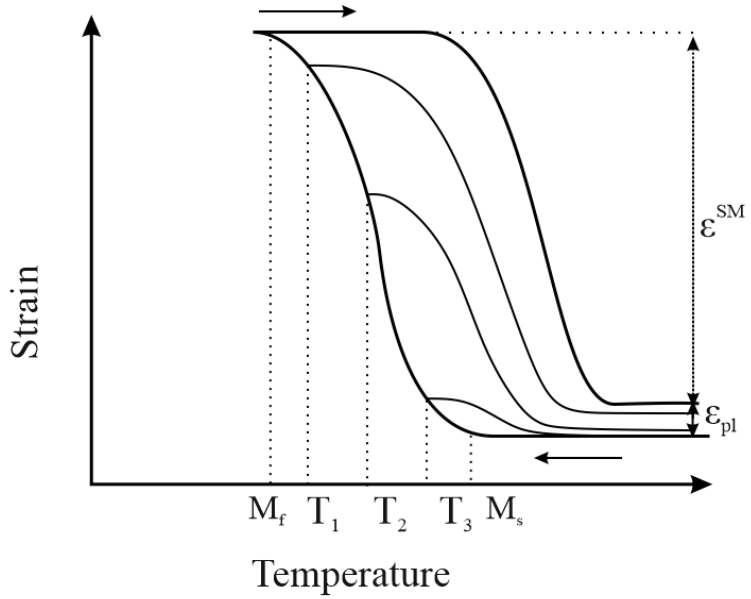

Figure 43. Scheme for determining temperatures T1, T2, T3 during thermal cycling in the temperature range of incomplete forward martensitic transformation

loaded with stress of 50 or 200 MPa, and then subjected to thermal cycling in the interval T÷ T_n (n = 1, 2, 3) under constant stress of 50 or 200 MPa. The temperatures T_n were determined in each cycle, taking into account the shift in the temperature of the forward transformation start. Based on the obtained strain-temperature dependencies ε(T), the values of the shape memory effect, irreversible strain, and temperatures of the start of the forward transition were determined, and the work performed by the alloy during heating was calculated using the formula: $A = \sigma\varepsilon^{SM}$.

Figure 44 illustrates the dependencies of the start temperatures of the forward transformation as a function of the cycle number, obtained during thermal cycling of the $Ni_{50}Ti_{50}$ alloy under loads of 50 MPa (a) and 200 MPa (b) through various fractions of

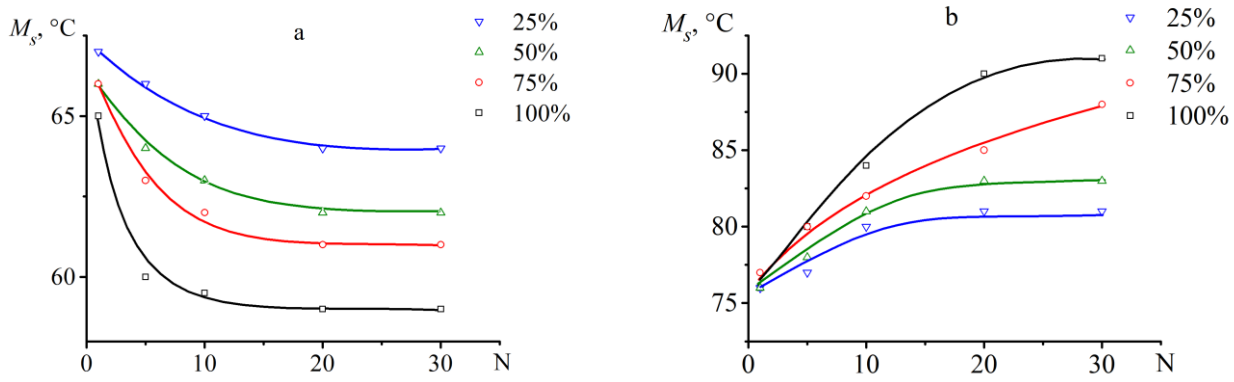

Figure 44. Dependencies of M_s(N) obtained during thermal cycling of the $Ni_{50}Ti_{50}$ alloy under a load of 50 MPa (a) and 200 MPa (b) through various fractions of the temperature interval of the forward martensitic transformation (indicated in the legend).

the temperature range of the forward martensitic transformation. When thermal cycling the $Ni_{50}Ti_{50}$ alloy under a load of 50 MPa, the M_s temperatures decreased with an increase in the number of cycles, while under a load of 200 MPa, they increased (the reasons for these differences are discussed in 1.2). The smaller the fraction of the temperature interval of the forward transformation, the less the change in the M_s temperature regardless of the stress and whether this temperature decreases during thermal cycling (under 50 MPa) or increases (under 200 MPa). Thus, the largest changes in the M_s temperature are observed when the second half of the forward transition is realized. Increasing the stress during thermal cycling intensifies this effect. For example, in Figure 44a, if the stress in the cycle was 50 MPa, then over 30 complete cycles, the M_s temperature decreased by 6°C, and

over 30 cycles through 50% of the forward transition, it decreased by 3°C. If during thermal cycling the stress was 200 MPa, then the M_s temperature increased by 14°C over 30 complete cycles and by 4°C over 30 cycles through 50% of the temperature range of the forward transition. This indirectly confirms that the greater the fraction of the forward transition realized during thermal cycling, the greater the change in defect density and transition temperatures.

Figure 45 depicts the dependencies of the shape memory effect (ε^{SM}) on the cycle number, obtained during thermal cycling of the $Ni_{50}Ti_{50}$ alloy under loads of 50 MPa (a) and 200 MPa (b) through various fractions of the temperature range of the forward martensitic transformation. It can be observed that the value of ε^{SM} decreased as the fraction of the temperature interval decreased, since the volume of the material undergoing martensitic transformations decreased. During thermal cycling under a load of 50 MPa, the values of ε^{SM} increased with an increase in the number of cycles, which is associated with the manifestation of the training effect [123,148–150]. However, this effect is most pronounced when the second half of the forward transition interval was realized during thermal cycling. For example, over 30 cycles, the value of ε^{SM} increased from 1.7% to 3.6% when cooling was carried out over the full transition interval, and from 0.8% to 1.7% when the fraction of the forward transition interval was 50%.

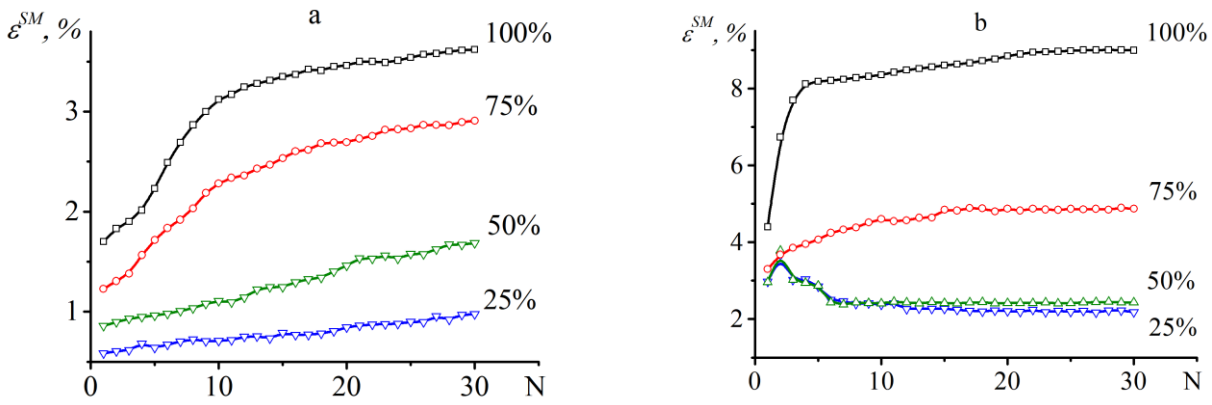

Figure 45. Dependencies of ε^{SM}(N) obtained during thermal cycling of the Ni50Ti50 alloy under loads of 50 MPa (a) and 200 MPa (b) through various fractions of the temperature interval of the forward martensitic transformation. The curves indicate the fraction of the temperature interval of the forward martensitic transformation.

The value of reversible strain, ε^{SM}, increased during thermal cycling under a stress of 200 MPa only if the fraction of the forward transformation during cooling was 100% or 75%. Decreasing the fraction of the forward transition from 100% to 75% resulted in a 1.4-fold decrease in reversible strain from 4.5% to 3.2% in the first cycle. However, by the thirtieth cycle, these values differed almost twofold, from 8% to 4.5%. This indicates that the training effect – the increase in reversible strain during thermal cycling – is most pronounced when the last quarter of the forward transition is realized during cycling under a stress of 200 MPa. If only 25% or 50% of the forward transformation was realized during cooling, the value of ε^{SM} changed non-monotonically with the number of cycles: it increased in the second cycle, decreased from the third to the seventh cycle, and remained unchanged during subsequent thermal cycling. Thus, the results of the study showed that the training effect is observed only when the second half of the temperature interval of the forward transition is realized during thermal cycling. This may be due to the fact that during cycling under stress, oriented internal stress fields are mainly formed in the second half of the temperature interval of the forward transition.

During thermal cycling of the $Ni_{50}Ti_{50}$ alloy under stress, plastic strain accumulates in each cycle (Figure 46).

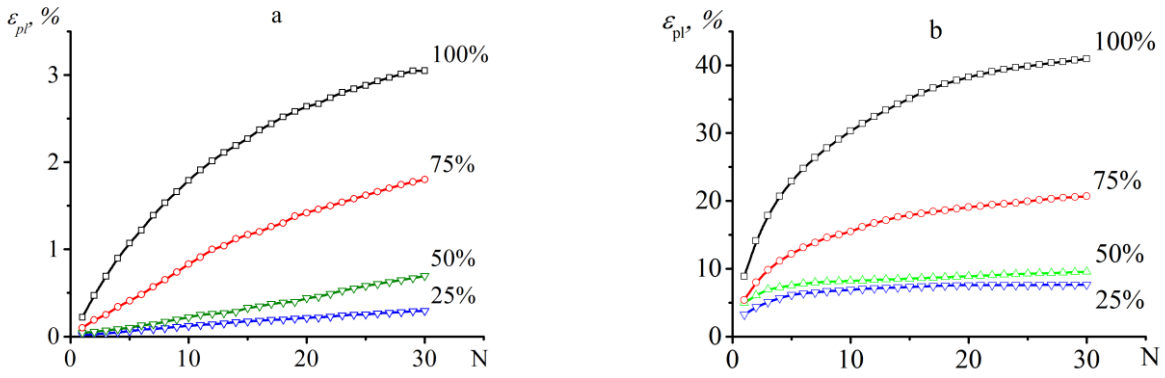

Figure 46. Variations in ε_{pl} during thermal cycling of the $Ni_{50}Ti_{50}$ alloy under a load of 50 MPa (a) and 200 MPa (b) through various fractions of the temperature interval of the forward martensitic transformation. The curves indicate the fraction of the temperature range of the forward martensitic transformation.

With an increase in the number of cycles, the alloy strengthens, and the intensity of plastic strain accumulation decreases, resulting in non-linear dependencies of $\varepsilon_{pl}(N)$. The value of plastic strain depended non-linearly on the fraction of the temperature interval.

In Figure 46, it can be seen that the main accumulation of defects occurs when the fraction of forward martensitic transformation exceeds 50% during thermocycling. Under a 200 MPa load during thermocycling, the accumulation of plastic strain is much greater than under 50 MPa, yet the same effect is observed – the primary change in plastic strain during thermocycling is observed when the fraction of forward martensitic transformation exceeds 50%. For instance, after 30 cycles under a 200 MPa load, accumulations of 7.6% and 9.5% plastic strain were observed for 25% and 50% of the forward martensitic transformation interval, respectively, while accumulations of 20.7% and 40.9% were observed for 75% and 100% realizations. A comparison of the results obtained with thermocycling through 75% and 100% of the forward martensitic transformation range showed that half of the plastic strain accumulates in the last quarter of the forward martensitic transformation, regardless of the value of the applied stress during thermocycling.

The dependencies of the work performed during heating on the cycle number are presented in Figure 47. Since thermal cycling was conducted under constant stress, the change in the amount of work performed was influenced only by changes in the values of ε^{SM}. Hence the work during thermocycling varies similarly to the reversible strain depending on the fraction of forward martensitic transformation realized during cooling. For $Ni_{50}Ti_{50}$ alloy thermocycled under 50 MPa and 200 MPa loads, the amount of work performed increased with the number of cycles. The greater the fraction of forward martensitic transformation during cooling, the greater the work performed in the first cycle and the more pronounced its variations during thermocycling. Increasing the stress during thermocycling affects the amount of work performed during heating, with the work performed under a 200 MPa load being approximately ten times greater than under a 50 MPa load.

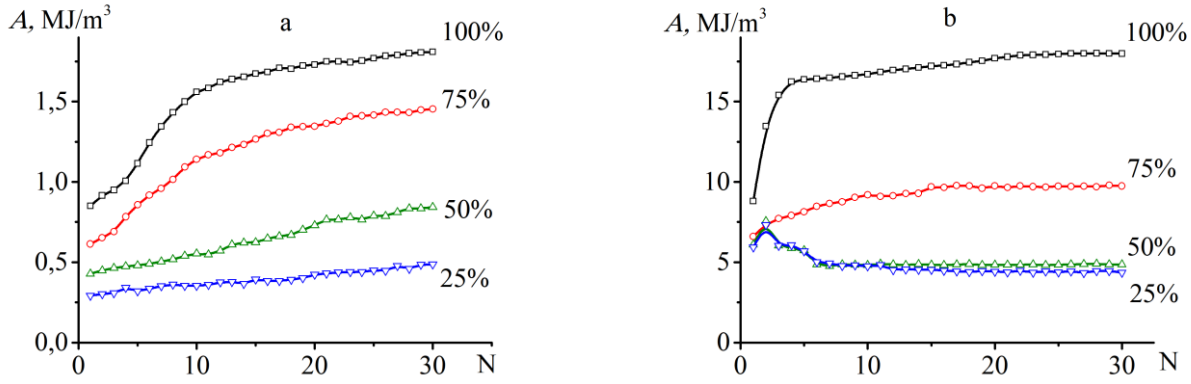

Figure 47. Variations in the values of work performed during heating by the NiTi alloy during thermocycling under a load of 50 MPa (a) and 200 MPa (b) through various fractions of the forward martensitic transformation range. The curves indicate the fraction of the forward martensitic transformation range.

Thus, reducing the fraction of the forward martensitic transformation range during thermocycling of the NiTi alloy under loads of 50 MPa and 200 MPa led to a decrease in plastic strain, a decrease in the temperature transition variations, reversible strain, and work performed. It has been established that significant changes in functional properties during thermocycling are observed when more than 50% of the forward transformation is realized during cooling. In this case, a significant accumulation of plastic strain occurs in the alloy, training effect is observed (increase in the value of shape memory effect), and transition temperatures vary. Moreover, the main changes in properties are observed when the last quarter of the forward transformation is realized during cooling. This is because the transformation from cubic austenitic B2 phase to monoclinic martensitic B19' phase is accompanied by up to 11% shear [151], which creates high internal stresses. At the initial stage, while the martensite fraction is small, the internal stresses can partially accommodate elastically, so the defect density changes insignificantly. The results of this study show that this occurs when the fraction of the forward transformation does not exceed 50%. Therefore, thermocycling through the first half of the forward transformation range is accompanied by very slight variations in functional properties and irreversible strain. Since the defect density changes weakly, the internal stresses are not high, therefore the total stress (external and internal) changes insignificantly, as a result, the training effect is not observed. At the final stage, elastic accommodation is impossible,

local stresses are very high and exceed the dislocation yield limit in the austenite state. This leads to intensive dislocation multiplication and movement, significantly increasing the defect density [37,48,98,99]. Therefore, at the final stage of the forward transformation, the most intensive accumulation of plastic strain and changes in functional properties occur. The increase in defect density leads to an increase in internal stresses, which, combined with external stresses, increase the effective stress acting during thermocycling, thereby manifesting the training effect. Thus, the results of the study showed that excluding the last half of the forward transformation during cooling allows stabilizing the properties of the NiTi alloy during thermocycling. However, this significantly reduces the reversible strain and work performed, which may be unacceptable for certain applications. If it is necessary to increase the reversible strain while minimizing changes in functional properties during thermocycling, it is necessary to increase external load and exclude the last quarter of the forward transformation.

2.2. Thermal cycling of the $Ni_{50}Ti_{50}$ alloy under load within temperature range of incomplete reverse martensitic transformation

Unlike the influence of the fraction of forward transformation on the variations in properties during thermocycling, which had been to some extent investigated prior to this study, the effect of the fraction of reverse transformation on the functional properties of the NiTi alloy during thermocycling had not been previously studied. In this dissertation, such investigations were conducted for the first time for the NiTi alloy. To achieve this, samples of the NiTi alloy (with the same composition, heat treatment, and martensitic transformations as described in section 2.1) were heated to a temperature of 180°C, at which the alloy was in the austenite state, loaded to 50 MPa or 200 MPa, and then cooled to a temperature of 30°C, at which the alloy was in the martensitic state. Subsequently, the sample was heated to temperatures T_1, T_2(or T_3 if available), calculated according to the following procedure. Based on the data described in section 1.2, which presents the results of property variations in the alloy during thermocycling through complete transformation ranges under stresses of 50 or 200 MPa, the temperatures A_s and A_f in the first cycle under the corresponding stress were determined, and the reverse transformation temperature range $\Delta A = A_f - A_s$ was calculated. Then, the values of $0.25 \cdot \Delta A$, $0.5 \cdot \Delta A$, and $0.75 \cdot \Delta A$ were calculated for cycles under 50 MPa stress, and $0.25 \cdot \Delta A$ and $0.5 \cdot \Delta A$ for cycles under 200 MPa stress (thermocycling through 75% of the reverse transformation fraction under 200 MPa stress was not investigated because in this case, the sample accumulated significant plastic strain, similar to what was observed during thermocycling through the complete transformation range). Temperatures at which the heating was stopped were chosen as $T_1 = A_s + 0.25 \cdot \Delta A$, $T_2 = A_s + 0.5 \cdot \Delta A$, and $T_3 = A_s + 0.75 \cdot \Delta A$ for thermocycling under 50 MPa stress, and $T_1 = A_s + 0.2 \cdot \Delta A$ and $T_2 = A_s + 0.5 \cdot \Delta A$ for thermocycling under 200 MPa stress (the values of these temperatures are presented in Table 2). Once the sample reached the corresponding temperature T_i, it underwent thermal cycling in the temperature range T_i - 30°C under the corresponding stress.

Table 2. Values of temperatures at which heating was interrupted during thermocycling in the incomplete temperature range of reverse martensitic transformation under loads of 50 and 200 MPa.

σ, MPa	A_s, °C	A_f, °C	T_1, °C	T_2, °C	T_3, °C
50	87	101	90	94	97
200	138	174	147	156	-

In Figure 48, the dependence of strain on temperature is presented, obtained in the NiTi alloy during cooling through the temperature range of forward martensitic

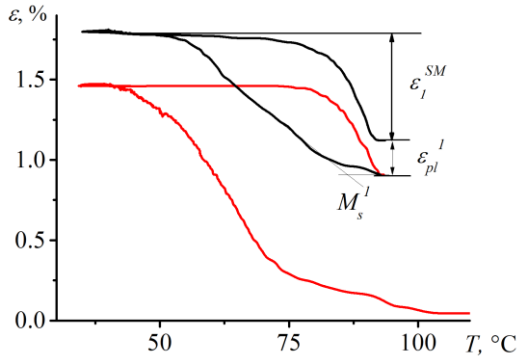

Figure 48. The dependences of strain on temperature obtained during cooling of the NiTi alloy from 180°C to 30°C under a stress of 50 MPa, heating to 94°C (red line), and in the first thermocycle within the temperature range of 94°C to 30°C (black line).

transformation (from 180 to 30°C), heating to the temperature T2 = 94°C, and in the first cycle T2÷30°C under a stress of 50 MPa, in which 50% of the temperature range of reverse martensitic transformation was realized. It can be observed that the accumulation of strain during cooling from 94°C starts at higher temperatures compared to cooling from 180°C. The end of strain accumulation during cooling is not dependent on the proportion of reverse transformation implemented before this cooling. It can be seen that in the first cycle, the deformation is not fully recovered upon heating, i.e., irreversible strain accumulates in the alloy. Based on the dependencies ε(T) obtained during the thermocycling of the NiTi alloy under stresses of 50 and 200 MPa, the values of shape memory effect (ε^{SM}), plastic stain (ε_{pl}), and the temperature at which strain accumulation begins during cooling (M_s) were calculated, as shown in Figure 48.

Figure 49 shows the dependencies of M_s(N) obtained during the thermocycling of the NiTi alloy under loads of 50 MPa and 200 MPa through various fractions of the reverse martensitic transformation temperature range.

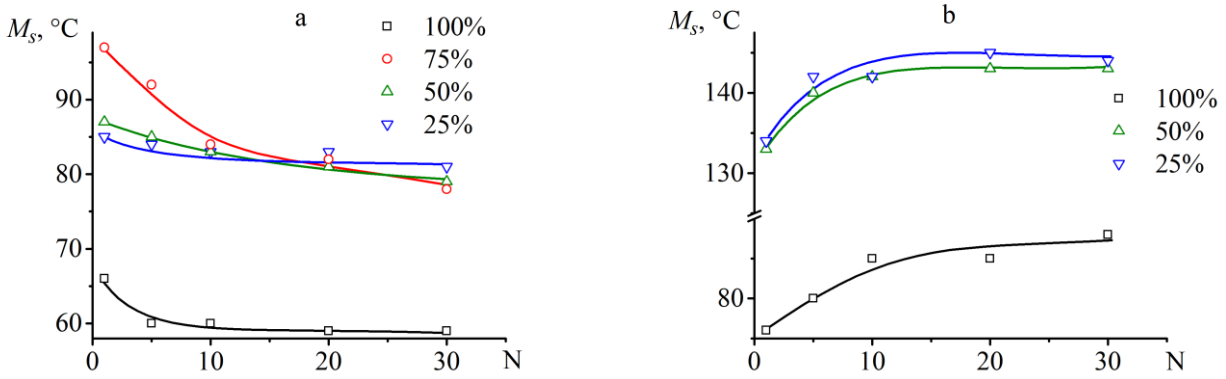

Figure 49. Dependencies of M_s(N) obtained during the thermal cycling of the $Ni_{50}Ti_{50}$ alloy under loads of 50 MPa (a) and 200 MPa (b) through various fractions of the reverse martensitic transformation temperature range (indicated in the legend).

As noted above, during thermal cycling through an incomplete reverse transformation range, the M_s temperature is significantly higher than during cycling through the full temperature range. For example, during cycling under a load of 50 MPa, the M_s temperature in the first cycle was 66°C and 85-97°C in the initial cycles through the incomplete reverse transformation range. During cycling under a load of 200 MPa, the M_s temperature was 76°C in the first full cycle and 133-136°C in the initial incomplete cycles. The increase in the start temperature of the forward transformation in incomplete cycles, compared to full cycles, is due to the presence of martensite in the alloy volumes that have not undergone the reverse martensitic transformation at the beginning of cooling. Therefore, there is no need to expend energy on martensite nucleation. During cooling, the untransformed martensitic crystals left after incomplete reverse transformation increase in size, requiring a significantly smaller thermodynamic stimulus than the formation of new crystals from the austenite. During cycling under a load of 50 MPa, the M_s temperature decreases regardless of the fraction of the reverse transformation range. Minimal changes in M_s temperature were observed when no more than 50% of the reverse transformation was realized during heating. During cycling under a load of 200

MPa, the M_s temperature increased regardless of the fraction of the reverse transformation range.

Figure 50 illustrates the dependencies of the recovered strain (ε^{SM}) values on the cycle number obtained during the thermal cycling of the $Ni_{50}Ti_{50}$ alloy under load through various fractions of the reverse martensitic transformation temperature range. It can be seen that with a decrease in the fraction of the reverse martensitic transformation temperature range, the ε^{SM} value decreased. For example, during the thermal cycling of the NiTi alloy under a load of 50 MPa, the ε^{SM} value was 1.7% in the full first cycle and 0.7% in the first cycle where 50% of the reverse transformation was realized. The decrease in the ε^{SM} value is associated with a reduction in the fraction of the material undergoing martensitic transformations during thermal cycling. With an increase in the number of cycles, the training effect (increase in the ε^{SM} value) was observed again only if the fraction of the reverse transformation realized during heating exceeded 50%. If the fraction of the reverse transformation temperature range did not exceed 50%, then the recoverable strain increased only in the first 2-5 cycles and then remained unchanged or slightly decreased, regardless of the fraction of the reverse transformation.

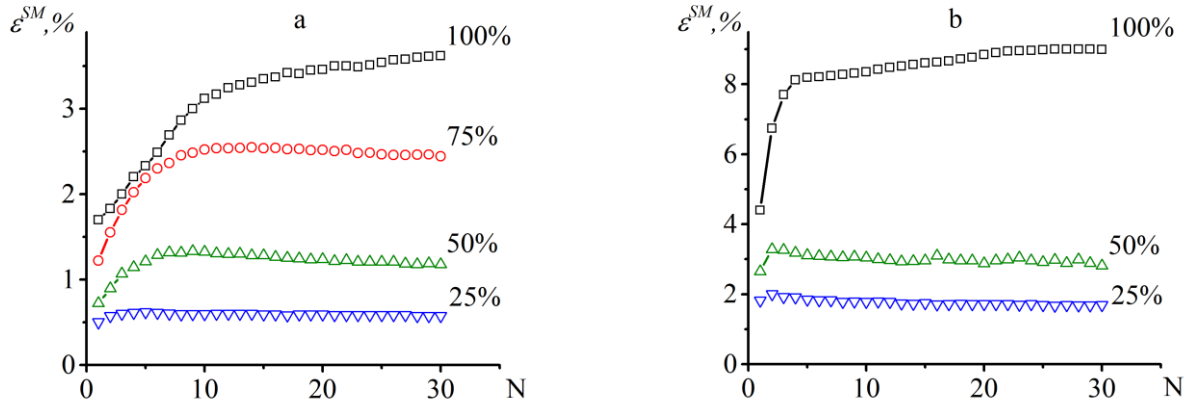

Figure 50. Dependencies of $\varepsilon^{SM}(N)$ during thermal cycling of the $Ni_{50}Ti_{50}$ alloy under loads of 50 MPa (a) and 200 MPa (b) through various fractions of the reverse martensitic transformation temperature range (indicated on the curves).

The recovery of strain during heating was not complete, meaning that irreversible strain accumulated in the alloy from cycle to cycle. Figure 51 shows the dependencies of the total plastic strain ε_{pl} on the number of cycles under loads of 50 MPa and 200 MPa.

In these dependencies, the zero cycle is assigned the plastic strain accumulated during cooling through the full range of the forward transformation preceding cycling in the incomplete reverse transformation range (see Figure 48 and the description of the methodology). The dependencies $\varepsilon_{pl}(N)$ were nonlinear, regardless of the fraction of the reverse transformation temperature range and the stress applied during cycling. The maximum accumulation of irreversible strain was observed when the fraction of the reverse transformation temperature range exceeded 50%. For example, during cycling under a load of 50 MPa for 30 cycles, 1.4% of strain accumulated when 50% of the reverse transformation was realized, compared to 3.1% when the reverse transformation was fully completed during heating. Under a load of 200 MPa for 30 cycles, 12.2% of strain accumulated when 50% of the reverse transformation was realized, compared to 41% when heating was conducted through the full temperature range of the reverse transformation. It is evident that the reduction in the value of plastic strain was significantly greater during cycling under a load of 200 MPa. For instance, if cycling through 50% of the interval under a load of 50 MPa reduced plastic strain by 2.2 times (from 3.1% to 1.4%), under a load of 200 MPa, plastic strain decreased by 3.4 times (from 41% to 12.2%).

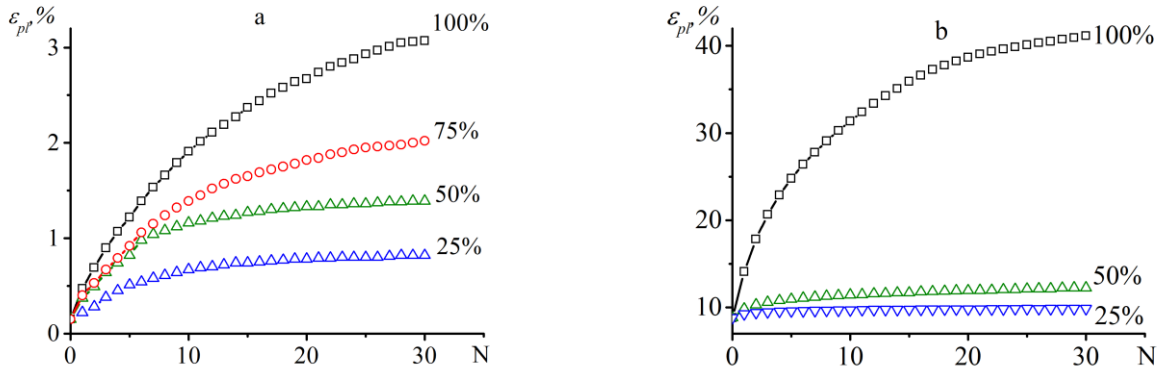

Figure 51. Dependencies of the values of $\varepsilon_{pl}(N)$ during thermal cycling of the NiTi alloy under loads of 50 MPa (a) and 200 MPa (b) through various fractions of the temperature range of the reverse martensitic transformation (indicated on the curves).

Based on the values of the shape memory effect and the stress acting in the cycle, the work performed by the alloy during heating was computed using the formula specified

in section 2.1. The dependencies of the values of *A*(N) obtained during thermal cycling of the $Ni_{50}Ti_{50}$ alloy under load through various fractions of the temperature range of the reverse martensitic transformation are presented in Figure 52. Since the stress during heating remained unchanged, the work value varied during thermal cycling similarly to the varied in reversible strain. As the realized fraction of the range decreased, the work value decreased because the proportion of material undergoing martensitic transformations decreased, and therefore reversible strain decreased. However, reducing the fraction of the temperature range of the reverse transformation significantly increased the stability of the work during thermal cycling. For example, during thermal cycling under a load of 50 MPa and a realization of 50% of the interval, the performed work increased from 0.36 MJ/m³ in the first cycle to 0.67 MJ/m³ in the 10th cycle, and from the 10th to the 30th cycle, the work values decreased to 0.59 MJ/m³ in the 30th cycle. In contrast, during thermal cycling through the full interval under a load of 50 MPa, the performed work increased from 0.85 MJ/m³ to 1.81 MJ/m³, more than doubling, with significant changes occurring over all 30 cycles. During thermal cycling under a load of 200 MPa with a realization of 50% of the interval, minimal variations in the performed work were observed, with A being 5.3% in the first cycle and 5.6% in the 30th cycle. Meanwhile, during thermal cycling through the full interval, the work increased from 8.8 MJ/m³ to 18 MJ/m³.

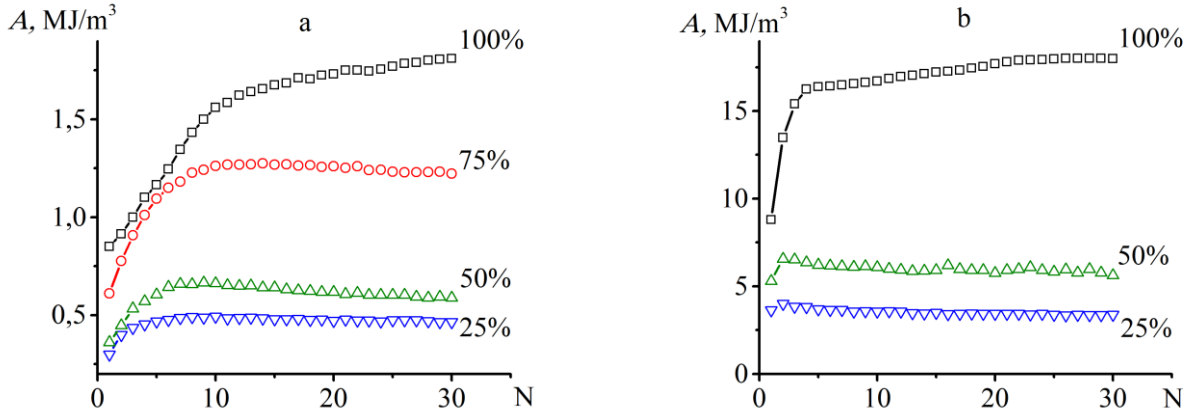

Figure 52. Dependencies of the values of *A*(N) during thermal cycling of the Ni50Ti50 alloy under a load of 50 MPa (a) and 200 MPa (b) through various fractions of the temperature range of the reverse martensitic transformation (indicated on the curves).

Thus, the results of the study allowed for the first time to establish the influence of the fraction of the temperature range of the reverse transformation on variations in the values of the shape memory effect, the work performed during heating, and the accumulation of irreversible strain during thermal cycling under constant stress. It has been shown that if no more than 50% reverse transformation is realized during heating, then variations in functional properties are observed only in the first few cycles. Irreversible strain is small and largely determined by the strain accumulated during the first cooling under stress through an incomplete reverse transformation range. The training effect is insignificant. If more than 50% of the temperature range of the reverse transformation is realized during thermal cycling, then significant changes in functional properties occur, a larger plastic deformation accumulates, and the training effect is manifested.

One could assume that the reasons for the influence of the fraction of the reverse transformation on the change in functional properties during thermal cycling are similar to the reasons for the influence of the direct transformation fraction, described in Section 2.1. However, during cooling, martensite crystals grow, creating high stresses, which leads to an increase in defect density and changes in all properties. During heating, reverse transformation occurs by moving the interphase boundary without the formation of austenite nuclei, i.e., during heating, martensite crystals collapse, so there is no reason for the occurrence of high stresses. In this case, the question arises as to what causes the accumulation of defects and plastic strain during reverse transformation? Since reverse transformation occurs with an increase in temperature, it is logical to assume that this is accompanied by processes of relaxation of the dislocation structure, which reduces the defect density.

Earlier, assumptions were made about the existence of factors causing alloy softening during reverse martensitic transformation in shape memory alloys. In [61,152], the authors drew attention to the fact that during thermal cycling, starting from a certain cycle, the rate of plastic strain accumulation per cycle becomes constant but not zero, and plastic deformation accumulates until sample failure [26,36,74]. Since the defect density

increases during cooling through the direct transformation interval, this strengthens the alloy, and, therefore, suppresses plastic strain. In this case, starting from a certain cycle, the rate of plastic strain accumulation should be zero; however, this is never observed in experiments. Therefore, the authors [61,152] suggested that softening occurs during reverse transformation, i.e., a decrease in the density of defects accumulated during the preceding cooling. If the strengthening acquired by the alloy during forward transformation becomes equal to the softening occurring during reverse transformation, the rate of plastic strain accumulation becomes constant. It is precisely the softening processes that can explain the influence of the fraction of the reverse transformation on the accumulation of plastic strain and variations in the functional properties of the NiTi alloy during thermal cycling. If the fraction of reverse transformation is small, then a lower temperature is reached during heating compared to heating through the full transformation interval. In this case, the recovery processes are insignificant, and therefore, the density of dislocations formed as a result of the first cooling through the temperature range of forward transformation does not change, the alloy remains strengthened, and during subsequent cycles, the variaitons in irreversible strain is determined only by the strain accumulated during the first cooling, and it weakly changes in subsequent cycles. The variations in the properties of the alloy during thermal cycling is insignificant, and the training effect is not manifested because internal stresses do not change. The smaller the fraction of reverse transformation realized during heating, the higher the temperature to which the alloy is heated in each cycle, the more intense the recovery processes, and the greater the decrease in defect density during heating. Consequently, the greater the increase in defect density during the next cooling, which leads to an increase in irreversible strain, variations in functional properties, and the manifestation of the training effect. Thus, it has been shown in the dissertation that by reducing the fraction of reverse transformation realized during heating, it is possible to reduce the intensity of irreversible strain accumulation and increase the stability of the functional properties of the NiTi alloy.

2.3. The influence of the fraction of the temperature range of forward and reverse martensitic transformation on the variations in properties of the NiTi alloy during thermal cycling under load

The results of the dissertation research showed that during thermal cycling under load within the temperature range of incomplete forward or reverse martensitic transformation, the stability of the strain values, the work done during heating, significantly increases, while the accumulation of plastic strain decreases. This raises the question of which thermal cycling mode is preferable for improving the stability of the NiTi alloy. To address this question, the study computed changes in functional properties and plastic strain over thirty cycles and analyzed the influence of the fraction of forward and reverse transitions on these values. Thus, the study calculated the change in the start temperature of the forward transition, denoted as $\Delta M_s^{30} = M_s^1 - M_s^{30}$; the change in the shape memory effect, denoted as $\Delta\varepsilon^{SM} = \varepsilon^{SM}_1 - \varepsilon^{SM}_{30}$; the cumulative plastic deformation over 30 cycles ε_{pl}^{30}, and the change in work, denoted as $\Delta A^{30} = A^1 - A^{30}$, where index 1 corresponds to the values measured in the 1st cycle, and index 30 corresponds to the values in the 30^{th} cycle.

Figure 53 illustrates the dependencies of ΔM_s^{30} on the fraction of the temperature range of forward or reverse martensitic transformation during thermal cycling under stresses of 50 and 200 MPa. It can be observed that the change in M_s temperature depends on which transition (forward or reverse) fraction was altered during thermal cycling. When cycling under a stress of 50 MPa through an incomplete forward transition interval, the value of ΔM_s^{30} linearly decreases with an increase in the fraction of the forward transition (Figure 53a). If cycling under a stress of 50 MPa was conducted within an incomplete reverse transformation interval, the value of ΔM_s^{30} nonlinearly depends on the transition fraction. Maximum changes in the value of M_s^{30} were observed when 75% reverse transition was realized during thermal cycling. In this case, the temperatures decreased by 19°C over 30 cycles, while with 50% interval realization, the value of ΔM_s^{30} was -4°C, and in the complete interval, it was -6°C.

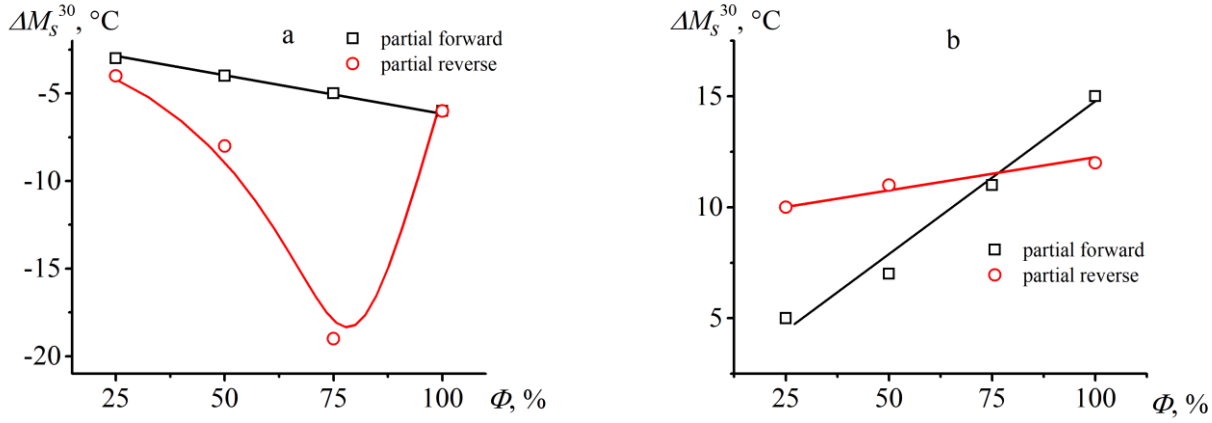

Figure 53. Variations in M_s temperatures in the $Ni_{50}Ti_{50}$ alloy after 30 thermal cycles under load of 50 MPa (a) and 200 MPa (b) through various fractions of the temperature range of forward or reverse martensitic transformation.

When thermal cycling under a stress of 200 MPa, the value of ΔM_s^{30} exhibited a linear dependence on both the fraction of forward and reverse transformations. The difference lay only in the slope of the $\Delta M_s^{30}(\Phi)$ line. Reduction in the fraction of forward transition significantly decreased the value of ΔM_s^{30} more than the fractions of reverse transition (Figure 53b). Consequently, the research results indicated that reducing the fraction of forward transition leads to better stabilization of transition temperatures compared to reducing the fraction of reverse transformation. This is because defect accumulation occurs during the forward transition. Growing martensitic crystals generate high stresses exceeding the dislocation yield limit, leading to increased defect density. Thus, the smaller the fraction of forward transition, the fewer martensitic crystals form, resulting in less increase in defect density and consequently smaller changes in transition temperatures. During heating, relaxation processes contribute to the change in defect density upon subsequent cooling. As the temperatures to which the samples were heated slightly differ from each other and are low (not exceeding 200°C), relaxation processes proceed slowly, thus the changes in temperatures during thermal cycling are less dependent on the fraction of reverse transition.

The variations in ε^{SM} values during thermal cycling under a stress of 50 MPa exhibited a linear dependence on the transformation fraction regardless of whether the fraction limited forward or reverse transitions (Figure 54a). The smaller the realized

fraction of the interval, the smaller the variation in ε^{SM} values. During thermal cycling under a stress of 200 MPa, the dependence $\varepsilon^{SM}(\Phi)$ was nonlinear and weakly depended on which transformation fraction was limited during thermal cycling. Decreasing the fraction of both transitions to 50% significantly reduced the values of $\Delta\varepsilon^{SM}_{30}$. The fact that the variation in shape memory effect during thermal cycling does not depend on which fraction of transition (forward or reverse) was limited is explained by the fact that the shape memory effect depends only on the fraction of the alloy undergoing martensitic transformation, which was the same for incomplete forward and reverse transitions.

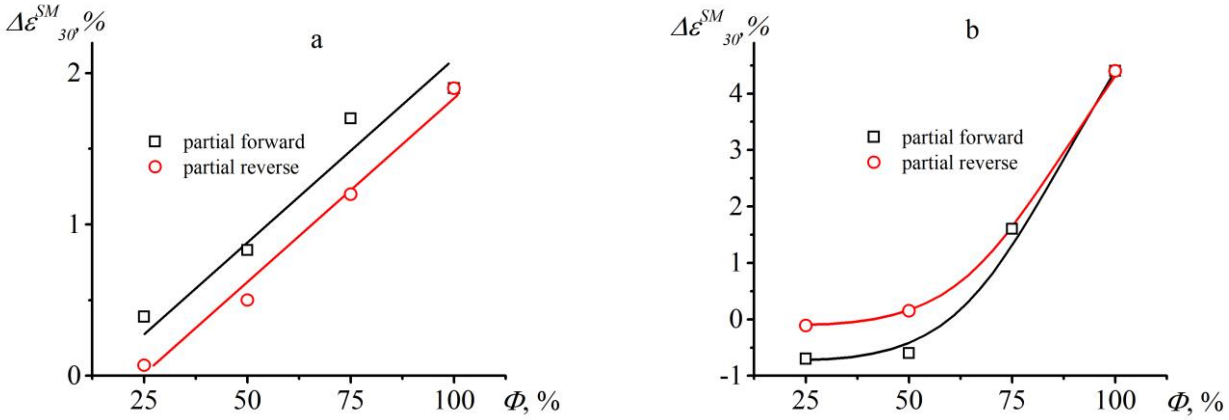

Figure 54. Dependence of $\Delta\varepsilon^{SM}_{30}$ values in the $Ni_{50}Ti_{50}$ alloy, measured over 30 thermal cycles under a load of 50 MPa (a) and 200 MPa (b), on the fraction of the temperature range of forward or reverse martensitic transformation.

The value of plastic strain accumulated after 30 thermal cycles under various conditions exhibited a nonlinear dependence on the fraction of the interval (Figure 55). Regardless of the applied stress during thermal cycling, reducing the fraction of both forward and reverse transitions decreased plastic strain, with the most significant changes observed when reducing the fraction to 50%. It is evident that reducing the fraction of forward transition more significantly reduces plastic strain than reducing the reverse transition fraction. This is because the increase in defect density, responsible for the change in plastic strain, occurs during the forward transformation when martensitic crystals grow. The less martensite is formed during cooling, the smaller the change in defect density, and hence the smaller the plastic strain. The fact that reducing the forward

transition interval to 50% reduces the intensity of plastic strain accumulation by 4-5 times suggests that the main increase in defect density occurs at the final stage of the forward transformation.

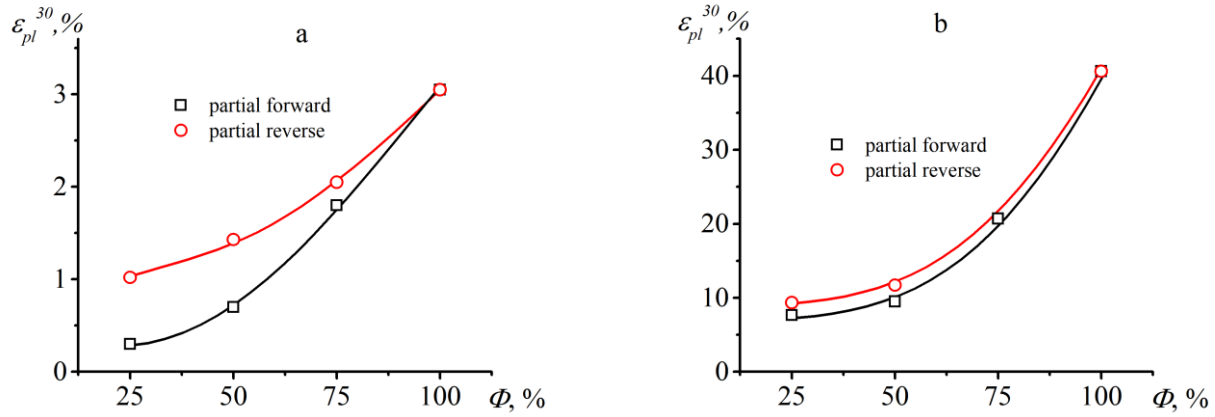

Figure 55. Dependence of ε_{pl} values measured in the NiTi alloy after 30 cycles under loads of 50 MPa (a) and 200 MPa (b) through various fractions of the temperature range of forward or reverse martensitic transformation on the realized fraction of the temperature interval.

In Figure 56, dependencies of the ΔA^{30} value on the fraction of the temperature range are presented. It can be observed that during thermal cycling under a stress of 50 MPa, the dependencies $\Delta A^{30}(\Phi)$ are linear and independent of which transition fraction was limited during thermal cycling. The larger the fraction, the greater the changes in the work done. For instance, during thermal cycling through an incomplete forward transition interval with 50% interval realization, the work done increased by 0.4 MJ/m³, while with 100% realization, the ΔA^{30} value was 0.95 MJ/m³. During thermal cycling through an incomplete reverse transformation interval, the ΔA^{30} value was 0.6 MJ/m³ with 50% interval realization.

During thermal cycling under a stress of 200 MPa, the dependencies $\Delta A^{30}(\Phi)$ were nonlinear, and the ΔA^{30} value changed sign. During thermal cycling through an incomplete forward transition range for 30 cycles with 50% realization, the work done decreased by 1.2 MJ/m³, as reversible strain decreased. Conversely, with 100% realization, the work done increased by 8.8 MJ/m³. During thermal cycling through an incomplete reverse transition interval (Φ = 50%), the ΔA^{30} value increased by 0.3 MJ/m³.

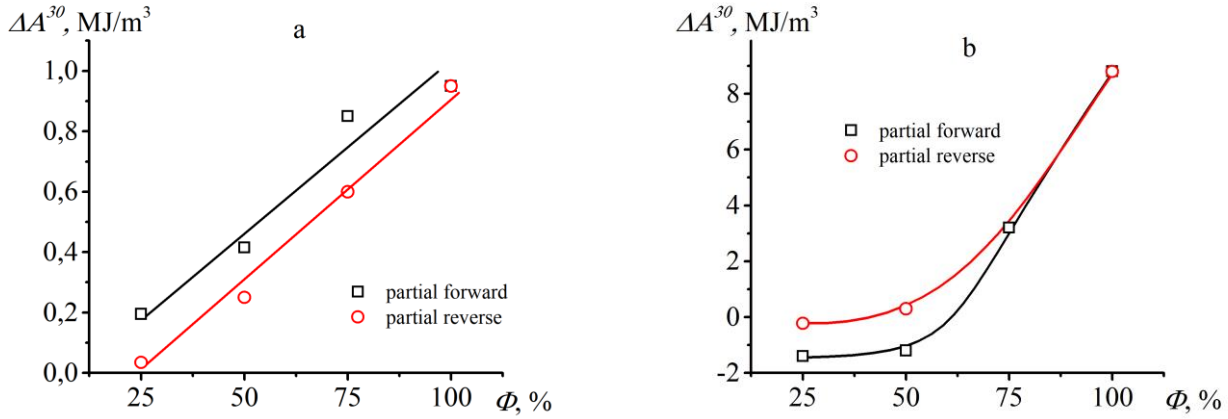

Figure 56. Dependencies of the value of the change in work done during heating over 30 cycles on the realized fraction of the temperature range, obtained for the NiTi alloy during thermal cycling under load of 50 MPa (a) and 200 MPa (b) through various fractions of the temperature range of forward or reverse martensitic transformation.

Thus, reducing the fraction of both forward and reverse transitions during thermal cycling decreases the accumulation of plastic strain, variations in shape memory effect values, and work done during heating, thereby improving the stability of the functional properties of the NiTi alloy. The research results showed that reducing the fraction of the forward transition is more effective in improving the stability of functional properties than reducing the fraction of the reverse transformation. This is because the main accumulation of defects occurs during the forward transition, when martensitic plates grow. Therefore, limiting the fraction of the forward transition has a greater impact on changing the properties of the NiTi alloy during thermal cycling compared to the fraction of the reverse transition, which only controls the intensity of the structure relaxation process, affecting the accumulation of defects during subsequent cooling.

2.4. Conclusions to Chapter 2

Based on the results presented in Chapter 2, the following conclusions can be drawn:

1. Decreasing the fraction of both forward and reverse temperature ranges reduces the variations in martensitic transformation temperatures, reversible strain, work done during heating, and the amount of plastic strain accumulated during thermal cycling of the NiTi alloy under stress. It was found that if the temperature range of the forward transition does not exceed 50% of the total range during thermal cycling, then the functional properties change only in the first 3-5 cycles and remain stable thereafter. It was demonstrated that variations in the functional properties of the alloy during thermal cycling under stress occur only when the temperature range of the forward transition exceeds 50%.

2. The influence of the fraction of the forward transition on the variations in the functional properties of the NiTi alloy during thermal cycling is related to the peculiarities of changes in defect density during the forward transition. At the initial stage of the forward transition ($\Phi \leq 50\%$), stress accommodation, created by the growing martensitic plate, occurs elastically, which is not accompanied by changes in defect density, thus the variations in martensitic transformation temperatures, reversible and irreversible strain are insignificant. At the final stage of the forward martensitic transition ($\Phi > 50\%$), the value of local stresses exceeds the dislocation yield stress, initiating dislocation multiplication and glide. As a result, the defect density increases, plastic strain accumulates, and functional properties change during thermal cycling.

3. The influence of the fraction of the reverse transition on the variations in the functional properties of the NiTi alloy during thermal cycling is determined by the processes of reverse transformation, which occur during heating and contribute to the nucleation and movement of defects during subsequent cooling. The greater the fraction of the reverse transition, the higher the temperature to which the sample is heated in the cycle, and the more intense the reverse processes are, resulting in a decrease in dislocation density. This leads to an increase in dislocation density in the alloy during subsequent cooling through the temperature range of the forward transition, resulting in increased plastic strain and variations in martensitic transformation temperatures.

4. The training effect - an increase in reversible strain during thermal cycling - is associated with the ability of the alloy to accumulate plastic strain during repeated thermal cycles. This effect is observed when the fraction of the forward or reverse transition during thermal cycling exceeds 50%. In this case, during thermal cycling under stress, irreversible strain accumulates actively in the alloy, accompanied by an increase in internal stresses. These stresses, combined with external stresses, increase the effective stress during thermal cycling, leading to an increase in the fraction of oriented martensite, which appears during cooling and disappears during heating, resulting in an increase in reversible strain.

5. Decreasing the fraction of the forward transition during thermal cycling under stress leads to better stabilization of the functional properties of the NiTi alloy compared to reducing the fraction of the reverse transition. This is because the main variations in defect density occur during the forward transition, so limiting the fraction of this transformation allows better control of variations in defect density and management of the functional properties of the NiTi alloy.

6. Decreasing the fraction of both forward and reverse transitions reduces reversible strain and work done during heating, but significantly improves the stability of these properties and reduces irreversible strain, which is important for devices with repeated actions. For example, reducing the fraction of the forward transition from 100% to 50% during thermal cycling of the alloy under a stress of 50 MPa reduces reversible strain by 2.3 times and plastic strain by 5 times.

7. Increasing the stress during thermal cycling results in variations in martensitic transformation temperatures, reversible strain, and accumulated irreversible strain, but does not fundamentally affect the nature of the dependencies of these quantities on the fraction of the temperature range of the forward and reverse martensitic transitions.

Chapter 3. Managing functional properties during thermal cycling of NiTi alloy in actuator mode

The stability of shape memory alloy properties is particularly important for actuator systems - devices that perform repetitive actions during heating and cooling cycles. These devices typically include a working element made of a shape memory alloy subjected to thermal cycling under variable stress generated by the elastic counterbody. This counterbody is a necessary component of the actuator design, serving as a reservoir of elastic energy. During the initial heating cycle, the deformation in the shape memory alloy element is recovered, leading to the deformation of the counterbody, which acts as an accumulator of elastic energy. Upon further cooling, during the direct martensitic transformation, the accumulated potential energy from the counterbody is used to deform the working element. Upon subsequent heating, the deformation in the shape memory alloy element is restored again, and the counterbody is deformed, repeating the described process [24–28,58,59,153]. For the actuator to operate steadily without requiring adjustment to its operation mode, the properties of the shape memory alloy element should remain unchanged during thermal cycling. Chapter 2 demonstrated that for NiTi-based alloys, property stabilization can be achieved by reducing the proportion of direct and/or reverse transformations. However, all the results in Chapter 2 were obtained under constant load thermal cycling conditions. Nevertheless, as noted above, in the actuator (drive) mode, stress decreases during the cooling of the shape memory alloy element and increases during heating. In other words, thermal cycling occurs under varying stress conditions, which may have an additional impact on the properties of NiTi alloy during thermal cycling. Additionally, for actuator operation, important parameters include the stiffness of the counterbody, the activation temperature range, and the method of pre-deformation of the shape memory alloy element. All these factors affect the stress variation during thermal cycling, and thus may influence the change in alloy properties. The literature lacks systematic studies on the influence of these parameters on the change in shape memory alloy properties during thermal cycling in the actuator mode, making it

difficult to develop optimal operating modes for the actuator where changes in its performance characteristics would be minimal. Therefore, an important task is to investigate changes in NiTi alloy properties during thermal cycling in the actuation mode. This task has been addressed in this work, and the results are presented in [65–68].

3.1. The influence of counterbody stiffness, pre-deformation method, and strengthening on the variation of niti alloy properties during thermal cycling in actuator mode

3.1.1. Objects and methods used for investigations of NiTi shape memory alloy properties variations during thermal cycling in actuator mode

The studies presented in sections 3.1, 3.2, and 3.3 were conducted on cast samples of the $Ni_{50}Ti_{50}$ alloy with a diameter of 4.0 ± 0.5 mm and a length of 30.0 ± 3 mm. These samples were quenched in water from a temperature of 900°C for 15 minutes and annealed at 500°C for 2 hours. After thermal treatment, the alloy underwent martensitic transformations B2 ↔ B19' at the temperatures M_s = 59°C, M_f = 37°C, A_s = 67°C, and A_f = 90°C. Figure 57 shows the experimental setup for studying the properties of shape memory alloys (SMAs) in the actuator mode. This setup consists of an electric motor (1) with a reducer (3), used to apply torque to the sample (12), which is mounted on a shaft with grips (5). A disk with a cord (7) is attached to a platform with a load and is used to apply constant load (stress) to the sample during cooling and heating. The angle of torsion of the two shaft parts is recorded by optical encoders (9), and the force moment is measured by a pendulum dynamometer (10). The stress value is estimated at the outer fiber using the assumption of ideal plasticity according to the equation (3.1):

$$\tau = \frac{1{,}5 * M_0 \mathrm{Sin}\varphi}{\pi * r^3} \quad (3.1)$$

where r is the sample radius, ϕ is the angle of elevation of the dynamometer lever, and $M_0 = m \cdot g \cdot h$, where m is the mass attached to the dynamometer lever, g is the acceleration due to gravity, and h is the length of the lever (Figure 57). The strain was calculated in the outer fiber according to equation (3.2):

$$\gamma = \frac{\varphi \cdot r}{l} \cdot 100\%, \quad (3.2)$$

where l is the length of the sample. The role of the elastic counter-body is performed by the pendulum dynamometer.

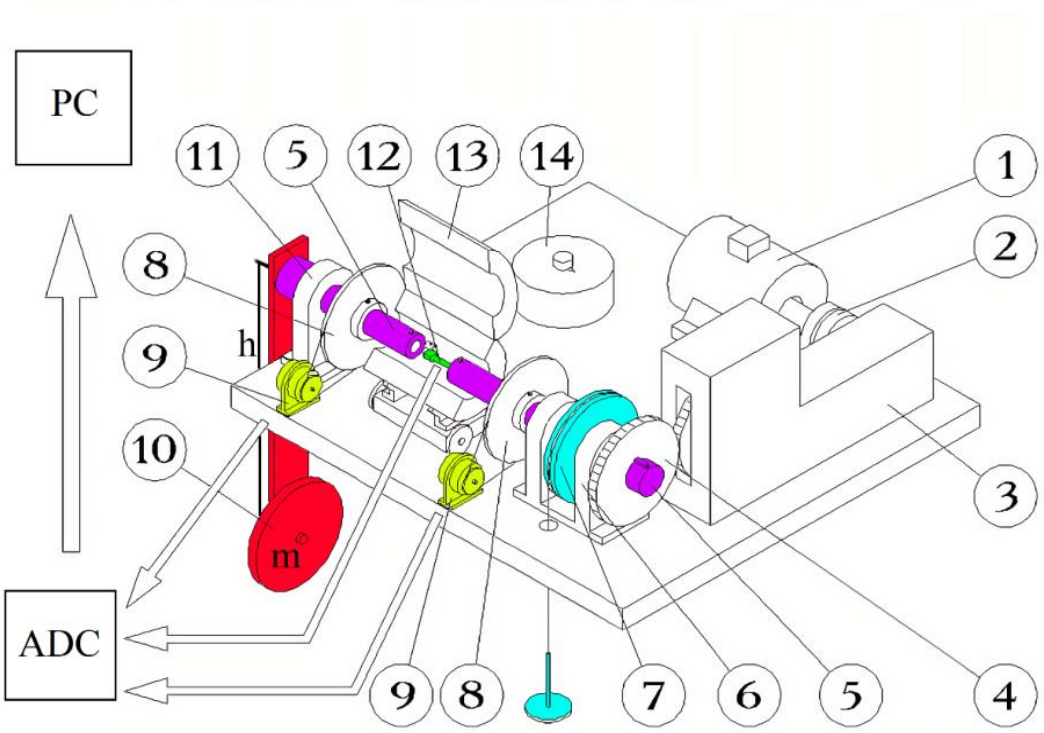

Figure 57. Experimental setup for torsional testing. 1 - electric motor, 2 - gearbox, 3 - transmission case, 4 - driving gear, 5 - shaft with grips, 6, 11 - supports with bearings, 7 - disk with cord used to apply constant load on the sample, 8 - disks for transmitting angular displacements to angle sensors, 9 - optical angle displacement sensors, 10 - pendulum dynamometer with load (m), 12 - sample, 13 – thermal chamber, 14 – thermal chamber control.

Since the increase in stress (τ_h) during heating is proportional to the recovered strain (γ_h), it can be written that $\tau_h = K \cdot \gamma_h$, where K is the linear coefficient characterizing the stiffness of the system, which can be computed using equations (3.1) and (3.2). Then, at small torsional angles, we obtain the following expression:

$$K = \frac{1{,}5 \cdot l \cdot M_0}{\pi \cdot r^4} \tag{3.3}$$

Equation (3.3) shows that the stiffness (K) depends on the torque (M_0), the value of which changes with the mass (m) attached to the dynamometer lever. Thus, the choice of stiffness K can be made by varying the mass m attached to the dynamometer lever.

For the operation of the drive, the NiTi alloy specimen must be pre-deformed. To study the influence of the method of pre-deformation on the drive parameters (recovered strain, recovery stress, and work), pre-deformation was carried out either by active

deformation or by cooling under stress. Active deformation of the specimen (Figure 58a) is performed using an electric motor (1), which generates a torque on the shaft (5) through the transmission system. To pre-deform the specimen by cooling under stress (Figure 58b), the specimen was heated to a temperature at which the alloy is in the austenite state and loaded to the selected stress by applying a mass to the plate connected to the disk (7). Then the specimen was cooled under this load through the temperature interval of direct martensitic transformation (down to room temperature) and unloaded (the load was removed from the plate).

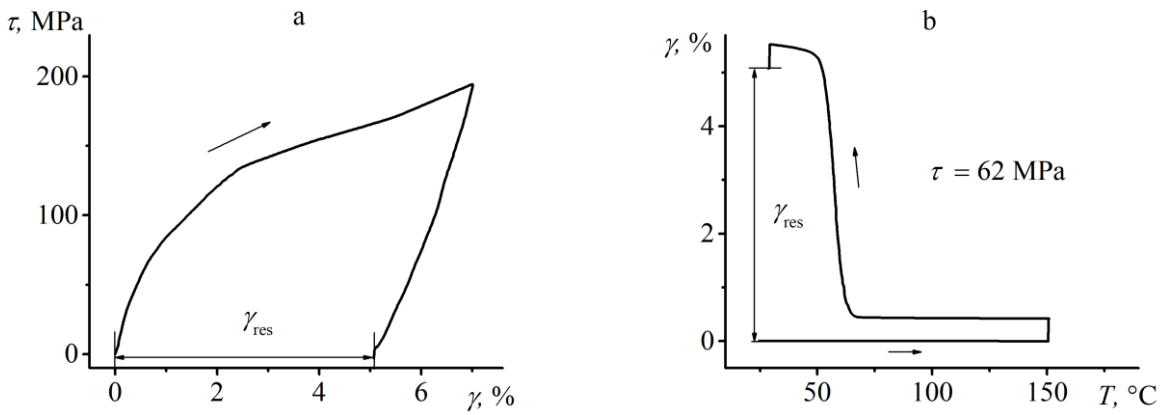

Figure 58. Two schemes of samples pre-deformation: active deformation in the martensite state (a) and cooling under constant stress (b).

Using the first scheme (Figure 58a), NiTi alloy specimens were deformed to 7% at room temperature (in the martensite state), then unloaded. After unloading, residual strain was measured in the specimens (γ_{res}=5.1±0.2%). Using the second scheme (Figure 58b), specimens were loaded at a temperature of 180°C (austenitic state) to 62 MPa. Then the specimen was cooled under constant stress of 62 MPa in the temperature range of direct martensitic transformation and then unloaded. The value of the constant stress of 62 MPa was chosen to provide residual strain values (measured after unloading at room temperature) close to the γ_{res} observed after active deformation in the martensitic state.

To initiate strain and stress variations during thermal cycling in actuator mode, after pre-straining by one method or another, the sample was connected to the dynamometric pendulum (10), and the right part of the shaft (5), where the second end of

the sample was attached, was fixed by locking the gear ring (4). Temperature control was carried out by a thermocouple fixed at the center of the working part of the sample. The sample was heated to 180°C and subjected to cooling-heating cycles in the temperature range of 180 to 30°C. During heating, strain was restored in the sample, leading to the deflection of the dynamometer (10) from the vertical position, which created a moment, resulting in increased stresses in the specimen. During cooling, under the stresses generated during the heating stage, the sample accumulated strain in the temperature range of forward martensitic transformation, and the position of the rod returned to the vertical. During the subsequent thermal cycles, the entire described procedure was repeated.

3.1.2. The impact of counterbody stiffness on the variation of functional properties of NiTi alloy

The value of stresses generated during heating directly depends on the stiffness of the counterbody. To investigate the influence of counterbody stiffness on the variation of properties of the NiTi alloy during thermal cycling in drive mode, 7 stiffness values were selected, as presented in Table 3. As mentioned earlier, stiffness was varied by adjusting the mass on the dynamometer. Samples, pre-deformed to 7%, were subjected to thermal cycling at all selected stiffness values. Table 3 shows the residual strain values after unloading. It is evident that the residual strain in all samples is 5.1 ± 0.2%, indicating that before thermal cycling in drive mode, all samples were under identical conditions.

Table 3. Counterbody stiffness (K), torque (M_0), and residual strain (γ_{res}) values in samples (γ_{res}) subjected to different pre-deformation procedures.

Sample №	M_0, N*m	K, GPa	Residual strain γ_{res}, %	
			Active deformation up to 7 % in marteniste	Cooling under stress 62 МПа
1	3.6	3.2	5,0	5.1
2	6.7	6.3	5.2	5.3
3	12.2	11.3	5.1	5.3
4	23.2	23.5	5.0	5.1
5	34.2	34.4	5.1	5.3
6	50.7	51.4	5.0	5.3
7	61.7	70.7	4.9	5.0

In Figure 59, dependencies of γ(T) and τ(T) obtained during the first heating and subsequent thermal cycle (K = 11.3 GPa) of a sample pre-deformed by 7% are shown. Additionally, changes in strain and stress in the tenth thermal cycle are presented. It is observed that strain recovery during heating is accompanied by stress generation (blue line). During subsequent cooling, direct transformation from the austenite phase to martensite occurs under stress created by the previous heating. Such cooling results in oriented martensite formation, leading to strain accumulation and stress relaxation (red

line). During the next heating, strain recovery and stress generation occur in the temperature range of reverse transformation (red line). During further thermal cycling, all described stages repeat. In the tenth cycle (green line), variations in strain and stress occur similarly to the first cycle, but the values of shape memory effect and reactive stresses change. It is observed that strain recovery during heating is incomplete, as non-closure is observed in the γ(T) dependence, indicating the accumulation of plastic strain during cycles (Figure 59a). However, stress never fully relaxes during cooling (Figure 59b), and the minimum stress value is 25±5 MPa.

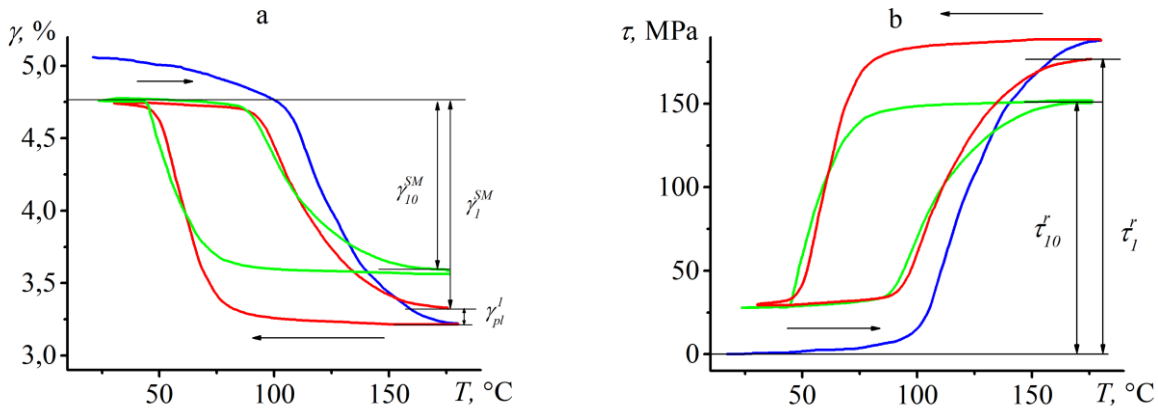

Figure 59. Dependencies of strain (a) and stress (b) on temperature obtained during the first heating after deformation (blue line), the first (red line), and the tenth (green line) cycles with a stiffness of K = 11.3 GPa for a sample actively deformed in the martensite state. Subscripts indicate the cycle number.

Based on the obtained curves γ(T) and τ(T), the values of the shape memory effect (γ^{SM}), irreversible deformation (γ_{pl}), and reactive stresses (τ_r) were measured, as shown in Figure 59. It can be observed that during the first heating of the deformed sample, 1.8% of deformation was recovered (blue line), while during the subsequent heating (red line), 1.4% of deformation was recovered (Figure 59a). The difference in the recovered strain during the first heating and the first cycle is due to the difference in the mechanism of oriented martensite formation: before the first heating, oriented martensite was formed by reorienting martensitic variants during active deformation in the martensitic state. Before heating in the first and subsequent cycles, oriented martensite was formed during cooling under variable stress, resulting in less accumulated deformation than during active

deformation. The reversible deformation is proportional to the proportion of oriented martensite; the smaller the proportion, the smaller the reversible deformation. Since the first heating, which was carried out immediately after pre-deformation, is only necessary to "cock" the drive, the variation in properties during this heating was not compared with the variation in properties in the thermal cycles (in the future, we will refer to the first heating as the "zero" cycle).

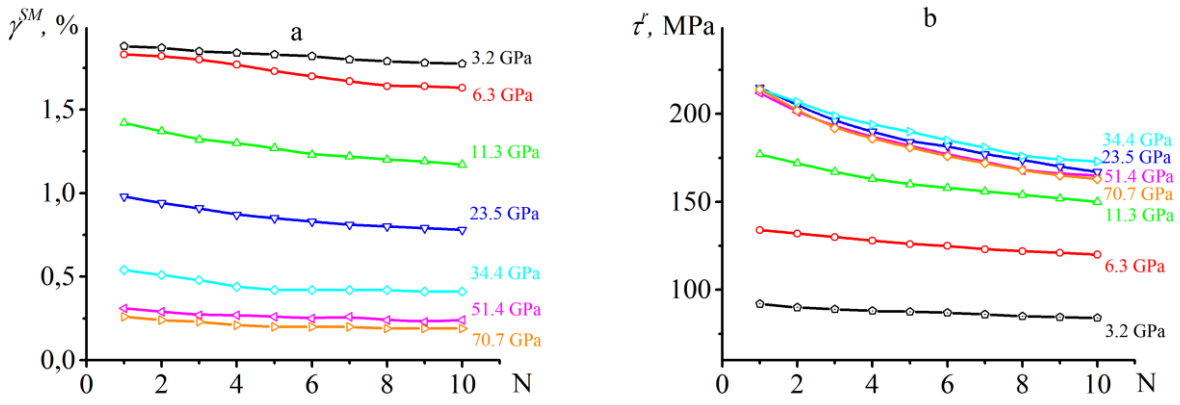

Figure 60. Dependencies of the shape memory effect value γ^{SM} (a) and maximum stress τ_r (b) on the number of thermal cycles (N), obtained for samples actively deformed in the martensite state.

Figure 60a shows the variation in the values of the shape memory effect γ^{SM} in samples deformed in the martensite state up to 7% and subjected to thermal cycling with different stiffness. It can be seen that the values of the shape memory effect decrease differently during thermal cycling, depending on the stiffness of the counter body. The minimum change in reversible strain during thermal cycling was observed at a stiffness of 3.2 GPa, and the maximum - at a stiffness of 71 GPa. In Figure 60b, it can be observed that the smallest variations in the values of reactive stresses during thermal cycling was observed at the lowest stiffness. An increase in the stiffness of the counter body from 3.6 to 23.5 GPa leads to an increase in reactive stresses in the first cycle. If the stiffness of the counter body exceeds 23.5 GPa, then the values of reactive stresses and their variations during thermal cycling do not depend on the stiffness of the system.

Figure 61 illustrates the dependencies of the shape memory effect and recovery stresses on the system stiffness, obtained in the first and tenth cycles. It is shown that the

recoverable strain (γ^{SM}) decreases with increasing stiffness of the counterforce (Figure 61a). Recovery stresses increase with stiffness up to 23.5 GPa and then remain unchanged (Figure 61b). Saturation in the $\tau_r(K)$ dependence is associated with reaching the limit of dislocation slip during stress generation, hence the stress does not increase, and plastic strain accumulates in the alloy. Thermal cycling reduces both the value of the shape memory effect and recovery stresses.

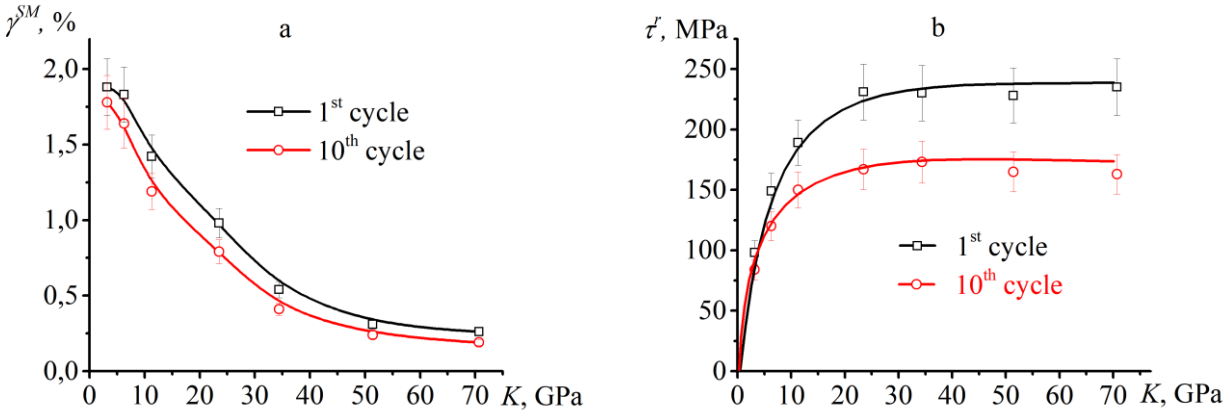

Figure 61. Dependencies of γ^{SM} (a) and τ_r (b) on the effective stiffness K, obtained for samples that were deformed in the martensite state.

Previously, it was assumed that maximum recovery stresses should be expected under conditions of rigid fixation, where stiffness can be considered infinite, and the maximum value of recoverable strain should occur under conditions of no stress, i.e., with zero stiffness. Typically, the dependence of recovery stresses on γ^{SM} is obtained by connecting the two extreme points directly (strain change during heating without stress and stress generation during heating with infinite stiffness) [12,15]. The results of this study show that the dependence of $\tau_r(\gamma^{SM})$ is nonlinear, both for the first and the tenth thermal cycle (Figure 62a). It can be observed that the recovery stresses remain constant for recoverable strains of less than 1% and decrease for $\gamma^{SM} > 1\%$. These findings are in good agreement with previous studies [12,15,18,22,154].

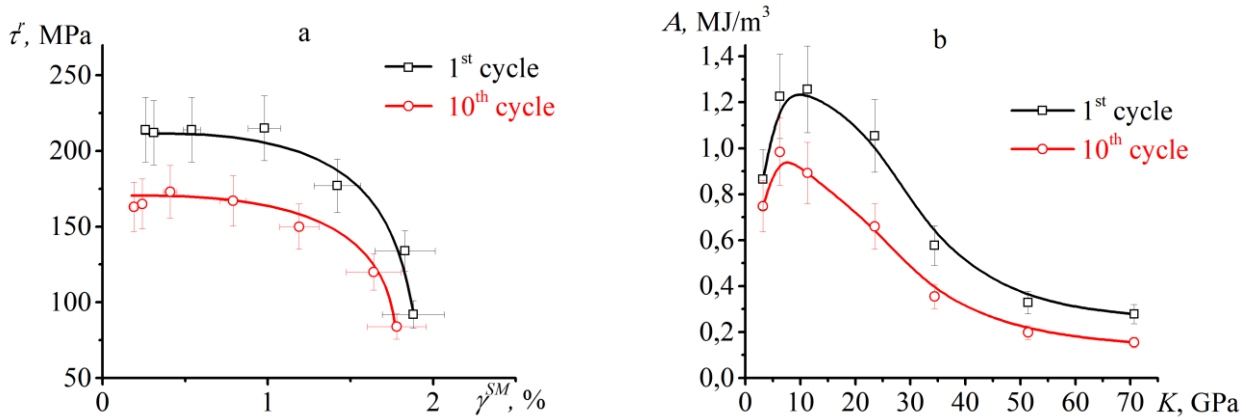

Figure 62. Relationship between the value of the shape memory effect γ^{SM} and recovery stresses τ_r (a). Dependency of work A on system stiffness K (b), obtained for specimens that were actively pre-deformed in the martensite state.

To determine the optimal stiffness of the system ensuring maximum drive efficiency, it is necessary to assess the work done during heating, which can be calculated using formula (3.4):

$$A = \frac{\Delta\tau\,\gamma^{SM}}{2}, \tag{3.4}$$

where $\Delta\tau$ is the change in recovery stress during heating, and γ^{SM} is the value of shape memory effect. In Figure 62b, the dependencies of the work done during heating on the stiffness of the system are shown, calculated for the first and tenth cycles. It can be seen that maximum work is performed when the stiffness of the counter-body is in the range of 6-10 GPa. With an increase in the number of thermal cycles, the efficiency decreases, but the position of the maximum remains unchanged.

Plastic (irreversible) strain (γ_{pl}) occurs both during the initial heating and during subsequent thermal cycling. Obviously, plastic strain accumulated during the pre-deformation process and "zero" cycle (first heating) affects the subsequent changes in reversible and irreversible strain during thermal cycling, as it leads to the strengthening of the alloy. However, in this case, the value of the pre-deformation was the same for all specimens. The total amount of plastic strain γ_{pl} is calculated as the sum of γ_{pl}^{N} measured in each cycle, and its variation during thermal cycling is shown in Figure 63. It can be seen that γ_{pl}^{0} measured in the "zero" cycle was greater than the cumulative γ_{pl} accumulated in the subsequent 10 thermal cycles. Increasing the stiffness of the system increases γ_{pl}

measured in the "zero" cycle but reduces the accumulation of plastic strain during subsequent thermal cycling. This is because the plastic strain accumulated during pre-deformation and the first heating (γ_{pl}^{0}) leads to the strengthening of the alloy, reducing variations in defect density during subsequent thermal cycling and, as a result, reducing the accumulation of γ_{pl}. The higher the stiffness of the system, the greater the plastic strain in the "zero" cycle, the greater the strengthening of the alloy, and the lower the intensity of plastic strain accumulation during thermal cycling. For example, during thermal cycling with K = 70.7 GPa, plastic strain in the "zero" cycle was 4.7%, while in the subsequent 10 thermal cycles it was 0.1%. For K = 3.2 GPa, these values are 2.1% and 0.6%, respectively.

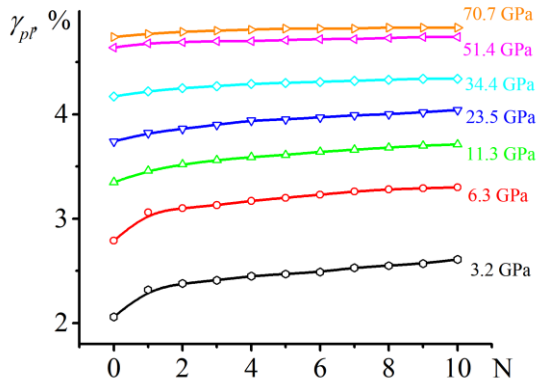

Figure 63. Variation of plastic strain during thermal cycling with different stiffness, measured in specimens of NiTi alloy pre-deformed in the martensite state.

3.1.3. Impact of pre-deformation method on functional properties variations of NiTi alloy during thermal cycling in actuator mode

In the second series of experiments, variations in reversible strain, recovery stresses, work output, and plastic strain during thermal cycling in the actuator mode were studied for samples pre-deformed by cooling under constant stress of 62 MPa (the choice of stress is explained in 3.1.1). Dependencies of γ(T) and τ(T) were obtained and analyzed in the same manner as in the first series. Figure 64 shows the dependencies of γ^{SM}, maximum recovery stress, and work output on stiffness, obtained in the initial thermal cycles.

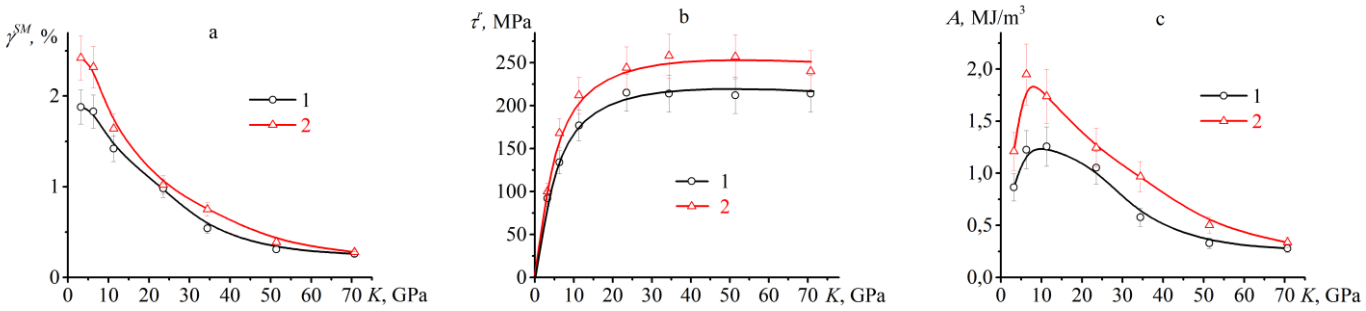

Figure 64. Dependencies of reversible strain (a), recovery stresses (b), and work (c) on the stiffness of the counter-body, obtained in the first thermal cycle, for samples pre-deformed in the martensite state (1) or cooled under constant stress (2).

It is evident that all parameters measured in samples pre-deformed by cooling under stress (the second method) were higher than those in samples pre-deformed in the martensite state (the first method). For example, at K = 6.3 GPa, the performance of samples pre-deformed by cooling under stress was 40% higher than that of samples pre-deformed in the martensite state. In both cases, a non-monotonic dependence of work output on stiffness was observed (Figure 64c), with the maximum work output reached at stiffness values between 6 and 10 GPa. With an increase in the number of thermal cycles, the difference in the values of reversible strain, recovery stresses, and work output of the alloy between samples pre-deformed by different methods decreases (Figure 65).

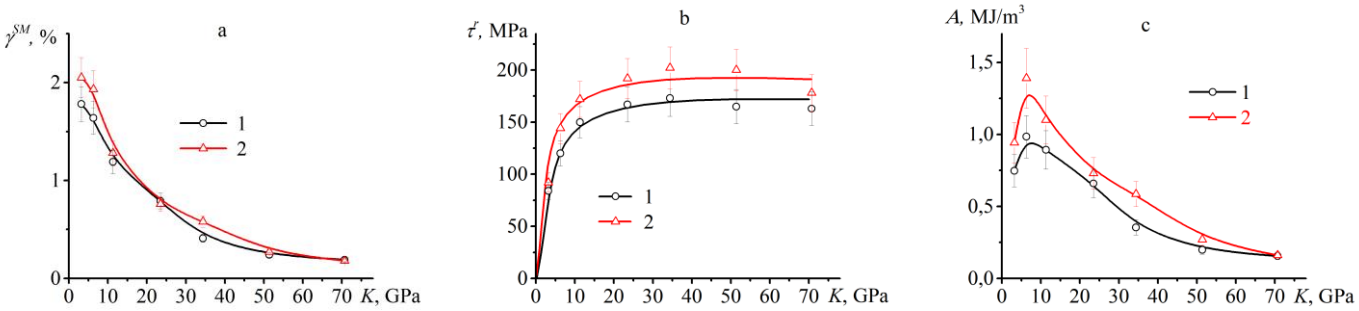

Figure 65. Dependencies of reversible strain (a), recovery stresses (b), and work (c) on the stiffness of the counter-face obtained in the tenth thermal cycle for samples pre-deformed in the martensite state (1) or cooled under constant stress (2).

On figures 64b and 65b, it can be observed that as the stiffness increases up to 23.5 GPa, the recovery stresses grow, reaching their maximum value. Afterwards, for K>23.5 GPa, they remain constant regardless of the pre-deformation method. To explain this phenomenon, let's analyze the changes in stress and strain during the first heating of the pre-deformed sample. Figure 66 presents a deformation diagram obtained at a temperature of 180°C (in the austenitic state), with points corresponding to the measured strain and stress values after the first heating with different stiffness values (stiffness values K are indicated near the points). The red points correspond to values obtained in samples pre-deformed by cooling under constant stress, while the green ones represent values obtained for samples pre-deformed in the martensite state. It can be seen that at low stiffness (K≤11.3 GPa), the stresses after heating are significantly lower than the stress corresponding to the $\sigma(\varepsilon)$ curve. Increasing the stiffness at which heating occurs increases the stress value, and the points approach the $\sigma(\varepsilon)$ curve. At high stiffness values, the stress generated by the sample reaches the yield point, and plastic strain occurs, while the recovery stress remains unchanged. This result is consistent with the findings of reference [155], where the authors indicate that the values of recovery stresses is limited by the corresponding stress value on the stress-strain curve in the austenite state.

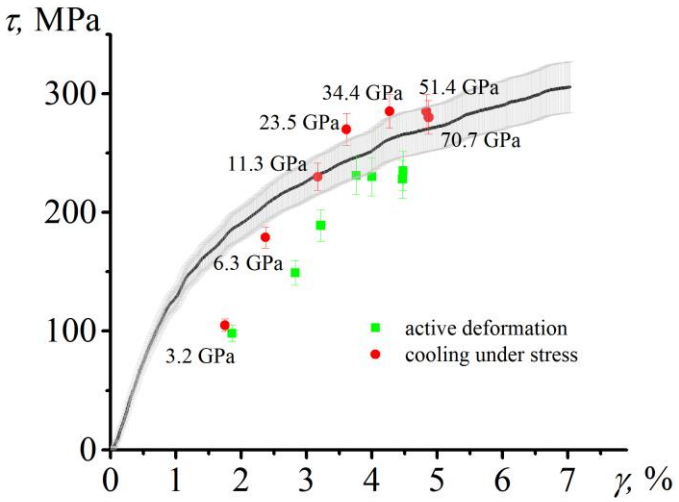

Figure 66. Deformation diagram obtained at 180°C (in fully austenite state) for NiTi alloy under torsional loading. Points represent the strain and stress values in samples after the first heating. The gray area indicates the statistical spread for the stress-strain curve.

The influence of stiffness on the irreversible strain after ten thermal cycles, measured in samples pre-deformed by different methods, is shown in Figure 67. It can be observed that if K < 30 GPa, the irreversible strain in the sample pre-deformed by cooling under stress is slightly less than in samples pre-deformed in the martensitic state. If K > 30 GPa, the value of γpl did not depend on the method of pre-deformation.

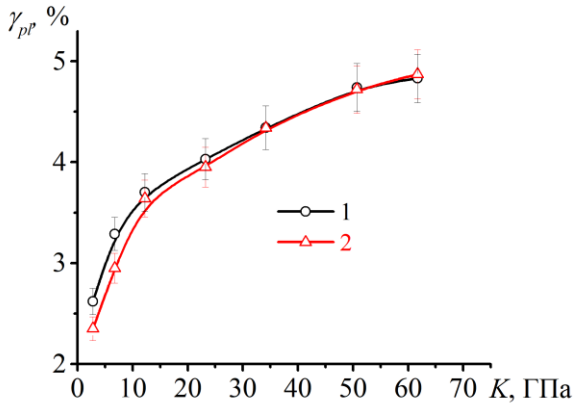

Figure 67. The influence of stiffness on the value of irreversible strain, measured after ten thermal cycles, in samples pre-deformed in the martensitic state or cooled under constant stress.

Comparison of the dependencies of $\gamma^{SM}(K)$, $\tau_r(K)$, and $A(K)$, $\gamma_{pl}(K)$ shown in Figures 64 and 67 revealed that pre-straining by cooling under constant stress provides higher values of recoverable strain, recovery stresses, and work, and leads to less accumulation of plastic strain at low stiffness values compared to active straining in the martensitic state. This is because the inelastic strain in SMA can be either reversible or irreversible. Reversible strain is caused by the formation of oriented martensite, which recovers when martensite disappears upon heating due to reverse transformation. Irreversible strain is caused by dislocation slip that occurs during pre-straining. The residual strain observed after straining is the sum of these two contributions. Comparing the two pre-straining methods assumes that the residual strain in the samples after straining was the same; however, the contributions of reversible and irreversible strain could be different. It is known that the process of oriented martensite formation during cooling under stress is associated with less irreversible strain than reorientation of martensite variants during straining in the martensitic state [156]. In this case, after pre-deforming by cooling under stress, the value of reversible strain (γ^{SM}) will be greater than after active straining in the martensitic state, leading to higher recovery stresses and, consequently, work performed during heating. During thermal cycling, regardless of the pre-deforming method, martensite forms during cooling under variable stresses, so the dependence of functional properties on the pre-deforming method disappears over cycles.

Thus, the results of the study showed that there is a complex, nonlinear relationship between the values of recoverable strain and maximum recovery stresses regardless of the pre-deforming method of the NiTi alloy. This is due to the fact that the level of generated stresses is limited by the magnitude of the dislocation slip limit in the austenitic state. The nonlinear dependence of the values of the shape memory effect and the generated forces on the stiffness of the counter sample leads to a non-monotonic dependence of the work performed during heating on the stiffness. The maximum work performed is observed at a stiffness of the counter sample ranging from 6 to 10 GPa. Pre-straining by cooling under constant stress enhances the functional properties of the alloy compared to pre-straining in the martensitic state. This is due to the influence of the straining method on the values of reversible strain. However, with cycles, the difference

becomes insignificant, since straining of the alloy occurs uniformly in each cycle - during cooling under variable stress through the temperature interval of forward transformation. Based on this, it can be concluded that both pre-straining methods can be used in the creation of actuators.

3.1.4. Influence of pre-straining in the austenite state on variations in the functional properties of NiTi alloy during thermal cycling in actuator mode

The results presented in sections 3.1.2 and 3.1.3 have shown that during actuator mode heating, the value of maximum recovery stresses is limited by the stress corresponding to the minimum strain observed after heating on the deformation diagram obtained in the austenite state. This stress can be increased by strengthening the alloy, so it can be assumed that to increase recovery stresses, it is necessary to increase the yield stress of the austenite, which is achieved by strengthening the alloy. Various methods of strengthening exist, such as cold rolling, severe plastic deformation, or preloading, and all of them have been successfully used to increase recovery stresses [157–159]. However, the mentioned studies investigated the influence of strengthening on recovery stresses during heating of the sample under rigid fixation conditions, i.e., under infinite stiffness. However, as shown in sections 3.1.2 and 3.1.3, the stiffness of the counterbody affects the value of recovery stresses and their variation during thermal cycling. Therefore, in this dissertation, we studied the influence of pre-strain imposed in the austenite state on recovery stresses, the value of the shape memory effect, and the work done during heating in one cycle in actuator mode with different stiffness.

Samples, their dimensions, and heat treatment described in section 3.1.3 were pre-strained to 10% or 20% at a temperature of 200°C (austenite state) and then unloaded. The samples were then loaded to 250 MPa with a counterbody stiffness of 8 GPa and cooled to room temperature. Upon cooling through the forward martensitic transformation temperature range, the sample accumulated strain, leading to stress relaxation (Figure 68). At room temperature, the sample was unloaded, and the counterbody stiffness was changed to the selected value (4.6 GPa, 8 GPa, 49.2 GPa, or 88.7 GPa), and subjected to a single thermal cycle in the range of 180÷30°C.

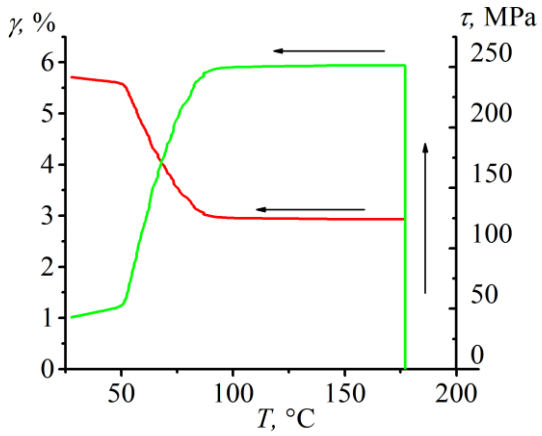

Figure 68. Stress (green line) and strain (red line) dependencies during the first cooling cycle (a) at a stiffness of 8 GPa.

Based on the dependencies of $\gamma(T)$ and $\tau(T)$, the value of the shape memory effect and maximum recovery stresses were determined as shown in Figure 58. Figure 69 illustrates the dependencies of the shape memory effect values and recovery stresses on stiffness obtained in the first cycle for samples with different pre-strain in the austenite state (0%, 10%, and 20%). It can be observed that pre-straining up to 10% or 20% does not affect the recovery stresses at a stiffness of 4.6 GPa, while at 8 GPa (Figure 69a), the value of reversible strain decreases (Figure 69b), leading to a reduction in the work performed by the alloy during heating. At the same time, pre-straining in the austenite state significantly increases the value of maximum recovery stresses at high stiffness values (49.2 GPa and 88.7 GPa). For instance, at a counterbody stiffness of 49.2 GPa, the recovery stresses increased from 245 MPa to 271 MPa after 10% pre-straining and to 294 MPa after 20% pre-straining, while the value of the shape memory effect remained unchanged. The different influence of plastic deformation on recovery stresses at different stiffness levels is due to the fact that at low stiffnesses, the maximum recovery stress does not reach the yield stress of the austenite (see Figure 66), so increasing the yield strength does not affect the recovery stress. At high counterbody stiffness values, the maximum recovery stress reaches the yield stress of the austenite, so its change due to strengthening affects the maximum recovery stress.

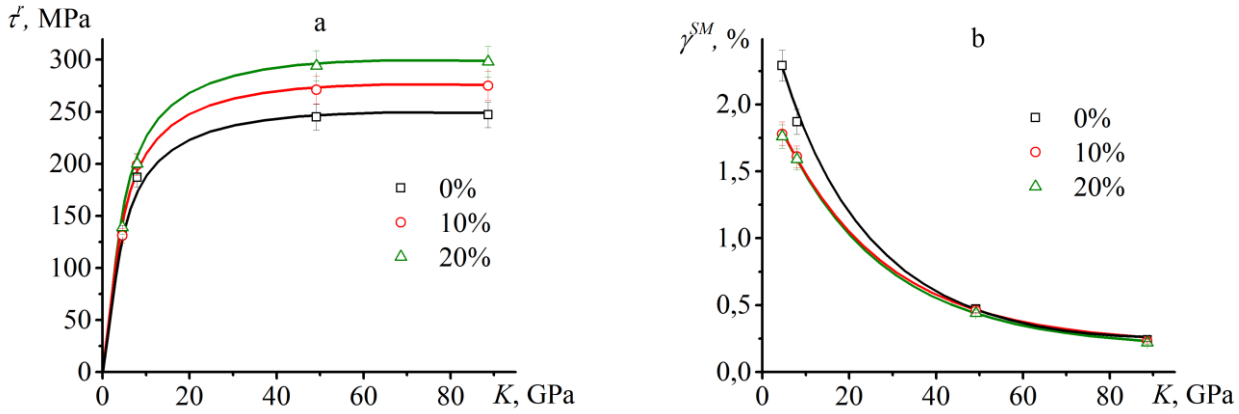

Figure 69. Dependencies of recovery stresses (a) and shape memory effect (b) values on stiffness obtained in the first thermal cycle in samples pre-strained in the austenite state to 0%, 10%, and 20%.

Variations in recovery stress and reversible strain lead to variations in work output, the dependencies of which on stiffness in the first cycle are presented in Figure 70.

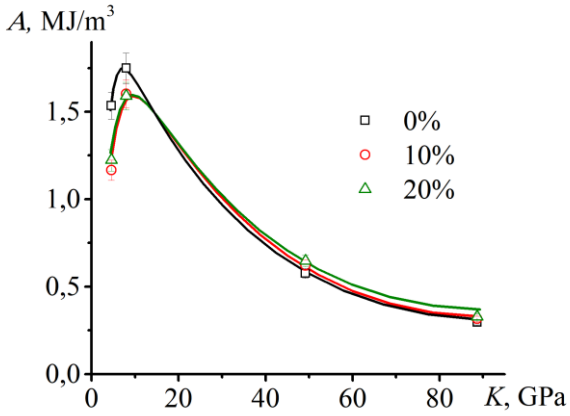

Figure 70. Dependencies of the work output on stiffness, obtained in samples pre-strained in the austenite state to 0%, 10%, and 20% in the first thermal cycle.

It can be observed that the maximum work performed by the alloy at a stiffness of 8 GPa was 1.75 MJ/m³ in the sample without pre-strain and 1.6 MJ/m³ in the sample pre-strained by 20% in the austenite state. At a stiffness of 88.7 GPa, the work performed by the alloy was 0.29 MJ/m³ without pre-strain and 0.33 MJ/m³ in the sample pre-strained by 20% in the austenite state. Thus, the results of the study showed that strengthening the austenitic phase through pre-strain allows for an increase in recovery stresses and the work performed in thermal cycles at high stiffness values. However, the reversible strain at

such stiffnesses is minimal, so even with high recovery stresses, the work performed during heating will be less than in NiTi alloy without pre-deformation, which undergoes thermal cycling in drive mode with low stiffness.

3.2. The influence of transformation fraction during thermal cycling in drive mode on variations in the functional properties of NiTi alloy

Chapter 2 demonstrated that thermal cycling through an incomplete martensitic transformation interval (both forward and reverse) significantly improves the stability of NiTi alloy properties and reduces the accumulation of plastic strain. However, the results in Chapter 2 were obtained for thermal cycling under constant stress. However, in actuators, the NiTi alloy component is connected to an elastic counterbody, which provides the device's multiple actuations. In this case, the NiTi alloy element is heated under increasing stress and cooled under decreasing stress. It has been previously established that changes in properties during thermal cycling depend not only on the transformation fraction but also on the value of the applied stress. Since stresses in the actuator vary during heating and cooling, the variations in the properties of the NiTi alloy element during thermal cycling in the actuator mode will be different compared to variations in its properties during thermal cycling under constant stress. Thus, it is necessary to study the influence of the forward and reverse martensitic transformation fraction on the changes in the properties of the NiTi alloy during thermal cycling in the actuator mode. This study was conducted in the present work, and the results were published in [64,65].

The setup and objects of the study are described in section 3.1.1. Since it was shown in section 3.1.3. that the cocking method does not affect the changes in the functional properties during thermal cycling of the NiTi alloy in the actuator mode, in this study, the specimens were pre-deformed in the martensitic state. The level of stresses generated during heating is determined by the stiffness of the counterbody and the value of the recoverable strain, which, in turn, depends on the value of the pre-deformation of the sample. In turn, the value of the recovery stresses may affect the variations in the properties of the NiTi alloy during thermal cycling in the actuator mode. To study the influence of pre-deformation on the variations in the functional properties of the NiTi alloy in the actuator mode, in this study, samples made of NiTi alloy were deformed in

the martensitic state to different values of pre-deformation: 3%, 5%, or 7%. After pre-deformation, the samples were unloaded, connected to the counterbody, and heated to 180°C. The mass on the lever was chosen to provide a stiffness of 8 GPa (selected based on data presented in section 0). Table 4 presents the values of residual strain after unloading, shape memory effect, plastic strain, and maximum generated stress in the zero cycle (during the first heating).

Table 4. Residual strain measured after pre-deformation (γ_{res}), value of shape memory effect (γ_0^{SM}) during the first heating, plastic strain (γ_{pl}^0), and recovery stresses measured during the first heating (τ_r^0).

γ_{giv}, %	γ_{res}, %	γ_0^{SM}, %	γ_{pl}^0, %	τ^r_0, MPa
3	1.6±0.1	0.9±0.1	0.7±0.1	73±3
5	3.3±0.1	1.5±0.1	1.8±0.1	120±5
7	5.1±0.2	2.2±0.2	2.9±0.1	180±5

It can be observed that all values increase with increasing pre-deformation. For example, increasing the pre-deformation from 3% to 7% led to an increase in γ_0^{SM} from 0.9% to 2.2%, and the value of τ^r_0 increased from 73 MPa to 180 MPa.

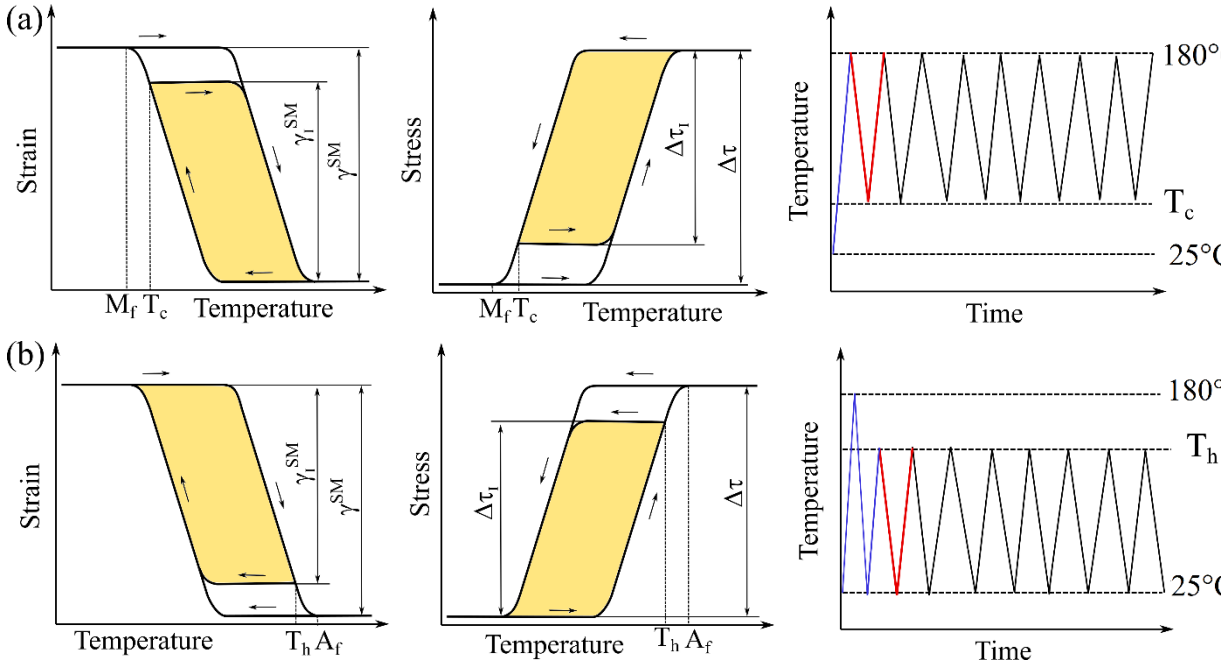

Figure 71. Thermocycling schemes in Mode I (a) and in Mode II (b). The red lines represent the first cycle.

To investigate the influence of the forward and reverse transformation fractions on the drive parameters samples were subjected to full transformation range cycling and two

thermocycling modes were used for partial transformation range cycling. In Mode I, samples were cooled and heated within the temperature range from 180°C to T_c, chosen within the temperatures of the direct transformation range ($M_s < T_c < M_f$), thereby altering the forward transformation fraction (Figure 71a). In Mode II, samples were cooled and heated within the range from T_h to 25°C, with T_h chosen within the temperatures of the reverse transformation range ($Af < T_h < As$), thus varying the reverse transformation fraction. For this, samples were heated to 180°C, cooled to 25°C (through the complete forward transformation range), and then heated to the temperature T_h. Subsequently, the sample underwent thermocycling within the temperature range from T_h to 25°C (Figure 71b).

Table 5. Sample labeling according to the value of pre-strain, mode used, and the fraction of work realized in the first cycle. The label "full" applies to samples subjected to thermocycling through the full temperature range of martensitic transformations.

γ_{giv}, %	**$\Phi = A_1^* / A_1^{full}$ (work output fraction realized on first cycle)**								
	1	**Regime I**				**Regime II**			
		90%	**75%**	**50%**	**25%**	**90%**	**75%**	**50%**	**25%**
3	3-full	3-0.9c	3-0.75c	3-0.5c	3-0.25c	3-0.9h	3-0.75h	3-0.5h	3-0.25h
5	5-full	5-0.9c	5-0.75c	5-0.5c	5-0.25c	5-0.9h	5-0.75h	5-0.5h	5-0.25h
7	7-full	7-0.9c	7-0.75c	7-0.5c	7-0.25c	7-0.9h	7-0.75h	7-0.5h	7-0.25h

The values of T_c and T_h were chosen such that in the first partial cycle, the work production (A_1*) equaled 25%, 50%, 75%, or 90% of the work performed in the first full cycle (A_1^{full}). The temperatures T_c and T_h were determined based on the data obtained during thermocycling in the complete range, where samples were cooled and heated in the drive mode within the temperature range from 180 to 25°C.

In Table 5, samples are labeled according to the value of pre-strain, thermocycling mode, and the fraction of work output realized in the first cycle. For instance, the sample "7-0.75c" underwent deformation of 7% and was subjected to thermocycling in Mode I with 75% work realization.

In Figure 72, dependencies of γ(T) and τ(T) are presented for the first heating cycle (black line) and during the first thermocycle (red line) in both modes for samples pre-strained by 7%. In Mode I, cooling was interrupted at the temperature T_c, which was higher than M_f, after which the sample was heated to a temperature of 180°C, which was above the A_f temperature (Figure 72a, b).

Regime I

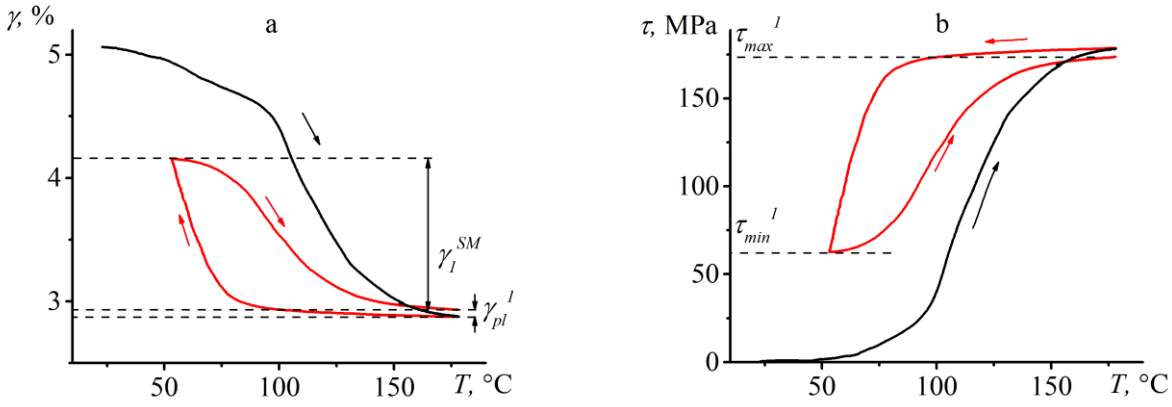

Regime II

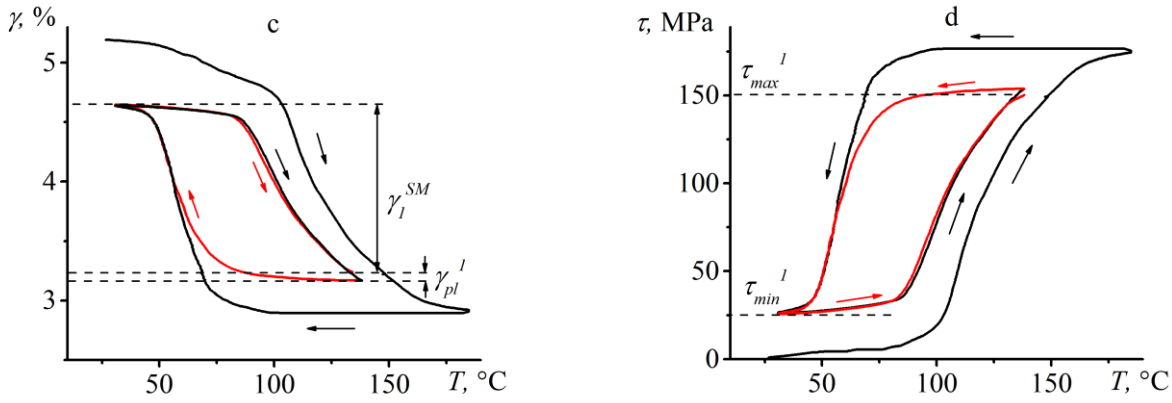

Figure 72. Variations in strain (a, c) and stress (b, d) during heating of samples pre-strained by 7% and subjected to heating and the first thermocycle in Mode I (a, b) or Mode II (c, d).

In Mode II, cooling was conducted to a temperature of 25°C, which was below the M_f temperature, and heating was halted until the completion of the reverse transformation at the temperature T_h (Figure 72c, d). During heating in the temperature range of the reverse transformation, strain recovery (γ_1^{SM}) was observed, and within the same range, stress generation occurred up to τmax1. Regardless of the selected mode, strain recovery was

not complete, indicating irreversible strain (γ_{pl}^{1}). Based on the dependencies of γ(T) and τ(T), the value of reversible strain (γ^{SM}), minimum (τ_{min}), and maximum (τ_{max}) stress during heating, and irreversible strain (γ_{pl}) were measured in each cycle, as shown in Figure 72.

Figure 73 depicts the variations in the values of γ^{SM}, τ_{max}, τ_{min}, A*, and γ_{pl} during the thermocycling of samples pre-deformed by 7%. It can be observed that the variation in recoverable strain (γ^{SM}) during thermocycling depends on the transformation ratio and the cycling mode (Figure 73 a, b). The smaller the fraction of direct or reverse transformation realized in the first cycle, the lesser the variations in γ^{SM} values. For instance, over 15 cycles in the full range, γ^{SM} decreased from 2% to 1.7%, whereas with a 25% transformation fraction in Mode I, γ^{SM} reduced from 0.99% to 0.97%.

The reduction in the value of γ^{SM} with an increase in the number of cycles in Mode I was significantly less than in Mode II. For instance, after fifteen cycles, the value of γ^{SM} decreased by 0.17% in Mode I (sample 7-0.9c) and by 0.3% in the full cycle or Mode II (samples 7-full or 7-0.9h).

Figures 73c,d depict the dependencies of minimum and maximum stress on the cycle number. If thermocycling was conducted within the full range of martensitic transformation temperatures or in Mode II, the minimum stress remained unchanged throughout the cycles, ranging from 28 to 33 MPa. If thermocycling was conducted in Mode I, the minimum stress remained constant throughout the cycles, and its value depended on the fraction of forward transformation: the smaller the fraction, the greater the minimum stress (Figure 73c). The maximum stress always decreased with an increase in the cycle number; however, the variations in τ_{max} during thermocycling in Mode I were less pronounced than in Mode II. For instance, over fifteen cycles, the maximum stress decreased from 175 to 169 MPa in Mode I (sample 7-0.75c) and from 149 to 133 MPa in Mode II (sample 7-0.75h).

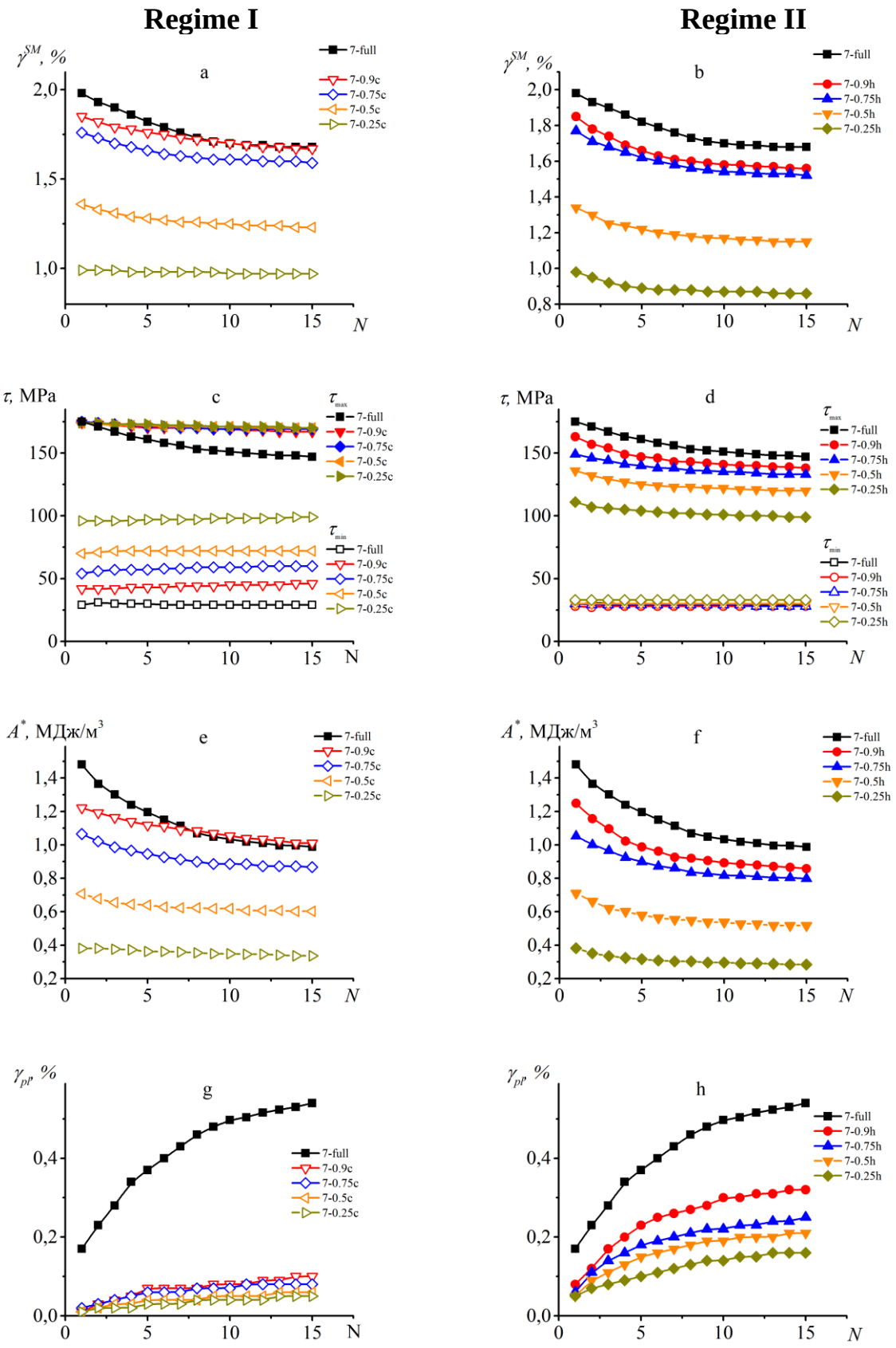

Figure 73. Variations in the values of γ^{SM} (a, b), τ_{min} (c, d), τ_{max} (c, d), A* (e, f), and γ_{pl} (g, h) during multiple thermocycling of NiTi alloy in Modes I and II. The pre-deformation was 7%.

Variations in the values of shape memory effect, maximum and minimum stress during thermocycling result in variations in the work performed by the alloy during heating. As shown in Figures 73e,f, the change in work output during thermocycling in Mode I was

less than in Mode II. In Mode I, the value of A decreased from 1.22 to 1.0 MJ/m^3 (in sample 7-0.9c), whereas in Mode II, it decreased from 1.22 to 0.85 MJ/m^3 (in sample 7-0.9h).

The dependencies of plastic strain on the cycle number during thermocycling in different modes are presented in Figures 73g,h. It can be observed that thermocycling in Mode I was accompanied by less variation in plastic strain compared to full cycles or Mode II. Thermocycling in Mode II resulted in less intense accumulation of plastic strain compared to full cycles but was significantly higher than in Mode I. For instance, the value of plastic strain was 0.1% after 15 cycles in Mode I (sample 7-0.9c), which was three times less than in Mode II (sample 7-0.9h) and five times less than in the full cycle (sample 7-full).

To determine the influence of pre-deformation on properties changes during thermocycling in incomplete martensitic transformation ranges, the change in the ratio of A_{15}^* to A_1^* (the ratio of work (A_{15}^*) measured in the 15th cycle to work A_1^* measured in the first cycle) was analyzed with varying transformation fractions in both modes (Figure 74).

It's evident that with an increase in the transformation fraction during thermocycling in Mode I, the value of A_{15}^*/A_1^* decreases in samples pre-deformed at 5% or 7%, and changes slightly in samples pre-deformed at 3% (Figure 74a). The reduction in A_{15}^*/A_1^* with an increase in the fraction is due to more pronounced accumulation of plastic strain. This accumulation, in turn, leads to variations in the values of strain recovery and reactive stresses. In Mode II thermocycling, the value of A_{15}^*/A_1^* increased with the growth of the transformation fraction in samples pre-deformed at 3% or 5%, and decreased in samples pre-deformed at 7% (Figure 74b). Comparison of the results obtained in the two modes for samples with the same Φ value shows that thermocycling in Mode I results in less variation in the work performed compared to Mode II. For

example, the value of A_{15}^*/A_1^* is 83% in Mode I (sample 7-0.9c) and 68% in Mode II (sample 7-0.9h).

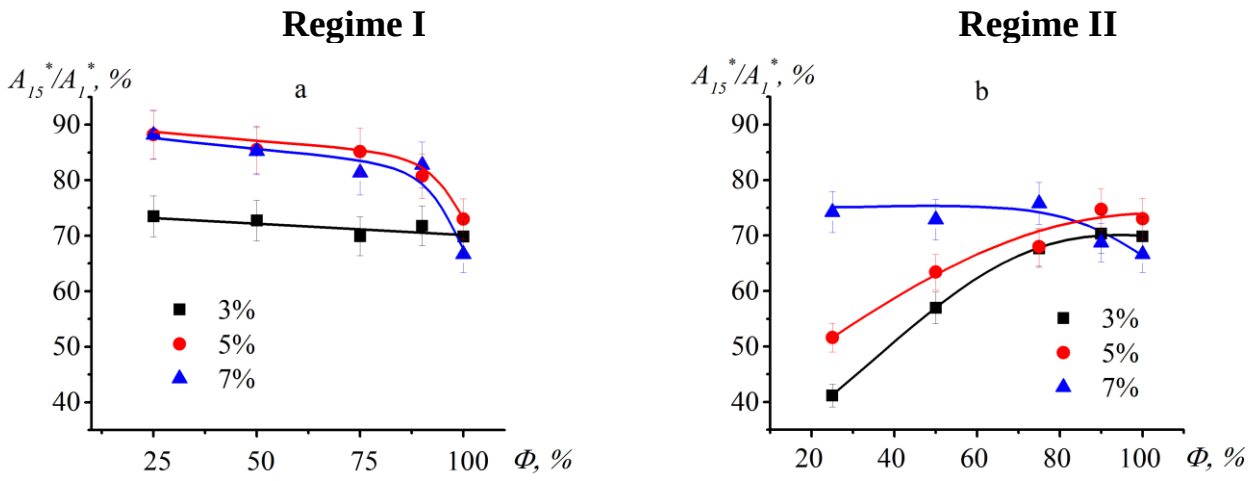

Figure 74. Dependencies of the change in workability A^* after 15 cycles in Mode I (a) or II (b) on the parameter Φ (the fraction of work realized in the first cycle) in samples pre-deformed in the martensite state.

Since the variation in strain recovery, reactive stresses, and work performed during thermocycling is related to plastic strain, let's consider how it changes depending on the realized fraction. Figure 75 shows the relationship between the value of plastic strain after 15 cycles in the incomplete temperature range of martensitic transformations and during thermocycling in a full cycle, depending on the fraction Φ. It's clear that in Mode I thermal cycling, reducing the parameter Φ significantly decreases plastic strain regardless of the pre-strain value. For instance, reducing Φ from 100% to 90% reduces plastic strain by a factor of 5. Further reduction in Φ has minimal impact on plastic strain (Figure 75a). In Mode II thermal cycling, the reduction in Φ results in varying reductions in plastic strain depending on the initial strain. The higher the initial strain, the greater the reduction in plastic strain with decreasing Φ.

Thus, the study findings demonstrate that variations in functional properties and the accumulation of irreversible strain during thermal cycling in NiTi alloy drive mode are influenced by the fraction of forward or reverse transformations. In Mode I (partial forward transformation), reduction in the fraction from 100% to 90% significantly decreased plastic strain accumulation, irrespective of the initial strain (Figure 75a).

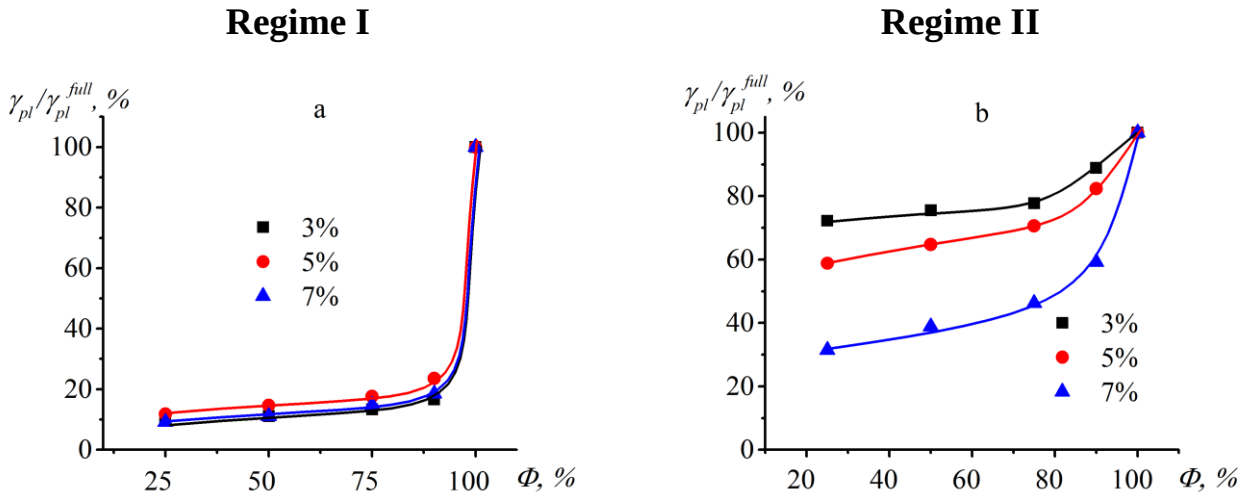

Figure 75. Relationship between the values of plastic strain accumulated over 15 thermal cycles in mode I (a) or II (b) and the plastic strain accumulated during thermal cycling over the full range, depending on the realized fraction of work output.

In samples pre-deformed to 5% and 7%, work decreased by 30-35% over 15 thermal cycles at Φ=100%, and by 20% at Φ=90% (Figure 74a). In Mode II (partial reverse transformation), the variation in plastic strain due to the reverse transition fraction depends on the initial strain value. Maximum changes were observed in samples pre-deformed to 7%. In these samples, reducing the reverse transition fraction from 100% to 90% decreased plastic strain by only 2 times (Figure 75b). Furthermore, plastic strain did not decrease by five times under any reverse transition fraction, as observed in Mode I. The change in the accumulated work over 15 thermal cycles at Φ=90% was nearly the same as at Φ=100% (Figure 74b). This indicates that reducing the reverse transition fraction by 10% does not enhance the stability of the alloy's functional properties. In all cases of reverse transition fraction, a reduction of over 20% in the accumulated work over 15 thermal cycles was observed (Figure 74b).

Thus, the results presented in Chapter 3, similar to those in Chapter 2, demonstrate that to improve the stability of NiTi alloy properties, reducing the direct transition fraction is more effective. This is because the direct transformation increases defect density. Therefore, limiting this process by reducing the direct transition fraction allows for controlling the stability of the alloy's functional properties during thermal cycling in drive mode. The results presented in Chapter 2, where samples were thermally cycled through

partial transformation ranges under constant load, showed that the main change in defect density occurs during the second half of the forward transition. Thus, excluding this part of the transformation helps stabilize the properties of the alloy. The results presented in Chapter 3 demonstrate that during thermal cycling in drive mode, excluding only the last 10% of the forward transformation significantly reduces plastic strain (by a factor of 5) and improves property stability. This difference is due to stress reduction during cooling in drive mode. As demonstrated in Chapter 2, the lower the stress at which martensite crystals form, the less the variation in defect density and plastic strain, leading to more stable functional properties during thermal cycling.

3.3. The influence of the temperature cycle position relative to the martensitic transition temperatures on the variation of the NiTi alloy functional properties during thermal cycling in drive mode within an incomplete temperature range

The results presented in Section 3.2 have shown that the variation of drive parameters (reversible strain, generated forces, work output) and the accumulation of plastic strain depend on the fraction of forward and reverse transformations realized during cooling or heating. However, the same transformation fraction can be achieved at different positions of the maximum and minimum temperatures in the cycle relative to the martensitic transition temperatures. As shown in the previous section, reducing the fraction of forward transformation during cooling by increasing the minimum cycle temperature (T_c) at a constant maximum cycle temperature significantly improves the stability of the NiTi alloy properties. Similarly, it has been shown in the same section that reducing the fraction of reverse transformation during heating by decreasing the temperature T_h at a constant lower boundary of thermal cycling also enhances the stability of NiTi properties and reduces the accumulation of irreversible strain. Thus, it can be assumed that there exists an optimal temperature range $T_{max} \div T_{min}$, where the minimum temperature T_{min} is above M_f and the temperature T_{max} is below A_f, in which the variation in the properties of the NiTi alloy during thermal cycling will be minimal. Therefore, one of the objectives of the dissertation was to investigate the influence of the position of the maximum and minimum temperatures in the cycle relative to the martensitic transition temperatures on the variations in the shape memory effect, reactive stresses, work performed during heating, and irreversible strain during thermal cycling. The temperatures T_{min} and T_{max} were selected to ensure a cycle in which the work was half of the work in the full cycle, the value of which is 1.4 MJ/m³. Six temperature ranges were chosen, and the maximum and minimum temperatures in each range are presented in Table 6. Additionally, in this table, sample 7 is indicated, which was thermally cycled in the temperature range of complete transitions, i.e., from 180 to 25°C. The value of the

preliminary deformation of the NiTi alloy element was 7%, and the mass of the counter sample was chosen to achieve a system stiffness of 8 GPa.

Table 6. Maximum and minimum temperatures of thermal cycling intervals (Martensitic transition temperatures according to DSC data M_s = 59°C, M_f = 37°C, A_s = 67°C and A_f =90°C).

Sample, №	**1**	**2**	**3**	**4**	**5**	**6**	**7**
T_{max}, °C	120	123	130	133	137	180	180
T_{min}, °C	25	44	47	49	51	55	25

The research methodology was as follows:

1. The sample was pre-deformed by 7% at room temperature and connected to a counterbody.
2. The sample was heated to 180°C in a drive mode (one side of the sample was fixed, while the other was connected to a dynamometric pendulum).
3. The sample underwent 15 thermal cycles in the temperature range T_{min} - T_{max}, the values of which are presented in Table 6.

Figure 76 shows the dependencies of strain on temperature obtained for samples 1

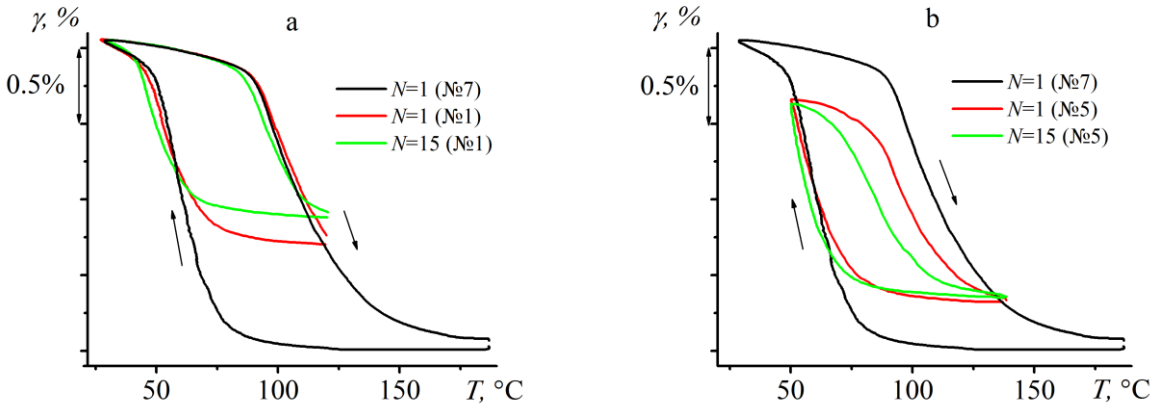

Figure 76. Dependencies of strain on temperature obtained during the first (red curve) and fifteenth (green curve) thermal cycles for sample 1 in the range of 120 to 25°C (a), and sample 5 (137 to 51°C) (b). The black curve represents the dependence of γ(T) for sample 7 in the range of 180 to 25°C.

and 5 in the 1st and 15th cycles, as well as for the first cycle in sample 7 (black curve). It can be seen that after fifteen thermal cycles, the value of the shape memory effect

significantly decreased in sample 1 (Figure 76a), while this parameter remained unchanged in sample 5. Based on γ(T) and τ(T), the values of γ^{SM}, plastic strain γ_{pl}, maximum τ_{max}, and minimum τ_{min} stresses in the cycle were determined, similar to what was done in Section 3.2. (Figure 72). The value of plastic strain γ_{pl} was calculated as the cumulative irreversible strain accumulated by the end of the current cycle.

Figure 77 depicts the dependencies of the transformation (recovered) strain (γ^{SM}), plastic strain, and maximum and minimum stresses on the cycle number during thermal

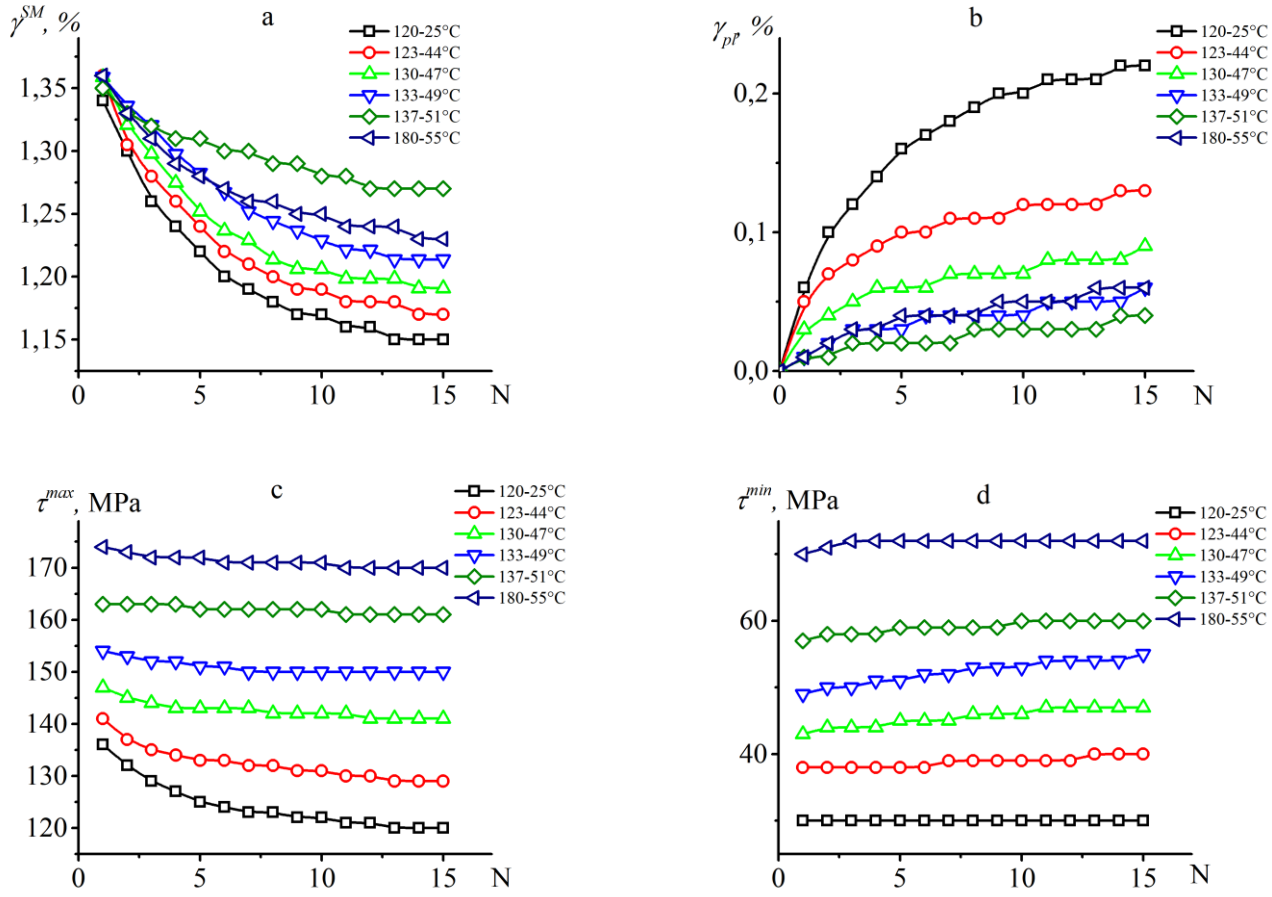

Figure 77. Dependencies of γ^{SM} (a), γ_{pl} (b), τ_{max} (c), τ_{min} (d) on the cycle number (N) obtained during thermal cycling in various temperature ranges. Values of T_{max} and T_{min} are indicated in the legend.

cycling in various temperature ranges. It is evident that with an increase in the number of cycles, the value of γ^{SM} decreases in all samples regardless of the cycling range (Figure 77a). However, the change in the value of forward transformation strain for one cycle depends on the position of the temperature range relative to the martensitic transformation temperatures. The greatest variation in γ^{SM} over 15 cycles was observed in sample No. 1

(T_{max} = 120°C and T_{min} = 30°C). The smallest variation in γ^{SM} was found when cycling in the range of 137÷51°C (sample No. 5). Increasing the values of T_{max} and T_{min} above 137°C and 51°C, respectively (T_{max} = 180°C, T_{min} = 55°C), deteriorates the stability of the forward transformation strain during cycling (sample 6).

The dependencies of accumulated plastic strain on the cycle number are shown in Figure 77b. It can be observed that the accumulation of plastic strain correlates with variations in the recovered strain values. The maximum accumulation of plastic strain was observed in sample 1, while the minimum variation in γpl was detected in sample 5. For instance, over 15 thermal cycles in the temperature range of 137÷51°C, the plastic strain increased by only 0.04% (sample 5). Conversely, if the thermal cycling was conducted in the range of 120÷51°C, the change in plastic strain amounted to 0.2%.

In Figures 77c and d, the dependencies of maximum and minimum stress on the cycle number obtained during thermal cycling of NiTi alloy samples in different temperature ranges are shown. The minimum variation in recovery stresses was observed in sample 5 (137÷51°C).

The variation of work A during thermal cycling in different temperature ranges is depicted in Figure 78a. With an increase in the number of cycles, the work decreases in all samples. The largest variation in completed work was found in sample 1 (120÷25°C), where the value of A decreased from 0.7 MJ/m^3 in the first cycle to 0.5 MJ/m^3 in the fifteenth cycle. The smallest change in the value of A, from 0.72 MJ/m^3 in the first cycle to 0.64 MJ/m^3 in the 15^{th} cycle, occurred during thermal cycling of sample 5 in the temperature range of 137÷51°C. Increasing the value of T_{max} above A_f (sample 6) worsens the stability of completed work during thermal cycling. In Figure 78b, the work and plastic strain measured in the 15th cycle for each temperature range are presented. It can be seen that after fifteen cycles, the maximum work and minimum plastic strain are observed during thermal cycling in the temperature range of 137÷51°C.

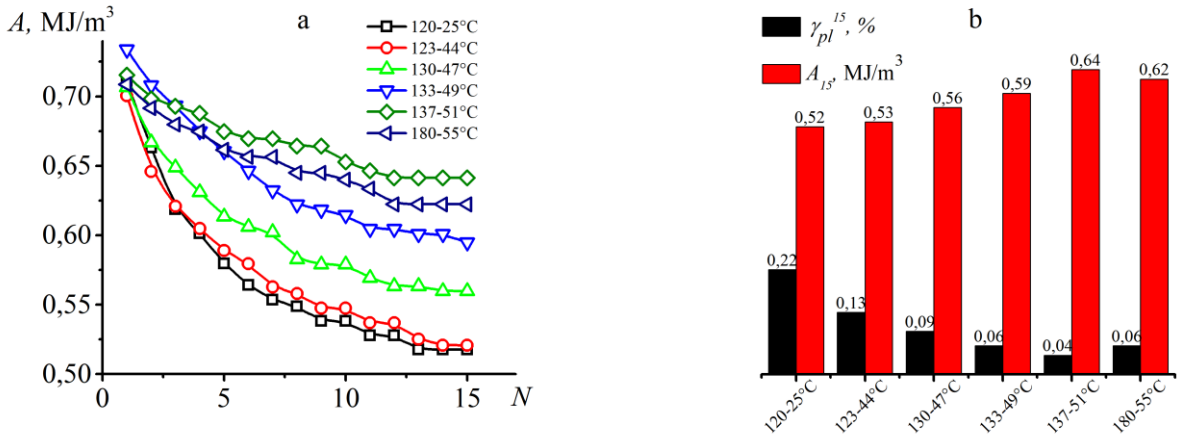

Figure 78. Dependence of work output (A) on the cycle number (N) obtained during thermal cycling of NiTi alloy samples in different temperature ranges (a). Work output and plastic strain measured in the 15th cycle (b) during thermal cycling of NiTi alloy samples in different temperature ranges.

The research results have shown that variations in the work output and accumulation of plastic strain during the thermal cycling of NiTi alloy depend not only on the fraction of forward transformations but also on the positions of T_{max} and T_{min} in the cycle relative to the start and finish temperatures of martensitic transitions. Increasing T_{min} from 25°C to 51°C, along with increasing T_{max} from 120°C to 137°C, led to an improvement in the stability of the alloy's functional behavior. Further increases in T_{min} from 51°C to 55°C and T_{max} from 137°C to 180°C worsened the stability of the work output. This is because increasing T_{min} from 25 to 51°C leads to the thermal cycling range encompassing only the first half of the forward transformation, while the main accumulation of plastic strain occurs during the final stage. Thus, thermal cycling of sample 1 was accompanied by the greatest accumulation of plastic strain since in this case T_{min} was lower than the M_f temperature, meaning the thermal cycling range included the second half of the forward transformation. In the case of sample 5, T_{min} was much higher than the M_f temperature, so the second half of the forward transition was hardly affected, resulting in minimal changes in plastic strain. Changing T_{max} from 120 to 137°C does not intensify the recovery processes upon heating, so the defect density remains unchanged. If T_{max} exceeded the A_f temperature (in sample 6), then the stability of the properties decreased because the recovery processes intensified upon heating. As a result, the defect

density decreased, making the alloy susceptible to accumulating plastic strain upon subsequent cooling, thus increasing plastic strain during thermal cycling.

Thus, two dependencies of plastic strain on temperature can be distinguished, one of which is determined by the fraction of forward transformation. In this case, the value of plastic strain increases as T_{min} decreases relative to M_s. The other dependence is determined by the intensity of recovery processes upon heating, so plastic strain increases with increasing T_{max}. Schematically, these dependencies can be represented as shown in Figure 79. It is evident that there is an optimal position for the temperatures T_{max} and T_{min}, at which the accumulation of plastic strain will be minimal. During the thermal cycling of the NiTi alloy in the drive mode within this range, the variations in its functional properties will be minimal.

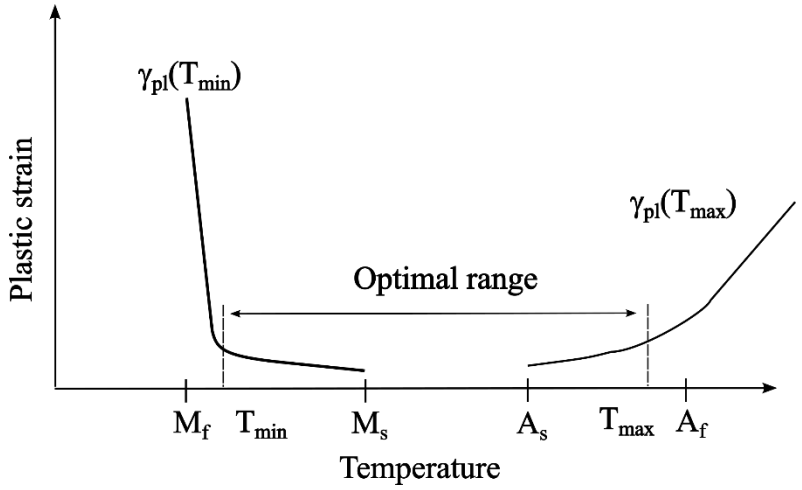

Figure 79. Optimal position of the temperature range for thermal cycling relative to the temperatures of martensitic transformations.

Based on the findings of the dissertation, recommendations can be formulated regarding the selection of optimal temperature, strain, and force regimes for NiTi alloy actuation:

1. Preliminary strain of the NiTi alloy element can be achieved through active deformation or stress-induced cooling. The value of the preliminary strain should be in the range of 5-7%.
2. The selection of the counter-body should ensure a stiffness of 6-10 GPa.

3. Thermal cycling of the actuator should be conducted in a manner that excludes the completion of the forward transformation during cooling. The less involvement of the second half of the forward transition during cooling, the better stability of the actuator parameters will be observed during thermal cycling. The maximum temperature in the cycle should be chosen slightly below the A_f temperature to reduce the contribution of the softening process to defects accumulation.

3.4. Variations in the functional properties of a torsional actuator with an working body made of NiTi alloy at high numbers of thermal cycles.

The results of the study described in 3.3. showed that there is an optimal range of thermal cycling where the operation of the actuator is accompanied by the least variation in device performance. However, these data were obtained with a small number of cycles (N = 15). For most practical applications, it is necessary for shape memory alloy-based actuators to reliably operate for thousands of cycles [9,16]. Moreover, it is known that the functional properties of shape memory alloys may not change monotonically depending on the number of thermal cycles [26,160]. To understand how the results obtained with a small number of cycles of thermal cycling can be applicable to actuators operating in real conditions (over 1000 cycles), investigations of reversible strain, recovery stresses, work output, and plastic deformation were conducted over 1000 cycles.

To address this issue, a torsional actuator operating in automatic mode was created. Figure 80 shows the overall view of the actuator. The working body made of NiTi shape memory alloy (1) is secured between the parts of the split shaft (2), one part of which has a rigid fastening, while the other is attached to a lever with a mass and a digital inclinometer. Automatic operation was ensured by the TRM-201 measurement regulator (4), which, upon the regulator's command, applies current to the induction heater circuit (5). Once the temperature reaches the required value, the circuit is disconnected, and the sample is cooled to the specified temperature. Once the desired temperature is reached during cooling, the regulator again applies current to the electrical circuit.

To eliminate the risk of anisotropy in the temperature field across the sample cross-section during induction heating, the frequency of the current was chosen to achieve a regime of volumetric (deep) heating. This mode is realized when the depth of current penetration equals half the diameter of the sample. The following formula was used to calculate the depth of current penetration:

$$Z_a = 503\sqrt{\frac{\rho}{\mu f}}, \qquad (3.5)$$

where ρ is the resistivity of the conductor material (60÷90 μΩ*cm for NiTi alloy), μ is the relative magnetic permeability (1.002), and f is the current frequency. Assuming the required depth of current penetration is 1 mm, using formula 3.5, we find the value of f to be 210 kHz.

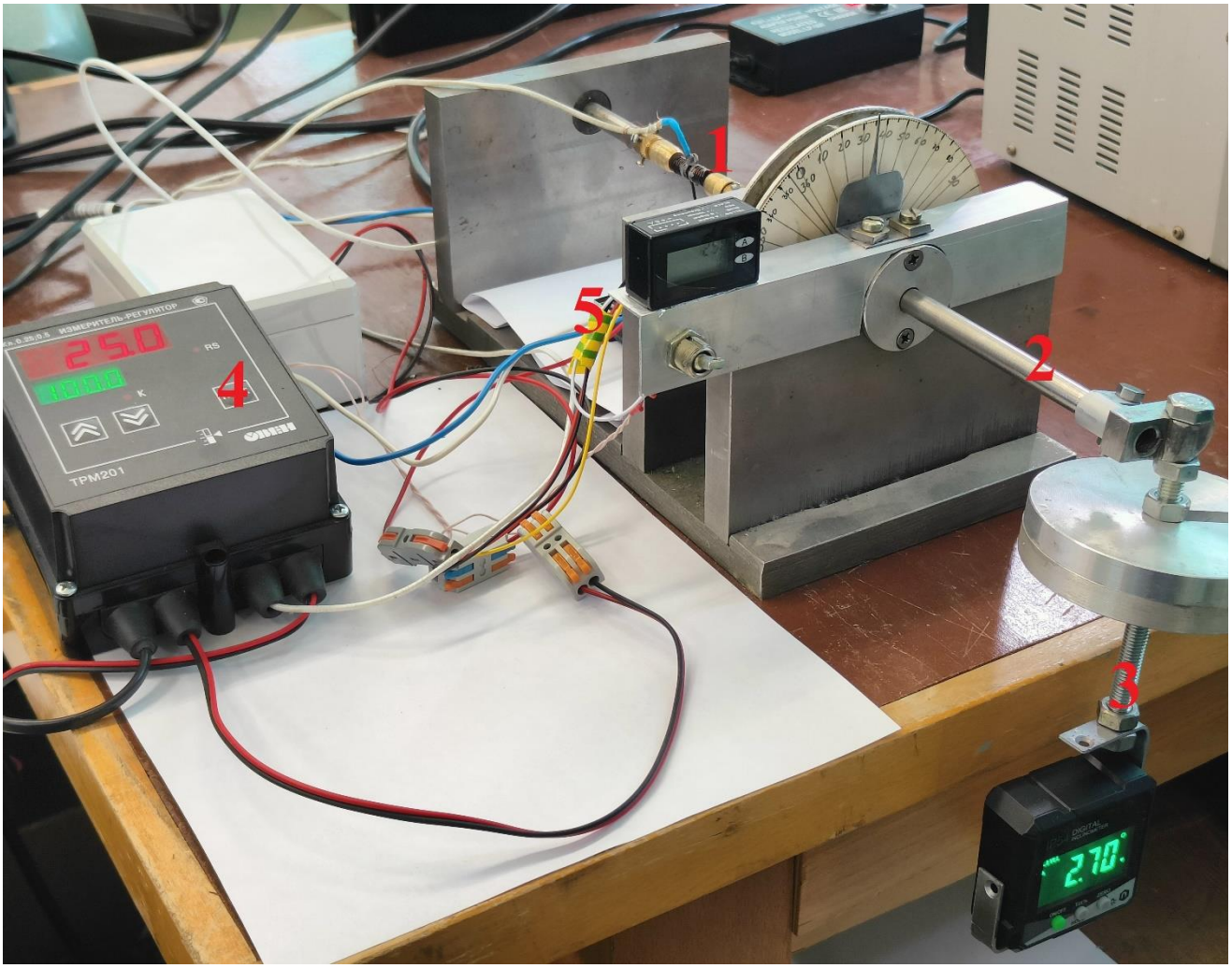

Figure 80. Photograph of the torsional actuator based on NiTi shape memory alloy. NiTi shape memory alloy working body (1), split shaft (2), lever with mass and digital inclinometer (3), TRM-201 measurement regulator (4), induction heater (5).

As the working element of the drive, samples of square cross-section measuring 2×2×40 mm were used, cut using an electroerosion machine from a NiTi alloy plate. The samples were subjected to quenching at 900°C for 20 minutes followed by annealing at 500°C for 500°C. After this heat treatment, the alloy underwent B2↔B19' transformations at the temperatures M_f=80°C, M_s=38°C, A_f=79°C, and A_s=108°C (according to DSC data). The samples were clamped and deformed (twisted) to 7% at

room temperature (in the martensite state) and then unloaded, resulting in residual strain of 4.7±0.1% (Figure 81).

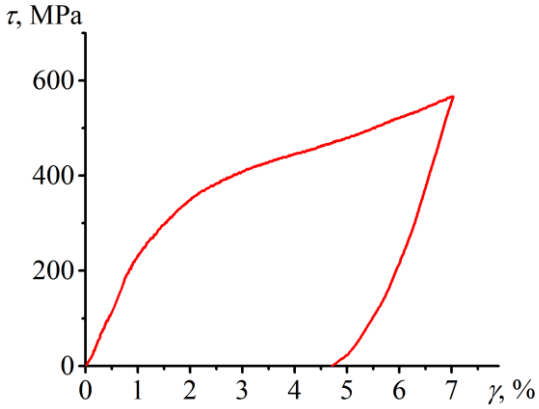

Figure 81. Deformation diagram of NiTi alloy obtained under torsional loading at room temperature (23°C).

After unloading, the samples underwent thermal cycling in the drive mode, during which the maximum and minimum deflection angles (φ) of the lever were recorded. To assess the influence of heating/cooling rates on the variations in the drive's working body parameters, two samples underwent 25 thermal cycles over the full temperature range of martensitic transformations from 180°C to 25°C at different rates. The first sample underwent thermal cycling at an average heating/cooling rate of 7°C/min, while the second sample was subjected to heating at a rate of 350°C/min and cooling at a rate of 150°C/min. Figure 82 shows the dependencies of shape memory effect values on the cycle number obtained during thermal cycling of NiTi alloy samples with low and high temperature change rates. It can be seen that the shape memory effect value increases in both cases, with the difference between the curves not exceeding 0.15%. Thus, heating and cooling at high rates do not affect the property variations during thermal cycling, allowing for the use of rapid heating and cooling of the NiTi alloy element in the drive.

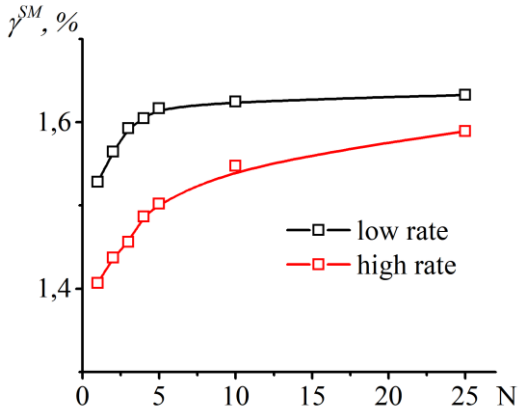

Figure 82. Dependencies of shape memory effect values on the cycle number obtained during thermal cycling in the temperature range of 180°C to 25°C of NiTi alloy with different heating/cooling rates.

To investigate the variation in the functional properties of the NiTi alloy during thermocycling through the temperature range of incomplete martensitic transformations, samples underwent 1000 thermocycles in various temperature intervals. The first sample underwent thermocycling across the full range of martensitic transformations from 180 to 25°C, with an initial cycle work output of 0.45 MJ/m3 (denoted as A_full). Two other samples underwent thermocycling in intervals of incomplete martensitic transformations. For this purpose, following the recommendations for selecting the optimal interval (section 3.3.), two intervals were determined: 115 to 58°C, where the initial cycle work output was 0.22 MJ/m3 - half of the work output in the full cycle (designated as A_0.5), and 115 to 51°C, where the work output in the initial cycle was 0.33 MJ/m3 - 75% of the work output in the full cycle (designated as A_0.75).

Figure 83 shows the dependencies of the shape memory effect magnitudes on the thermocycle number during thermocycling of the NiTi alloy in different temperature intervals.

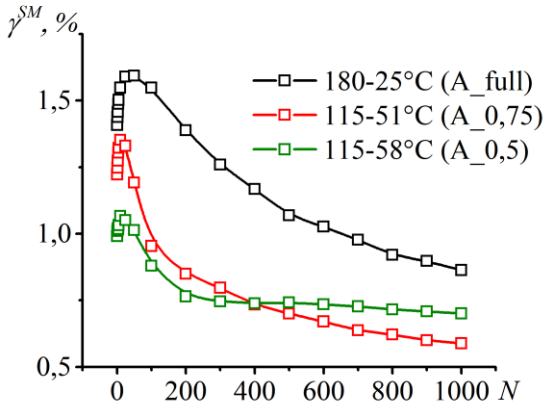

Figure 83. Dependencies of shape memory effect values on the thermocycle number obtained during thermocycling in various temperature ranges of the NiTi alloy.

It is observed that the values of γ^{SM} in all samples vary non-monotonically with an increase in the number of thermocycles. As the number of cycles increases to 10-50, the γ^{SM} value increases, and then decreases. For example, in sample A_full, the γ^{SM} value was 1.4% in the first cycle, reached a maximum at the 50th cycle (1.6%), and decreased to 0.86% at the 1000th cycle. In sample A_0.75, the γ^{SM} value increased from 1.22% to 1.35% by the tenth cycle, then decreased to 0.6% by the 1000th thermocycle. In the temperature interval of 115÷58°C, the γ^{SM} value also reached a maximum by the tenth cycle, increasing from 1% to 1.1%, and decreased to 0.7% at the 1000th cycle. In all presented dependencies, a linear decrease in the γ^{SM} value was observed after the five hundredth thermocycle, for which the slope was calculated. For sample A_full, the slope is -4.07×10^{-4} %/cycle, for the interval of 115÷51°C, it was -2.02×10^{-4} %/cycle, and the smallest decrease in the γ^{SM} value with cycles was observed in sample A_0.5, for which the slope was -0.87×10^{-4} %/cycle. It should be noted that due to the slower decrease in the γ^{SM} values during thermocycling in the 115÷58°C interval, the γ^{SM} value in sample A_0.5 was higher than in sample A_0.75 at the 1000th thermocycle.

The increase in γ^{SM} values in the initial cycles may be attributed to "training," which is caused by the increase in defect density leading to the formation of oriented internal stresses. These stresses add to the external load, increasing the effective stress and thereby enhancing reversible deformation.

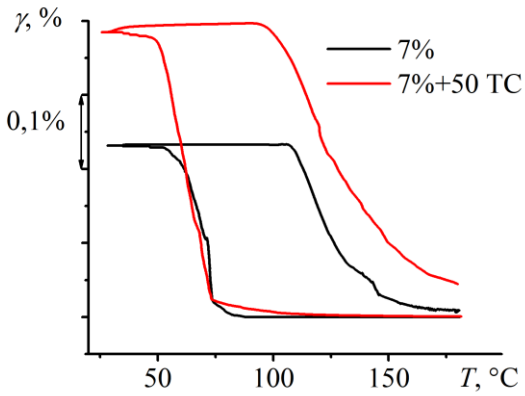

Figure 84. Variations in strain during thermocycling in the unloaded state of NiTi alloy samples after pre-deformation in the martensitic state by 7% (black line) and after deformation followed by thermocycling (red line).

To test this hypothesis, one sample pre-deformed to 7% in the martensite state was subjected to heating and a single thermocycle in the range of 180 to 25°C, while the second sample, after deformation to 7%, underwent 50 thermocycles in the drive mode (180 to 25°C), after which the sample was heated, cooled, and heated again. During this process, the variation in sample strain during cooling and heating in the unloaded state, i.e., the two-way shape memory effect (TWSME) (Figure 84), was observed. It can be seen that in the sample subjected to 50 thermocycles, the value of the reversible shape memory effect is 0.35%, which is 0.14% higher than in the sample not subjected to 50 thermocycles. Since the manifestation of the TWSME, like the training effect, is caused by fields of oriented internal stresses, an increase in the value of the TWSME indicates an increase in the values of internal stresses, which in turn leads to an increase in the value of the shape memory effect in the initial cycles.

Figure 85 shows the dependencies of the minimum - τ_{min} (a) and maximum τ_{max} (b) stresses during heating. The dependencies $\tau_{min}(N)$ for all samples have a complex character.

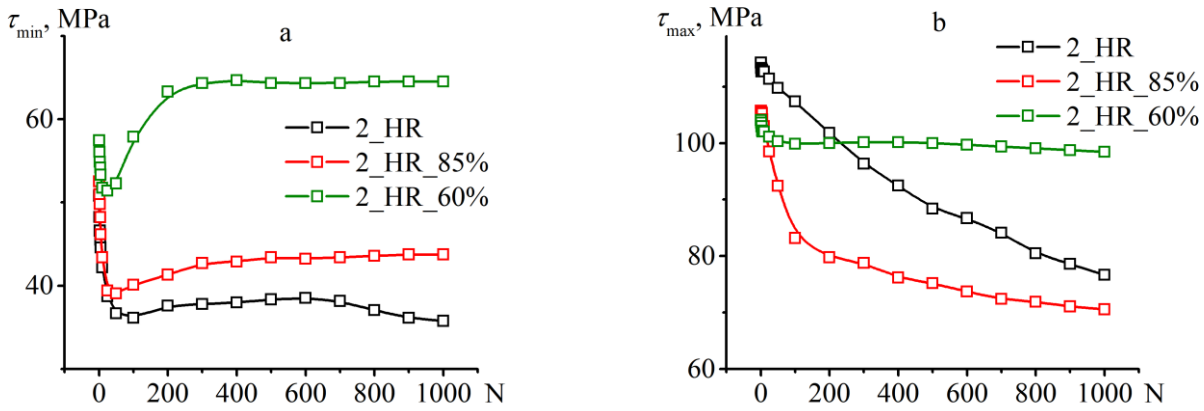

Figure 85. Dependencies of the minimum (a) and maximum (b) stress values on the number of thermocycles obtained during thermocycling in different temperature intervals of the NiTi alloy.

At the beginning of thermocycling, the values of τ_{min} decrease in all samples until reaching a minimum. Then, in the A_0.75 and A_0.5 samples, the values of τ_{min} increased with the number of thermocycles until saturation. In the sample subjected to thermocycling over the full range, the τ_{min} value decreased from the 1st to the 100th cycle, increased from the 100th to the 600th cycle, and then decreased again after the 600th cycle. In Figure 85b, it can be seen that the τ_{max} value decreased in all samples with increasing thermocycle number, and the larger the fraction of the temperature range, the greater the decrease in maximum recovery stress during thermocycling.

Figure 86 shows the variation in work during thermocycling through different temperature ranges. In all samples, the work increased at the beginning of thermocycling and then decreased. To compare the intensities of work decrease during thermocycling, the slope of the linear portion (for N > 500) of the A(N) dependence was calculated. The smallest slope was observed in the A_0.5 sample, where this value amounted to -0.26×10^{-4} MJ/m^3 per cycle. In the A_full sample, this value was -1.76×10^{-4} MJ/m^3 per cycle. Due to the lower intensity of work decrease in the A_0.5 sample, its work value exceeded that of the A_0.75 sample in the 500th cycle.

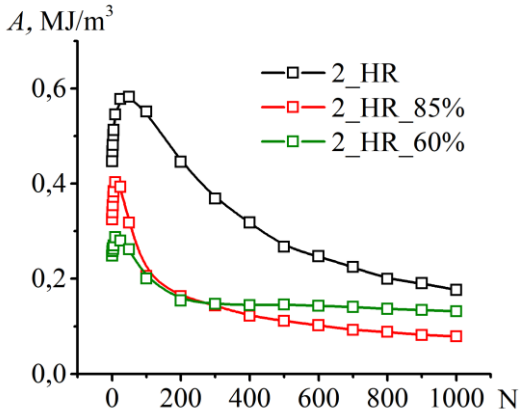

Figure 86. Dependence of work output values on the thermocycle number obtained during thermocycling in various temperature ranges of NiTi alloy.

Thus, the study validated the results obtained on a small cycle basis (see Section 3.3) for the operation of a NiTi alloy torsional drive over 1000 cycles. It was demonstrated that the optimal thermocycling regimes, selected based on the recommendations presented in Section 3.3., significantly improved the stability of the drive characteristics under conditions approximating operational ones. Based on this, it can be asserted that the results of this study are applicable to the development and creation of multiple-action drives with shape memory alloy elements based on NiTi. It was shown that during thermocycling of NiTi samples in the range of temperatures of incomplete martensitic transformations, the stability of the functional properties of the drive's working element was higher compared to thermocycling in the full interval.

3.5. Conclusions to Chapter 3

Based on the results presented in Chapter 3, the following conclusions can be drawn:

1. Nonlinear dependencies of the shape memory effect and recovery stresses values on the stiffness of the counterbody lead to a non-monotonic relationship between the work performed during heating and the stiffness of the counterbody. The maximum work is performed by the NiTi alloy when the stiffness of the counterbody is between 6-10 GPa.

2. Maximum recovery stresses generated during heating of the NiTi alloy are nonlinearly related to the value of the strain recovered during heating. This is because increasing the stiffness of the counterbody beyond 23.5 GPa does not affect the level of maximum recovery stresses. The limitation of maximum recovery stresses during heating is associated with reaching the dislocation yield strength, after which their increase ceases.

3. The stiffness of the counterbody does not affect the nature of the variations in the shape memory effect, recovery stresses, and work output, which decrease during thermocycling. The influence of the counterbody stiffness on the variation in plastic strain is not due to the stiffness itself, but rather to the plastic strain acquired by the sample during the "zero" cycle (during the first heating). The greater the plastic strain during the "zero" cycle, the less it varies during thermocycling.

4. The method of pre-deformation, which is necessary to "set" the actuator, only affects the work output properties in the first cycles. This is because the contributions of reversible and irreversible strain to the overall residual strain depend on the method of pre-deformation (active strain in the martensitic state or cooling under stress). After cooling under stress, the fraction of reversible strain is higher, so during the first heating in actuator mode, a greater strain is recovered, resulting in higher recovery stresses than after active strain in martensite. This influences the change in strain and stresses during subsequent cooling. With cycles, the influence of the pre-deformation method on the work output of the NiTi alloy weakens, and by the 10th cycle, it becomes insignificant,

as martensite begins to form under variable stress from the first cycle. Therefore, after the 10th thermocycle, variations in strain and recovery stress occur similarly in all pre-deformation methods of the alloy.

5. Strengthening of the austenitic phase due to pre-deformation at high temperatures increases maximum recovery stresses only at high stiffness. Since reversible strain after pre-deformation remains low, the amount of work performed during heating with high stiffness in hardened samples is lower than that with low stiffness in unhardened NiTi alloy samples.

6. The influence of the fraction of forward and reverse transformations on the variations in work output of the NiTi alloy and its strain variation during thermocycling in actuator mode is similar to what was observed during thermocycling under constant stress. Reducing the fraction of forward transformation is more effective for stabilizing the properties of the alloy than reducing the fraction of reverse transformation. During thermocycling of the NiTi alloy in actuator mode, reducing the fraction of forward transformation by 10% allows reducing the accumulated strain by 5 times with the same number of cycles, improving the stability of the alloy properties. Reducing the fraction of reverse transformation by 75% does not allow reducing the amount of irreversible strain by more than three times.

7. The value of pre-deformation required to "set" the actuator affects the characteristics of the actuator only in the "zero" cycle, but practically does not affect the change in these properties during thermocycling in actuator mode through an incomplete range of direct martensitic transformation. During thermocycling through an incomplete range of reverse transformation, the greater the pre-deformation, the stronger the influence of the fraction of reverse transformation on the variations in work output properties.

8. There is an optimal temperature range for the working cycle of the actuator, where the minimum temperature is such that the second half of the forward transformation is excluded during cooling, and the maximum temperature does not exceed the A_f temperature to suppress recovery processes during heating.

9. Recommendations have been developed for the temperature, deformational, and force characteristics of the actuator that minimize changes in the device's operating parameters during thermocycling.

10. The results of the study, obtained based on a 15-cycle basis, were tested during the operation of a prototype torsional actuator based on a 1000-cycle basis. It has been shown that the selection of optimal cycle temperatures based on recommendations made on a small cycle basis significantly improves the stability of the torsional actuator's operating parameters.

Conclusions

The dissertation work encompassed a comprehensive investigation of the variations in the work output of NiTi alloy during thermal cycling under various temperature, strain, and stress conditions. Thermal cycling of the NiTi alloy was conducted without stress, under constant stress, or in a drive (actuator) mode where stress decreased during cooling and increased during heating. The thermal cycling involved varying the fraction of forward and reverse transformations, both individually and in coordination. Additionally, the position of the temperature cycle relative to the martensitic transition temperatures was varied.

The preliminary strain of the samples differed in value and implementation method (active strain or cooling under stress), as well as in the temperature of deformation. Variations in the work output of the NiTi alloy were investigated under all thermal cycling regimes. The following conclusions can be drawn from the dissertation work:

1. A relationship was established between the variations in martensitic transition temperatures and defect density, which is nonlinear. It was shown that variations in defect density, determined by two processes - increasing defect density during forward martensitic transformation and decreasing defect density during reverse transformation - directly affect the variations in temperatures and sequences of martensitic transitions in the NiTi alloy. Intensification of recovery processes by increasing the maximum temperature in the cycle or during isothermal holding helps reduce defect density, thus restoring temperatures and sequences of martensitic transitions in the alloy. However, reducing defect density through recovery processes leads to an increased ability to accumulate defects upon subsequent cooling. The defect structure formed during thermal cycling is unstable and changes with variations in the maximum temperature in the cycle, holding time, or stress changes. This is because during thermal cycling, dislocations form in the austenite phase, where the yield stress is lower than in the martensite phase. The martensite phase inherits the dislocation structure of the austenite phase,

leading to the generation of high internal stresses, which relax with changes in the maximum temperature in the cycle or during holding, resulting in changes in transition temperatures.

2. Direct observations of interphase boundary movement during cooling and heating of the NiTi alloy in a transmission electron microscope column showed that in the annealed NiTi alloy, there is no correspondence between the sequences of crystal appearance during cooling and their disappearance during heating. Moreover, microstructural memory, i.e., the martensite structure, is not reproduced during thermal cycling. This may be due to the redistribution of defects, leading to changes in internal stresses, which additionally influence the changes in transition temperatures. If a dislocation structure is formed in the alloy during active deformation, microstructural memory is observed, and there is correspondence between the sequences of martensite crystal appearance during cooling and their disappearance during heating.
3. Reducing the fraction of the temperature range for both forward and reverse transformations contributes to a decrease in the rate of change of martensitic transformation temperatures, the values of reversible strain, the work done during heating, and the plastic strain accumulated during thermal cycling of the NiTi alloy under stress. It was established that if the temperature range for forward transformation during thermal cycling does not exceed 50% of the total range, the work output changes only in the first 3-5 cycles and remain unchanged thereafter. It was shown that reducing the fraction of forward transformation during thermal cycling under stress leads to better stabilization of the work output of the NiTi alloy compared to reducing the fraction of reverse transformation. This is because the main changes in defect density occur during forward transformation.
4. The training effect - the increase in reversible strain during thermal cycling is associated with the ability of the alloy to accumulate plastic strain during multiple thermal cycles. This effect is observed when the fractions of forward or reverse transformation during thermal cycling exceed 50%. In this case, during thermal cycling under stress, irreversible strain accumulates actively in the alloy,

accompanied by an increase in internal stresses. These stresses, combined with external ones, increase the effective stress during thermal cycling, resulting in an increased proportion of oriented martensite, which appears during cooling and disappears during heating, thus increasing reversible strain.

5. Reducing the fractions of both forward and reverse transformations included in the thermal cycling range reduces reversible strain and the work done during heating, while significantly improving the thermo-cyclic stability of these properties and reducing irreversible strain, which is important for devices subjected to multiple actions. For example, reducing the fraction of forward transformation from 100% to 50% during thermal cycling of the alloy under 50 MPa stress reduces reversible strain by 2.3 times and plastic strain by 5 times.
6. The influence of the stiffness of the counterbody, the method of pre-strain, and the strengthening of the austenite phase on the properties variations of the NiTi alloy during thermal cycling in the drive mode has been established. It has been shown that nonlinear dependencies of the values of the shape memory effect and recovery stresses on the stiffness of the counterbody lead to the dependence of the work performed during heating on the counterbody stiffness being non-monotonic, with a maximum observed at a stiffness of 6-10 GPa. It has been established that the stiffness of the counterbody does not affect the nature of the changes in the values of the shape memory effect, recovery stresses, and work performed, which decrease during thermal cycling. It has been shown that the method of pre-strain, necessary for "cocking" the drive, only affects the functional properties in the initial cycles. This is because the method of pre-strain determines the values of reversible strain, which directly influences the maximum recovery stress. After cooling under stress, the value of reversible strain is higher than after active deformation, so during the first heating in the drive mode, a greater deformation is restored, thus the level of recovery stresses will be higher than after active deformation in martensite. With cycles, the influence of the method of pre-strain of the NiTi alloy on the functional properties weakens, becoming insignificant by the 10th cycle. Strengthening of the austenite phase due to pre-strain at high temperature increases the maximum

recovery stresses only at high counterbody stiffnesses and does not affect the level of recovery stresses formed during heating with optimal stiffness.

7. The "recovery stresses-reversible strain" diagram is nonlinear due to the fact that for counterbody stiffnesses above 23.5 GPa, recovery stresses practically do not increase after they reach the yield stress of the austenite phase.
8. The influence of the fractions of forward and reverse transformations included in the temperature range of thermal cycling on the variations in the functional properties of the NiTi alloy and its plastic strain during thermal cycling in the drive mode is similar to that observed during thermal cycling under constant stress. Reducing the fraction of forward transformation more effectively stabilizes the properties of the alloy during thermal cycling than reducing the fraction of reverse transformation. During thermal cycling of the NiTi alloy in the drive mode, reducing the fraction of forward transformation by 10% allows reducing the accumulated plastic strain by 5 times with the same number of cycles, indicating an improvement in the stability of the alloy properties. Reducing the fraction of reverse transformation by even 75% does not allow reducing the values of irreversible strain by more than three times.
9. To achieve satisfactory values of reversible strain and recovery stresses in combination with good thermo-cyclic stability of the properties, it is necessary to use the optimal temperature range of the working cycle of the drive, where the minimum temperature is such that the second half of the forward transformation is excluded during cooling, and the maximum temperature does not exceed the A_f temperature.
10. Recommendations have been developed for the temperature, deformation, and force characteristics of the drive that minimize changes in the operating parameters of the device during thermal cycling. It has been shown that choosing the optimal cycle temperatures based on recommendations made on a small cycle basis significantly improves the stability of the operating parameters of a torsional drive that has undergone 1000 cycles.

References

1. Kurdyumov G.V., Khandros L.G. On thermoelastic equilibrium during martensitic transformations // Proceedings of the USSR Academy of Sciences. 1949. Vol. 66, No. 2. P. 211–214. (In Russian)
2. Kurdyumov G.V. Nondiffusion (martensitic) transformations in alloys // Journal of Technical Physics. 1948. Vol. 18, No. 8. P. 999–1025. (In Russian)
3. Otsuka K., Ren X. Physical metallurgy of Ti–Ni-based shape memory alloys // Prog. Mater. Sci. Elsevier Ltd, 2005. Vol. 50, № 5. P. 511–678.
4. Pelton A.R., Stöckel D., Duerig T.W. Medical Uses of Nitinol // Proc. Int. Symp. Shape Mem. Mater. 1999. 2000. Vol. 327–328. P. 63–70.
5. Duerig T., Pelton A., Stöckel D. An overview of nitinol medical applications // Mater. Sci. Eng. A. 1999. Vol. 273–275. P. 149–160.
6. Stoeckel D. Shape memory actuators for automotive applications // Mater. Des. 1990. Vol. 11, № 6. P. 302–307.
7. Humphreys A., Wicks N., Mckinley G.H. Intelligence in Novel Materials // Oilf. Rev. 2008. P. 32–41.
8. Fu Y. et al. TiNi-based thin films in MEMS applications: A review // Sensors Actuators, A Phys. 2004. Vol. 112, № 2–3. P. 395–408.
9. Mohd Jani J. et al. A review of shape memory alloy research, applications and opportunities // Mater. Des. Elsevier Ltd, 2014. Vol. 56. P. 1078–1113.
10. Shape Memory Alloy Market Report – Forecast (2022-2027)" by IndustryARC [Electronic resource]. URL: https://www.industryarc.com/Report/16235/shape-memory-alloy-market.html%0A.
11. Rossi C. et al. SMA-Based Muscle-Like Actuation in Biologically Inspired Robots: A State of the Art Review // Smart Actuation Sens. Syst. - Recent Adv. Futur. Challenges. 2012.
12. Ostropiko E.S., Razov A.I. Functional properties of TiNi conical working elements in the holding and release device // Cybern. Phys. 2018. Vol. 7, № Volume 7, 2018,

Number 4. P. 216–219.

13. Ostropiko E., Razov A., Cherniavsky A. Investigation of TiNi shape memory alloy for thermosensitive wire drive // MATEC Web Conf. / ed. Schryvers N., Van Humbeeck J. 2015. Vol. 33. P. 03021.
14. Concilio A., Ameduri S. Influence of structural architecture on linear shape memory alloy actuator performance and morphing system layout optimisation // J. Intell. Mater. Syst. Struct. 2014. Vol. 25, № 16. P. 2037–2051.
15. Ameduri S., Concilio A. A shape memory alloy torsion actuator for static blade twist // J. Intell. Mater. Syst. Struct. 2019. Vol. 30, № 17. P. 2605–2626.
16. Ameduri S. et al. A Shape Memory Alloy Application for Compact Unmanned Aerial Vehicles // Aerospace. 2016. Vol. 3, № 2. P. 16.
17. Suzuki Y., Kagawa Y. Dynamic tracking control of an SMA wire actuator based on model matching // Sensors Actuators, A Phys. Elsevier B.V., 2019. Vol. 292. P. 129–136.
18. Kim Y. et al. Bidirectional rotating actuators using shape memory alloy wires // Sensors Actuators, A Phys. Elsevier B.V., 2019. Vol. 295. P. 512–522.
19. Huang W. On the selection of shape memory alloys for actuators // Mater. Des. 2002. Vol. 23, № 1. P. 11–19.
20. Follador M. et al. A general method for the design and fabrication of shape memory alloy active spring actuators // Smart Mater. Struct. 2012. Vol. 21, № 11. P. 115029.
21. Hadi A. et al. Developing a novel continuum module actuated by shape memory alloys // Sensors Actuators, A Phys. Elsevier B.V., 2016. Vol. 243. P. 90–102.
22. Conrad K. et al. Staggered nitinol wire actuator array for high linear displacement and force-to-mass ratio // Crit. Rev. Biomed. Eng. 2019. Vol. 47, № 2. P. 121–129.
23. Husainov M.A. et al. Force characteristics of spherical segments made of Ti-Ni shape memory alloys // Bulletin of TSU. 2010. Vol. 15, No. 3. P. 3–7.(In Russian)
24. Li Y.F. et al. Constrained recovery properties of NiTi shape memory alloy wire during thermal cycling // J. Alloys Compd. 2014. Vol. 588. P. 525–529.
25. Benafan O. et al. Constant-Strain Thermal Cycling of a Ni50.3Ti29.7Hf20 High-Temperature Shape Memory Alloy // Shape Mem. Superelasticity. Springer

International Publishing, 2016. Vol. 2, № 2. P. 218–227.

26. Furuya Y., Park Y.C. Thermal cyclic deformation and degradation of shape memory effect in Ti-Ni alloy // Nondestr. Test. Eval. 1992. Vol. 8–9, № 1–6. P. 541–554.
27. Benafan O. et al. Thermomechanical cycling of a NiTi shape memory alloy-macroscopic response and microstructural evolution // Int. J. Plast. Elsevier Ltd, 2014. Vol. 56. P. 99–118.
28. Belyaev S.P. et al. Cyclic shape memory and the operating capacity of titanium nickelide // Strength Mater. 1989. Vol. 21, № 6. P. 748–752.
29. Poncet P. Applications of superelastic nitinol tubing [Electronic resource] // Memory corporation, USA. 1994. URL: http://www.memry.com/sites/default/files/documents/Applications_Superelastic–NiTI_tube.pdf (accessed: 04.02.2014).
30. Fadlallah S.A. et al. An overview of NiTi shape memory alloy : Corrosion resistance and antibacterial inhibition for dental application // J. Alloys Compd. Elsevier B.V., 2014. Vol. 583. P. 455–464.
31. Matsumoto H. Irreversibility in transformation behavior of equiatomic nickel–titanium alloy by electrical resistivity measurement // J. Alloys Compd. 2004. Vol. 368, № 1–2. P. 182–186.
32. Lin H., Wu S. Strengthening effect on shape recovery characteristic of the equiatomic TiNi alloy // Scr. Metall. Mater. 1992. Vol. 26, № c. P. 59–62.
33. Stachowiak G.B., McCormick P.G. Shape memory behaviour associated with the R and martensitic transformations in a NiTi alloy // Acta Met. 1988. Vol. 36. P. 291–297.
34. Tanaka K. et al. Analysis of thermomechanical behavior of shape memory alloys // Mech. Mater. 1992. Vol. 13, № 3. P. 207–215.
35. LI Y. et al. Effects of thermomechanical cycling on the shape memory behavior and transformation temperatures of a Ni50.2Ti49.8 alloy // Rare Met. The Nonferrous Metals Society of China, 2008. Vol. 27, № 5. P. 522–525.
36. Eggeler G. et al. Structural and functional fatigue of NiTi shape memory alloys // Mater. Sci. Eng. A. 2004. Vol. 378, № 1–2. P. 24–33.

37. Miyazaki S., Igo Y., Otsuka K. Effect of thermal cycling on the transformation temperatures of TiNi alloys // Acta Met. 1986. Vol. 34. P. 2045–2051.
38. Jones N.G., Dye D. Martensite evolution in a NiTi shape memory alloy when thermal cycling under an applied load // Intermetallics. Elsevier Ltd, 2011. Vol. 19, № 10. P. 1348–1358.
39. Belyaev S., Resnina N., Zhuravlev R. Deformation of Ti–51.5at.%Ni alloy during thermal cycling under different thermal-mechanical conditions // J. Alloys Compd. Elsevier B.V., 2013. Vol. 577. P. S232–S236.
40. Tong Y. et al. Thermal cycling stability of ultrafine-grained TiNi shape memory alloys processed by equal channel angular pressing // Scr. Mater. 2012. Vol. 67. P. 1–4.
41. Tang W., Sandström R. Analysis of the influence of cycling on TiNi shape memory alloy properties // Mater. Des. 1993. Vol. 14, № 2. P. 103–113.
42. Zheng Y., Li J., Cui L. Repeatable temperature memory effect of TiNi shape memory alloys // Mater. Lett. Elsevier B.V., 2009. Vol. 63, № 11. P. 949–951.
43. Wayman C.M., Cornelis I., Shimizu K. Transformation behavior and the shape memory in thermally cycled TiNi // Scr. Metall. 1972. Vol. 6, № 2. P. 115–122.
44. Wasilewski R. Martensitic transformation and fatigue strength in TiNi // Scr. Metall. 1971. Vol. 5, № 3. P. 207–211.
45. Wayman C.M., Cornelis I., Shimizu K. Transformation behaviour and the shape memory in thermally cycled TiNi // Scr. Metall. 1972. Vol. 6. P. 115–122.
46. McCormick P.G., Liu Y. Thermodynamic analysis of the martensitic transformation in NiTi—II. Effect of transformation cycling // Acta Metall. Mater. 1994. Vol. 42, № 7. P. 2407–2413.
47. Resnina N., Belyaev S. Multi-stage martensitic transformations induced by repeated thermal cycling of equiatomic TiNi alloy // J. Alloys Compd. 2009. Vol. 486, № 1–2. P. 304–308.
48. Pelton A.R. et al. Effects of thermal cycling on microstructure and properties in Nitinol // Mater. Sci. Eng. A. Elsevier B.V., 2012. Vol. 532. P. 130–138.
49. Ezaz T. et al. Plastic deformation of NiTi shape memory alloys // Acta Mater. Acta

Materialia Inc., 2013. Vol. 61, № 1. P. 67–78.

50. Benjamin M. Irradiation swelling, creep, thermal shock and thermal cycling fatigue analysis of cylindrical controlled thermonuclear reactor first wall // Nucl. Eng. Des. 1974. Vol. 28, № 1. P. 1–30.
51. Resnina N. et al. The effect of isothermal holding on reversible and irreversible strain in TiNi shape memory alloy // Mater. Today Proc. Elsevier Ltd, 2017. Vol. 4, № 3. P. 4748–4752.
52. Sibirev A., Belyaev S., Resnina N. Variation in TiNi Alloy Properties on Room Temperature Holding // Acta Phys. Pol. A. 2018. Vol. 134, № 3. P. 671–674.
53. Sibirev A., Belyaev S., Resnina N. Influence of holding between the thermal cycles on recovery in martensitic transformation temperatures in TiNi alloy // Lett. Mater. 2019. Vol. 9, № 1. P. 103–106.
54. Sibirev A., Belyaev S., Resnina N. Unusual Multistage Martensitic Transformation in TiNi Shape Memory Alloy after Thermal Cycling // Mater. Sci. Forum. 2013. Vol. 738–739. P. 372–376.
55. Sibirev A., Resnina N., Belyaev S. Relationship between the variation in transformation temperatures, resistivity and dislocation density during thermal cycling of Ni50Ti50 shape memory alloy // Int. J. Mater. Res. 2019. Vol. 110, № 5. P. 387–392.
56. Sibirev A. et al. In situ transmission electron microscopy study of martensite boundaries movement on cooling and heating of the NiTi shape memory alloy // Mater. Lett. Elsevier B.V., 2022. Vol. 319. P. 132267.
57. Resnina N. et al. In situ TEM observation of the martensite interface movement on heating – cooling – heating of the pre-deformed NiTi shape memory alloy // Mater. Lett. Elsevier B.V., 2023. Vol. 347, № November 2022. P. 134641.
58. Belyaev S., Resnina N., Sibirev A. Peculiarities of residual strain accumulation during thermal cycling of TiNi alloy // J. Alloys Compd. Elsevier B.V., 2012. Vol. 542. P. 37–42.
59. Belyaev S., Resnina N., Sibirev A. Accumulation of Residual Strain in TiNi Alloy During Thermal Cycling // J. Mater. Eng. Perform. 2014. Vol. 23, № 7. P. 2339–

2342.

60. Sibirev A., Belyaev S., Resnina N. Softening process during reverse martensitic transformation in TiNi shape memory alloy // J. Alloys Compd. Elsevier B.V, 2016. Vol. 661. P. 155–160.
61. Belyaev S. et al. Variation in kinetics of martensitic transformation during partial thermal cycling of the TiNi alloy // Thermochim. Acta. Elsevier B.V., 2014. Vol. 582. P. 46–52.
62. Sibirev A., Belyaev S., Resnina N. The influence of counter-body stiffness on working parameters of NiTi actuator // Sensors Actuators A Phys. Elsevier B.V., 2021. Vol. 319, № 112568.
63. Sibirev A. V., Belyaev S.P., Resnina N.N. Influence of preliminary straining on the recovery stress in tini shape memory alloy working element // Lett. Mater. 2021. Vol. 11, № 2. P. 209–212.
64. Sibirev A., Belyaev S., Resnina N. Improvement of the NiTi actuator performance stability by decreasing its operating temperature range // Sensors Actuators A Phys. Elsevier B.V., 2023. Vol. 363. P. 114743.
65. Sibirev A. V., Belyaev S.P., Resnina N.N. Influence of temperature range on NiTi SMA actuator performance during thermal cycling // Lett. Mater. 2023. Vol. 13, № 3. P. 249–254.
66. Belyaev S. et al. Shape memory effects in [001] Ni 55 Fe 18 Ga 27 single crystal // Smart Mater. Struct. IOP Publishing, 2017. Vol. 26, № 9. P. 095003.
67. Sibirev A. et al. Shape Memory Effects and Work Output of [001] Ni55Fe18Ga27 Single Crystals in Torsion Mode // J. Mater. Eng. Perform. Springer US, 2020. Vol. 29, № 4. P. 2185–2189.
68. Belyaev S. et al. Influence of Detwinning on the Shape Memory Effect in Ni55Fe18Ga27 Single Crystals // J. Mater. Eng. Perform. 2019. Vol. 28, № 7. P. 4234–4240.
69. Chang L.C., Read T.A. Plastic deformation and diffusionless phase changes in metals-the Gold-Cadmium beta phase // Trans. AIMS, J. Met. 1951. Vol. 191. P. 47–52.

70. Kurdyumov G.V. Microstructural study of the kinetics of martensitic transformations in copper-tin alloys // Journal of Technical Physics. 1949. Vol. 7. P. 32–36. (In Russian)
71. Basinski Z.S., Christian J.W. Crystallography of deformation by twin boundary movements in indium-thallium alloys // Acta Metall. 1954. Vol. 2, № 1. P. 101–113.
72. Nishida M., Wayman C.M., Honma T. Phase transformations in a Ti50Ni47.5Fe2.5 shape memory alloy // Metallography. 1986. Vol. 19, № 1. P. 99–113.
73. Shimizu K. Effect of ageing and thermal cycling on shape memory alloys // J Electron Microsc. 1985. Vol. 34. P. 277–278.
74. Van Humbeeck J. Cycling effects. Fatigue and degradation of shape memory alloys // J. Phys. IV. 1991. Vol. 1. P. C4-199.
75. Liu Y., McCormick P.G. Factors influencing the development of two-way shape memory in NiTi // Acta Met. Mater. 1990. Vol. 38. P. 1321–1326.
76. Jean R., Duh J. The thermal cycling effect on Ti-Ni-Cu shape memory alloy // Scr. Metall. Mater. 1995. Vol. 32, № 6. P. 885–890.
77. Amengual A., Likhachev A., Cesari E. An experimental study of the partial transformation cycling of shape-memory alloys // Scr. Mater. 1996. Vol. 34, № 10. P. 1549–1554.
78. Wang Z.G.G., Zu X.T.T., Fu Y.Q.Q. Study of incomplete transformations of near equiatomic TiNi shape memory alloys by DSC methods // Mater. Sci. Eng. A. 2005. Vol. 390, № 1–2. P. 400–403.
79. Paradis A., Terriault P., Brailovski V. Modeling of residual strain accumulation of NiTi shape memory alloys under uniaxial cyclic loading // Comput. Mater. Sci. Elsevier B.V., 2009. Vol. 47, № 2. P. 373–383.
80. Gall K., Maier H.. Cyclic deformation mechanisms in precipitated NiTi shape memory alloys // Acta Mater. 2002. Vol. 50, № 18. P. 4643–4657.
81. Lin G.M., Lai J.K.L., Chung C.Y. Thermal cycling effects in Cu-Zn-Al shape memory alloy by positron lifetime measurements // Scr. Metall. Mater. 1995. Vol. 32, № 11. P. 1865–1869.

82. García R. Stabilization of martensite in Cu-Zn-Al shape memory alloys: effects of γ precipitates and thermal cycling // Scr. Mater. 2000. Vol. 42. P. 531–536.
83. Dunne D.P., Kennon N.F. The structure of martensite in a CU-ZN-AL Alloy // Scr. Metall. 1982. Vol. 16, № 6. P. 729–734.
84. Besseghini S., Villa E., Tuissi A. Ni- Ti- Hf shape memory alloy: effect of aging and thermal cycling // Mater. Sci. Eng. A. 1999. Vol. 275. P. 390–394.
85. Liang X. et al. Thermal cycling stability and two-way shape memory effect of Ni–Cu–Ti–Hf alloys // Solid State Commun. 2001. Vol. 119. P. 381–385.
86. Xin Y., Li Y., Liu Z. Thermal stability of dual-phase Ni58Mn25Ga17 high-temperature shape memory alloy // Scr. Mater. Acta Materialia Inc., 2010. Vol. 63, № 1. P. 35–38.
87. Uchil J., Kumara K.G., Mahesh K.K. Effect of thermal cycling on R-phase stability in a NiTi shape memory alloy // Mater. Sci. Eng. A. 2002. Vol. 332, № 1–2. P. 25–28.
88. Matsumoto H. Transformation behaviour with thermal cycling in NiTi alloys // J. Alloys Compd. 2003. Vol. 350, № 1–2. P. 213–217.
89. Salamon M.B., Meichle M.E., Wayman C.M. Premartensitic phases of Ti50Ni47Fe3 // Phys Rev B. 1985. Vol. 31. P. 7306.
90. Wasilewski R.J., Butler S.R., Hanlon J.E. On the Martensitic Transformation in TiNi // Met. Sci. J. 1967. Vol. 1, № 1. P. 104–110.
91. Robertson S.W., Pelton A.R., Ritchie R.O. Mechanical fatigue and fracture of Nitinol // Int. Mater. Rev. 2012. Vol. 57, № 1. P. 1–37.
92. Wilson A.J.C. Recovery and recrystallization of metals edited by L. Himmel // Acta Crystallogr. 1964. Vol. 17, № 8. P. 1090–1090.
93. Uchil J. et al. Thermal and electrical characterization of R-phase dependence on heat-treat temperature in Nitinol // Phys. B. 1998. Vol. 253, № 1–2. P. 83–89.
94. Matsumoto H. Electrical resistivity of NiTi with high transformation temperature // J. Alloys Compd. 2004. Vol. 370, № 1–2. P. 244–248.
95. Uchil J., Mahesh K., Kumara K.G. Electrical resistivity and strain recovery studies on the effect of thermal cycling under constant stress on R-phase in NiTi shape

memory alloy // Phys. B Condens. Matter. 2002. Vol. 324, № 1–4. P. 419–428.

96. Wu S.K., Lin H.C., Chou T.S. A study of electrical resistivity, internal friction and shear modulus on an aged Ti49Ni51 alloy // Acta Metall. Mater. 1990. Vol. 38, № 1. P. 95–102.
97. Kaack M. et al. Ultrasonic attenuation by dislocation formation in NiTi shape memory alloys // Mater. Sci. Eng. A. 2004. Vol. 378, № 1–2. P. 119–121.
98. Simon T. et al. On the multiplication of dislocations during martensitic transformations in NiTi shape memory alloys // Acta Mater. 2010. Vol. 58, № 5. P. 1850–1860.
99. Seiner H. et al. Kwinking as the plastic forming mechanism of B19’ NiTi martensite // Int. J. Plast. 2023. Vol. 168, № May. P. 103697.
100. Liu Y., McCormick P.G. Thermodynamic analysis of the martensitic transformation in NiTi—I. Effect of heat treatment on transformation behaviour // Acta Metall. Mater. 1994. Vol. 42, № 7. P. 2401–2406.
101. Kocer M. et al. Measurement of Dislocation Density by Residual Electrical Resistivity // Mater. Sci. Forum. 1996. Vol. 210–213. P. 133–140.
102. Kanaan A., Mazloum A., Sevostianov I. On the connections between plasticity parameters and electrical conductivities for austenitic, ferritic, and semi-austenitic stainless steels // Int. J. Eng. Sci. Elsevier Ltd, 2016. Vol. 105. P. 28–37.
103. Hane K.F., Shield T.W. Microstructure in the cubic to monoclinic transition in titanium–nickel shape memory alloys // Acta Mater. 1999. Vol. 47, № 9. P. 2603–2617.
104. Wang X., Verlinden B., Van Humbeeck J. Effect of post-deformation annealing on the R-phase transformation temperatures in NiTi shape memory alloys // Intermetallics. Elsevier Ltd, 2015. Vol. 62. P. 43–49.
105. Salzbrenner R., Cohen M. On the thermodynamics of thermoelastic martensitic transformations // Acta Metall. 1979. Vol. 27. P. 739–748.
106. Wollants P., Roos J.R., Delaey L. Thermally- and stress-induced thermoelastic martensitic transformations in the reference frame of equilibrium thermodynamics // Prog. Mater. Sci. 1993. Vol. 37, № 3. P. 227–288.

107. Zhigilei L. Dislocations: Stress field and Energy [Electronic resource] // University of Virginia, MSE 6020: Defects and Microstructure in Materials. URL: http://people.virginia.edu/~lz2n/mse6020/notes/D-stress-energy.pdf.
108. Morris J.W. Overview of Dislocation Plasticity [Electronic resource]. URL: http://www.mse.berkeley.edu/groups/morris/MSE205/Extras/dislocation plasticity.pdf.
109. Kurdyumov G.V., Khandros L.G. ON THE "THERMOELASTIC" EQUILIBRIUM ON MARTENSITIC TRANSFORMATIONS // Dokl. Akad. Nauk SSSR. 1949. Vol. 66, № 2. P. 211–214.
110. Sandrock G.D., Hehemann R.F. The Observation of Surface Relief during the Martensitic Transformation in TiNi // Metallography. 1971. Vol. 456, № 4. P. 451–456.
111. Otsuka K. et al. Characteristics of the Martensitic Transformation in TiNi and the Memory Effect // Metall. Trans. 1971. Vol. 2, № September 1971. P. 2585–2588.
112. Yang S. et al. Martensite stabilization and thermal cycling stability of two-phase NiMnGa-based high-temperature shape memory alloys // Acta Mater. Acta Materialia Inc., 2012. Vol. 60, № 10. P. 4255–4267.
113. Belyaev S. et al. Martensite Stabilization Effect in the Ni50Ti50 Alloy After Preliminary Deformation by Cooling Under Constant Stress // Shape Mem. Superelasticity. Springer US, 2020. Vol. 6, № 2. P. 223–231.
114. Belyaev S. et al. Damage of the martensite interfaces as the mechanism of the martensite stabilization effect in the NiTi shape memory alloys // J. Alloys Compd. 2022. Vol. 921. P. 166189.
115. Tsoi K. a., Schrooten J., Stalmans R. Part I. Thermomechanical characteristics of shape memory alloys // Mater. Sci. Eng. A. 2004. Vol. 368, № 1–2. P. 286–298.
116. Morin M., Trivero F. Influence of thermal cycling on the reversible martensitic transformation in a Cu-Al-Ni shape memory alloy // Mater. Sci. Eng. A. 1995. Vol. 196, № 1–2. P. 177–181.
117. Belyaev S., Resnina N. Stability of mechanical behavior and work performance in TiNi-based alloys during thermal cycling // Int. J. Mater. Res. Hanser, 2013. Vol.

104, № 1. P. 11–17.

118. Urbina C., De la Flor S., Ferrando F. Effect of thermal cycling on the thermomechanical behaviour of NiTi shape memory alloys // Mater. Sci. Eng. A. 2009. Vol. 501, № 501. P. 197–206.
119. He X. et al. Transformation behaviour with thermal cycling in Ti50Ni43Cu7 shape memory alloy. 2006. Vol. 427. P. 327–330.
120. Filip P., Mazanec K. Influence of cycling on the reversible martensitic transformation and shape memory phenomena in TiNi alloys // Scr. Metall. Mater. 1994. Vol. 30, № c. P. 67–72.
121. Suresh K.S., Bhaumik S.K., Suwas S. Effect of thermal and thermo-mechanical cycling on the microstructure of Ni-rich NiTi shape memory alloys // Materials Letters. Elsevier, 2013. Vol. 99. P. 150–153.
122. Belyaev S. et al. Influence of chemical composition of NiTi alloy on the martensite stabilization effect // J. Alloys Compd. Elsevier B.V, 2019. Vol. 787. P. 1365–1371.
123. Atli K.C. et al. The effect of training on two-way shape memory effect of binary NiTi and NiTi based ternary high temperature shape memory alloys // Mater. Sci. Eng. A. Elsevier, 2013. Vol. 560. P. 653–666.
124. Tobushi H., Date K., Miyamoto K. Characteristics and Development of Shape-Memory Alloy Heat Engine // J. Solid Mech. Mater. Eng. 2010. Vol. 4, № 7. P. 1094–1102.
125. Belyaev S.P., Kuz'min S.L., Likhachev V. a. Ability of the composite 50 Ti-47 Ni-3 Cu to transform heat energy into mechanical work upon cyclic temperature change // Strength Mater. 1984. Vol. 16, № 6. P. 863–866.
126. Belyaev S., Resnina N., Zhuravlev R. Work production and variation in shape memory effects during thermal cycling of equiatomic TiNi alloy // J. Mater. Eng. Perform. 2014. Vol. 23, № 7. P. 2343–2346.
127. Resnina N. et al. Efficiency and work performance of TiNi alloy undergoing B2 ↔ R martensitic transformation // Int. J. Mater. Res. 2014. Vol. 105, № 5. P. 440–449.
128. Oikawa K. et al. Magnetic and martensitic phase transitions in ferromagnetic Ni-Ga-Fe shape memory alloys // Appl. Phys. Lett. 2002. Vol. 81, № 2002. P. 5201–

5203.

129. Heczko O. et al. Thermodynamic, kinetic, and magnetic properties of a Ni54 Fe19 Ga27 magnetic shape-memory single crystal // Phys. Rev. B - Condens. Matter Mater. Phys. 2008. Vol. 77, № 17. P. 1–7.
130. Efstathiou C. et al. Fatigue response of NiFeGa single crystals // Scr. Mater. 2007. Vol. 57. P. 409–412.
131. Efstathiou C. et al. Full-field strain evolution during intermartensitic transformations in single-crystal NiFeGa // Acta Mater. 2008. Vol. 56. P. 3791–3799.
132. Chumlyakov Y. et al. Shape memory effect and high-temperature superelasticity in high-strength single crystals // J. Alloys Compd. Elsevier B.V., 2013. Vol. 577, № SUPPL. 1. P. S393–S398.
133. Font J. et al. Thermal stability and ordering effects in Ni-Fe-Ga ferromagnetic shape memory alloys // Mater. Sci. Eng. A. 2008. Vol. 481–482, № 1-2 C. P. 262–265.
134. Hamilton R.F. et al. Thermal and stress-induced martensitic transformations in NiFeGa single crystals under tension and compression // Scr. Mater. 2006. Vol. 54. P. 465–469.
135. Sehitoglu H., Wang J., Maier H.J. Transformation and slip behavior of Ni2FeGa // Int. J. Plast. 2012. Vol. 39. P. 61–74.
136. Yu H.J. et al. Effect of annealing and heating/cooling rate on the transformation temperatures of NiFeGa alloy // J. Alloys Compd. 2009. Vol. 470. P. 237–240.
137. Zhu Y., Dui G. Micromechanical modeling of stress-strain behaviors with intermartensitic transformation in NiFeGa alloys // Mech. Mater. Elsevier Ltd, 2010. Vol. 42, № 4. P. 429–434.
138. Yu H.J. et al. Phase transformations and magnetocaloric effect in NiFeGa ferromagnetic shape memory alloy // J. Alloys Compd. 2009. Vol. 477. P. 732–735.
139. Morito H. et al. Effects of partial substitution of Co on magnetocrystalline anisotropy and magnetic-field-induced strain in NiFeGa alloys // J. Magn. Magn. Mater. 2005. Vol. 290-291 PA. P. 850–853.
140. Hamilton R.F. et al. Mechanical response of NiFeGa alloys containing second-

phase particles // Scr. Mater. 2007. Vol. 57. P. 497–499.

141. Yu H.J. et al. Effect of Ge addition on the martensitic transformation temperatures of Ni-Fe-Ga alloys // Mater. Sci. Eng. A. 2009. Vol. 507. P. 37–41.
142. Bachagha T., Suñol J.-J. All-d-Metal Heusler Alloys: A Review // Metals (Basel). 2023. Vol. 13, № 1. P. 111.
143. Gruner M.E. et al. Modulations in martensitic Heusler alloys originate from nanotwin ordering // Sci. Rep. 2018. Vol. 8, № 1. P. 8489.
144. Kaufmann S. et al. Modulated martensite: why it forms and why it deforms easily // New J. Phys. 2011. Vol. 13, № 5. P. 053029.
145. Timofeeva E.E. et al. Development of thermoelastic martensitic transformations in ferromagnetic [011]-oriented NiFeGa single crystals in compression // Russ. Phys. J. 2012. Vol. 54, № 12. P. 1427–1430.
146. Belyaev S.P., Resnina N.N., Volkov A.E. Influence of irreversible plastic deformation on the martensitic transformation and shape memory effect in TiNi alloy // Mater. Sci. Eng. A. 2006. Vol. 438–440. P. 627–629.
147. Liu Y. et al. Partial thermal cycling of NiTi // J. Alloys Compd. 2008. Vol. 449, № 1–2. P. 144–147.
148. Lahoz R., Puértolas J. Training and two-way shape memory in NiTi alloys: influence on thermal parameters // J. Alloys Compd. 2004. Vol. 381. P. 130–136.
149. Rehman S.U. et al. Effect of precipitation hardening and thermomechanical training on microstructure and shape memory properties of Ti50Ni15Pd25Cu10 high temperature shape memory alloys // J. Alloys Compd. Elsevier B.V., 2014. Vol. 616. P. 275–283.
150. Atli K.C., Karaman I., Noebe R.D. Work output of the two-way shape memory effect in Ti50.5Ni24.5Pd25 high-temperature shape memory alloy // Scr. Mater. Acta Materialia Inc., 2011. Vol. 65, № 10. P. 903–906.
151. Prokoshkin S.D. et al. Crystal lattice of martensite and the reserve of recoverable strain of thermally and thermomechanically treated Ti-Ni shape-memory alloys // Phys. Met. Metallogr. 2011. Vol. 112, № 2. P. 170–187.
152. Volkov A.E. Microstructural modeling of alloy deformation during repeated

martensitic transformations // Proceedings of the Academy of Sciences. Ser. Physics. 2002. Vol. 66, No. 9. P. 1290–1297. (In Russian)

153. Sibirev A. et al. Simulation of plastic strain accumulation during thermal cycling of TiNi alloy // Mater. Today Proc. 2017. Vol. 4, № 3. P. 4743–4747.
154. Hong K.-N. et al. Recovery Behavior of Fe-Based Shape Memory Alloys under Different Restraints // Appl. Sci. 2020. Vol. 10, № 10. P. 3441.
155. Georges T., Brailovski V., Terriault P. Experimental Bench for Shape Memory Alloys Actuators Design and Testing // Exp. Tech. 2013. Vol. 37, № 6. P. 24–33.
156. Coluzzi B. et al. Effect of thermal cycling through the martensitic transition on the internal friction and Young's modulus of a Ni50.8Ti49.2alloy // J. Alloys Compd. 2000. Vol. 310, № 1–2. P. 300–305.
157. Filip P., Mazanec K. The influence of thermal and mechanical treatment on the reactive stresses in TiNi shape memory alloys // J. Mater. Process. Technol. 1995. Vol. 53, № 1–2. P. 139–146.
158. Filip P., Mazanec K. Influence of work hardening on the reactive stress in a TiNi shape memory alloy // Mater. Sci. Eng. A. 1994. Vol. 174, № 2. P. L41–L43.
159. Lim Y.G. et al. Enhancement of recovery stresses of the Ni-50.2Ti alloy by severe plastic deformation using a high-ratio differential speed rolling technique // Scr. Mater. Elsevier Ltd, 2016. Vol. 124. P. 95–98.
160. Abuzaid W., Sehitoglu H. Functional fatigue of Ni50.3Ti25Hf24.7 – Heterogeneities and evolution of local transformation strains // Mater. Sci. Eng. A. Elsevier B.V., 2017. Vol. 696. P. 482–492.